
**ADDIS ABEBA UNIVERSITY**

**SCHOOL OF GRADUATE STUDIES**

**SCHOOL OF EARTH SCIENCES**

# PETROGENESIS OF BIMODAL BASALT-RHYOLITE SUITE FROM DEBRE SAHIL/ GUNA AREA, SOUTHEASTERN ETHIOPIA

BY

TEGENE WUBISHET SHEWANGIZAW

ADVISOR:

PROFESSOR DEREJE AYALEW

**A Thesis Submitted to School of Graduate Studies of Addis Ababa University, in Partial Fulfillment of the Requirements for the Degree of Masters of Earth Sciences in Geochemistry.**

**30th May, 2018**

**Addis Ababa, Ethiopia**


# ADDIS ABABA UNIVERSITY

## COLLEGE OF NATURAL SCIENCES

## SCHOOL OF EARTH SCIENCES

# PETROGENESIS OF BIMODAL BASALT-RHYOLITE SUITE FROM DEBRE SAHIL/ GUNA AREA, SOUTHEASTERN ETHIOPIA

BY

TEGENE WUBISHET SHEWANGIZAW

ID. NO: GSR/3907/09

ADVISOR:

PROFESSOR DEREJE AYALEW

**A Thesis Submitted to School of Graduate Studies of Addis Ababa University, in Partial Fulfillment of the Requirements for the Degree of Masters of Earth Sciences in Geochemistry.**

**30th May, 2018**

**Addis Ababa, Ethiopia**

# ADDIS ABABA UNIVERSITY

# COLLEGE OF NATURAL SCIENCES

# SCHOOL OF EARTH SCIENCES

**PETROGENESIS OF BIMODAL BASALT-RHYOLITE SUITE FROM DEBRE SAHIL/ GUNA AREA, SOUTHEASTERN ETHIOPIA**

BY

**TEGENE WUBISHET SHEWANGIZW**

**Approved by the Examining Committee**

| | | |
|---|---|---|
| Dr. Balemwal Atnafu | _____ | _____ |
| Head, School of Earth Sciences | Signature | Date |
| Prof. Dereje Ayalew | _____ | _____ |
| Advisor | Signature | Date |
| Prof. Gezahegn Yirgu | _____ | _____ |
| Examiner | Signature | Date |
| Dr. Mulugeta Alene | _____ | _____ |
| Examiner and chairperson | Signature | Date |

## Declaration of originality

I hereby declare that the thesis entitled "The petrogenesis of bimodal basalt-rhyolite suite from Debre Sahil /Guna area, Southeastern Ethiopia", is my original work prepared for the partial fulfillment of the degree of masters in science in the School of Earth Science, Addis Ababa University during the year of 2018 under the supervision of Professor Dereje Ayalew. In addition, I am assuring that this work has not been presented or submitted to any other University or institution for the award of any degree or diploma in any case. All materials are well referenced and acknowledged.

| | **Signature** | **date** |
|---|---|---|
| **Tegene Wubishet Shewangizaw** | _____ | _____ |

I hereby declare this is his original work as part of his masters of science in Earth Science (Geochemistry).

| | **Signature** | **date** |
|---|---|---|
| **Professor Dereje Ayalew** | _____ | _____ |

## ACKNOWLEDGMENT

Firstly, I would like to thank very much the two institutions, Addis Ababa and Mizan-Tepi Universities for providing me the opportunity to grasp my master's degree.

My deepest gratitude goes to my Advisor Professor Dereje Ayalew for his follow up, invaluable advice, constructive comment and suggestion, encouragement, discussion and limitless support at various times and continuous support throughout the entire thesis and his friendly approach throughout my research.

Prof. Gezahegn Yirgu is the second person to give my respect and acknowledgment for having a valuable technical discussion with him and guidance.

During the research work, I got a lot of support from my friends, and colleagues Belete Bayicheken, Hayelom Mengesha, Girma Hailu, Hagos Hiluf, Ahmed Musa, Demisachew Yilma, Senidu Demissie and Samuel Getachew are deeply acknowledged for their great support as well as motivation.

My acknowledgment goes to my family for giving me courage and unforgettable support.

The last but not the least, my gratitude goes to local peoples of Guna Wereda for helping me during the field work.

# TABLE OF CONTENTS

**Contents** **page**

# LIST OF FIGURES

# LIST OF TABLES

## ACRONYMS

| | |
|---|---|
| AAE | Addis Ababa Embayment |
| AAZ | arcuate accommodation zone |
| ALS | Australian Laboratory Science |
| a.s.l | Above mean sea level |
| BT | Boru Toru structural high |
| CFB | continental flood basalt |
| CMER | Central Main Ethiopian Rift |
| CIPW | (Cross, Iddings, Pirsson and Washington) |
| DEM | Digital elevation model |
| EARS | East African Rift System |
| EIGS | Ethiopian Institute of Geological Survey |
| Fig. | Figure |
| GPS | Global positioning system |
| ICP-AES | Inductively coupled plasma Atomic emission spectrometry |
| ICP-MS | Inductively coupled plasma mass Spectrometry |
| HREE | Heavy rare earth element |
| HT | High Titanium |
| HT1 | High Titanium one |
| HT2 | High Titanium two |
| Km | Kilometer |
| LOI | Loss on ignition |
| LREE | Light rare earth elements |
| LT | Low Titanium |
| MK | Midre Kebd structural high |
| ME-4ACD81 | Multi element four acid digestion 81 |
| MER | Main Ethiopian rift |
| MEVD | Multi element variation diagram |
| MORB | Mid-oceanic ridge basalt |
| MREE | medium Rare earth element |
| NMER | Northern Main Ethiopian rift |

| | |
|---|---|
| NNE-SSW | North North east South South east |
| N-S | North South |
| NW | North west |
| NE | North east |
| OIB | Ocean island basalt |
| PM | Partial melting |
| ppb | parts per billion |
| ppm | parts per million |
| PPL | Plane polarized light |
| REE | Rare earth element |
| SA-NMERTZ | Southern Afar Northern Main Ethiopian Rift transition zone |
| SMER | Southern Main Ethiopian Rift |
| SRTM | Shuttle Radar Topography Mission |
| TAS | Total Alkali Silica |
| Wt% | Weight percent |
| WFB | Wonji fault belt |
| WFZ | Woito fault zone |
| XPL | Cross polarized light |
| YTVTL | Yerer- Tulu Welel volcano tectonic lineament |

## ABSTRACT

The Debre Sahil volcanic rocks are part of southeastern province, eastern shoulders of Northern MER. The area is located approximately 302 Km from Addis Ababa. The main objective of the research study was to understand the petrogenetic evolution of bimodal volcanic suite. To achieve the objectives, starting from the beginning different methods have been applied. The methods are; field observation, petrographic data analysis, and geochemical data analysis. The major volcanic rock units are pyroxene- olivine phyric basalt (upper basalt), olivine-pyroxene phyric basalt (lower basalt), white rhyolite, rhyolitic ignimbrite and glassy rhyolite. The petrographic study show that the mafic volcanic product of the area is characterized by olivine, clinopyroxene, plagioclase and Fe-Ti oxide crystal phases with microlite groundmass, whereas the rhyolitic rocks are dominated by alkali feldspar, plagioclase, quartz and lithic fragments with glassy groundmass. The geochemical analysis results indicate the Debre Sahil rocks are bimodal in composition, mafic and silicic, lacking intermediate composition. The mafic rocks are alkaline basalt and the silicic rocks are dominantly peralkaline rhyolites. Furthermore, these results indicate that the Debre Sahil volcanic rocks are sourced from spinel bearing peridotite with some residual garnet mantle source. Moreover, the basalt-rhyolite suite is proved to be genetically related to each other by fractional crystallization process. Selected trace element ratios such as Zr/Sm (25.3- 34.15), Zr/Hf (34.12-40.73), Nb/Ta (15.96-21.23), La/Nb (0.77-0.96), Nb/La (1.04-1.29) and Ba/Nb (10.27-21.67) indicates that the study samples are comparable with primitive mantle values, and thus are originated from enriched mantle source or OIB type source.


**Key words**: Debre Sahil bimodal suite, Fractional crystallization, Crustal contamination, mantle melting condition (magma generation).

# CHAPTER ONE

# 1. INTRODUCTION

## 1.1. Background

The Ethiopian continental flood basalt (CFB) province (30 Ma), was formed due to the impingement of the Afar mantle plume beneath the Ethiopian lithosphere (Dereje Ayalew et al., 2002). This province consists of major sequences of rhyolitic ignimbrites generally found on top of the flood basalt sequence (Dereje Ayalew et al., 2002). In most of continental flood basalt provinces, the volcanic suites are bimodal basalt-rhyolite nature with a distinct lack of intermediate compositions (Dereje Ayalew and Gezahegn Yirgu, 2003) with the dominant process of fractional crystallization for their evolution (Dereje Ayalew and Gibson, 2009). The flood volcanism is predominantly composed of basaltic lavas together with rhyolitic ignimbrites and pyroclastic-fall deposits, and rhyolitic lavas (Dereje Ayalew et al., 2002; Kieffer et al., 2004). Based on $^{40}Ar/^{39}Ar$ dating (Ukstins et al., 2002), basaltic flood volcanism could have begun in Ethiopia significantly earlier than 30.9 Ma. The "volcano-stratigraphic profiles and dating indicate that along the rift margin in north-central part of Ethiopia volcanism might have been initiated significantly earlier with the greatest eruption rates and volume occurring from ~ 31 to 28 Ma (Hofmann et al., 1997; Ukstins et al., 2002)". These rocks are distributed in different parts of the country having various volcanic rocks, thickness, chemical composition and chronological ages (Mengesha Tefera et al., 1996).

Most of the flood basalts and rhyolites erupted in a short time period (1-2 My) at 31–29 Ma, (Hofmann et al., 1997) to form a wide volcanic plateau, and are a good example of the youngest major continental volcanic plateau (Kieffer et al., 2004). According to (Mengesha Tefera et al., 1996) the name Arsi and Bale basalts were given to the flood basalt succession of the Southeastern plateau where the flood basalt activity culminated by the formation of large volcanic edifices which formed some of the highest peaks on the southeastern plateau. These basalts are commonly felsic on the upper parts. The age of the southeastern Ethiopian flood basalt ranges from 30 to 22 Ma (Siefemichael Berhe et al., 1987). In mineralogical composition (Mohr, 1983; Mohr & Zanettin, 1988; Pik et al., 1998) the flood basalts are aphyric and sparsely phyric and contain phenocrysts of plagioclase and clinopyroxene with or without olivine.

The detailed geology and geochemistry of igneous province of the southeastern Ethiopian volcanic plateau are not well studied except for some regional studies (Siefemichael Berhe et al., 1987 and Nelson, 2009). This research project is designed to understand and examine the petrogenetic evolution of bimodal basalt-rhyolitic rocks of the eastern rift shoulder/

Southeastern Ethiopian plateau flood basalt through the integration of petrographic and geochemical data investigations.

## 1.2. General description of the Study Area

### 1.2.1. Location

The study area is located around Debre Sahil, in Oromia Region, Southeastern Ethiopia, which is about ~302 km southeast of Addis Ababa. Geographically the study area is bounded between 8°18'46" to 8°23'40"N latitude and 39°53'24" to 39°57'46"E longitude with a total coverage area of 72 km$^2$.

### 1.2.2. Accessibility

The study area is accessible by the gravel road which is running from Adama through Donni, Abomasa, Angada to Arba-Dima town. It is also accessed by the road that runs from Adama through Arsi Negele to Debre Sahil/ Guna village. The mappable area is accessed by footpath and trails stretching to different locations of the study area.

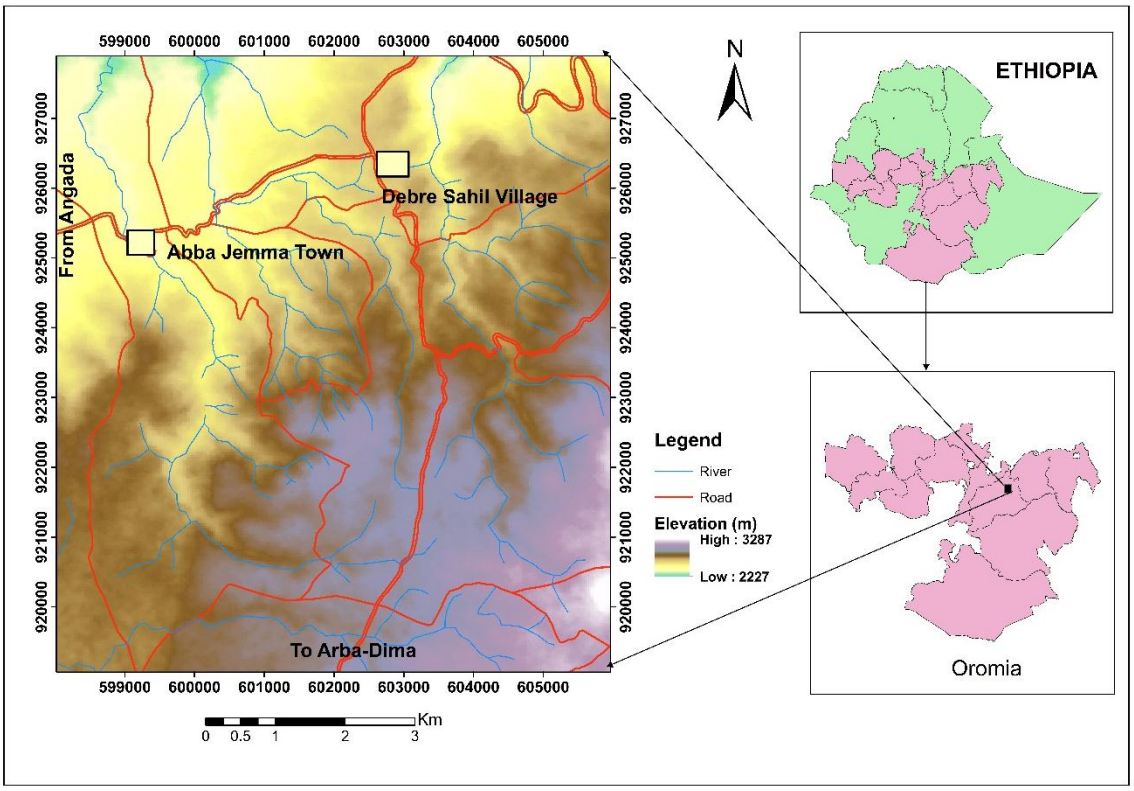


***Fig. 1.1***. Location and accessibility map of the study area

### 1.2.3. Physiography

The study area is characterized by different topographic features such as ridges, hills and flat surface. Hill topography is found in the southwestern, eastern and northeastern parts, while the central and the southwestern part has flat type nature. The hills or plateaus of the area are constituted by rhyolitic rocks, & some pyroxene-olivine phyric basalt unit, whereas the flat surfaces are mainly constituted by rhyolite and some olivine-pyroxene phyric basalt rock units. Generally, the ridges have N-S trending with a series of a saddle and steep slopes.

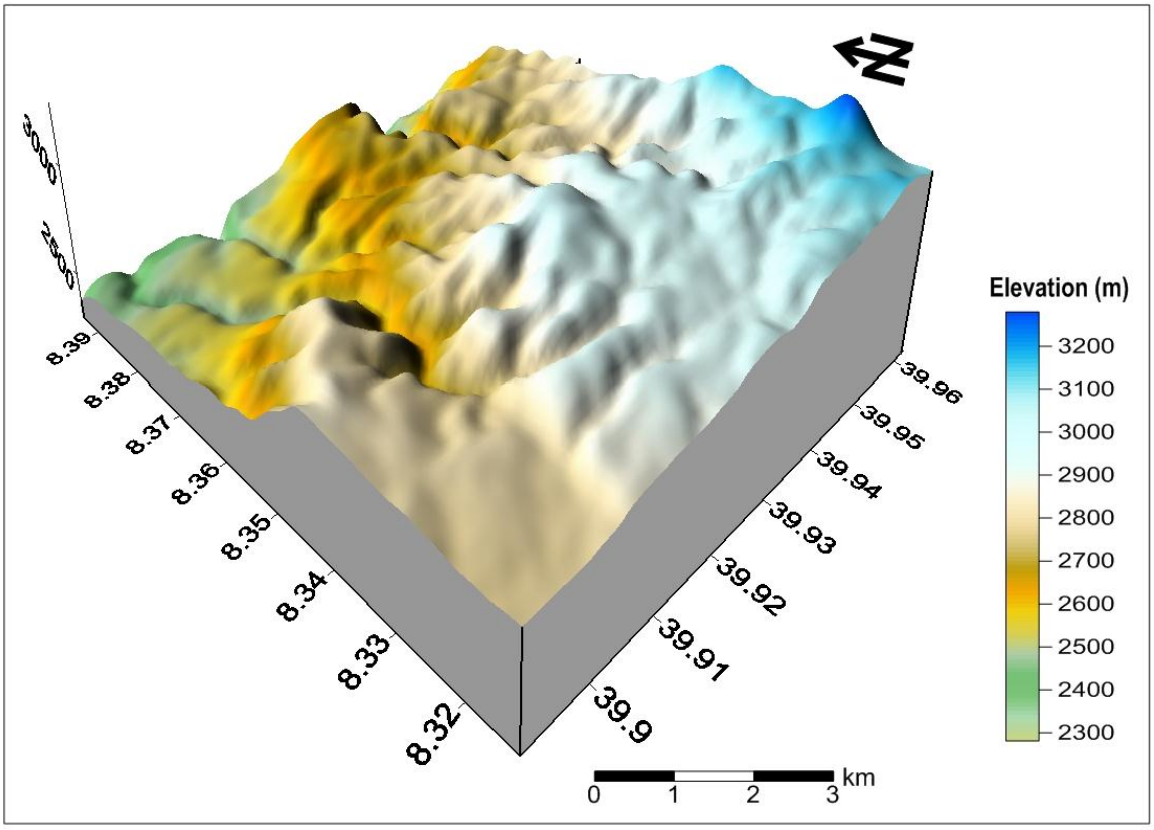


**Fig. 1.2**. Physiographic map of the study area

### 1.2.4. Drainage pattern

The study area is drained with the Abba Jemma and Sorbayi main river, and other small tributaries. Most of the streams flow seasonally and joining with the main Abajema river flowing together towards the northern direction of the study area. The drainage pattern of the stream shows a variation of density of water flow because of the seasonal variation. Overall, the study area is characterized by dendritic drainage pattern.

### 1.2.5. Climatic Condition

The climate condition around the area of the study shows warm and temperate climatic condition. In winter there is much less rainfall than in summer season. The climatic condition of the area is mainly expressed by average temperature and average precipitation. According to Climate-Data.org in http://en.climate-data.org/location/2108/ the annual average temperature is 16.2 $^{0}$C and the annual average rainfall is 1099 mm. June is the hottest month of the year with an average temperature of 17.3 $^{0}$C whereas November has the lowest average temperature of 14.9 $^{0}$C.

### 1.2.6. Soil

The Debre Sahil area is characterized among the regions that have medium to high soil fertility and it is covered by thick soil. This is due to weathering and erosion process. It is also suitable for growth of vegetation; because, the soil of the rock unit is fertilized. However, the soil at the flat area is little bit fertile than the hill top soils.

### 1.2.7. Vegetation

The study area is generally characterized by sparsely distributed vegetation coverage. However, the vegetation on the northeastern & northwestern parts of the study area is slightly denser than the other parts. The vegetation types found in the study area are Podocarpus (zigiba), Junperous procera (Tid), shrubs, bushes and Eucalyptus (Bahirzaf). Eucalyptus is grown by the local people for soil conservation. In addition, the local people cultivate some types of crops on the gentle slope landmass. The common types of crops cultivated in the study area are Teff, Wheat, Bean, Pea, Barley, Sorghum, and Maize. The harvesting season is between October and December at which the rainfall becomes lower in amount.

## 1.3. Objectives

### 1.3.1. General objective

The main objective of the present study is to investigate the petrogenetic evolution of bimodal basalt-rhyolite rock units of Debre Sahil area.

### 1.3.2. Specific objectives

- ✓ To produce geological map of the area at the scale of 1:25,000, with a collection of the representative sample.
- ✓ To describe the petrography of the rock with the aim at understanding the mineral composition.
- ✓ To understand the elemental composition of the rock with the aim at constraining the source and genesis of the rock of the area.

### 1.4. Statement of Problem

The southeastern Ethiopian volcanic plateau is not well studied as compared to the Northwestern Ethiopian plateau. Although, there are a number of studies focused on the rift area (e.g. Tadiwos Chernet et al., 1999; Gaspron et al., 1993; Bonini et al., 2005; Peccerillo et al.,2003; 2007; Furman, 2007; Giordano et al., 2014, Dereje Ayalew et al., 2000; 2016 and Mulugeta Alene et al., 2017). However, as compared to with the rift area, the rift shoulders are not well studied. Moreover, lack of a detailed geological map of any particular section of the Ethiopian igneous province makes it difficult to correlate much of the existing high-quality geochemical data from various parts of the Ethiopian igneous province. As a result, only very limited data and general features are known for the local study area. The aim here is to examine the source and Petrogenesis of volcanic rocks of Debre Sahil area using petrographic and geochemical analysis.

### 1.5. Materials and Methodology

#### 1.5.1. Materials

During the different phases of the study, a variety of tools are used; including a topographic map at the scale of 1: 25,000, geologic map at the scale of 1: 50,000, DEM_30m, GPS, compass, hand lens (10 x magnifications); digital Camera. The samples have been collected in closable plastic bags. Utilized, Software's include ArcGIS 10.3.1, ERDAS Imagine 10, Starter 4, surfer 10, Google Earth, Global Mapper version 11 and Microsoft Excel 2010, Petrographic 2 beta, GCDKIT Tool, CIPW normative Excel and geochemical tool.

#### 1.5.2. Methodology

The following different methods and approaches have been conducted in order to accomplish the general and specific objectives of the present study systematically.

##### 1.5.2.1. Revision of previous works

Some of the major activity conducted during the revision of previous works were collection of previous technical reports, journals, textbooks, extracting of relevant information from the satellite image and aerial photograph, reviewing and compiling of literature (published and unpublished reports) related to the study area.

##### 1.5.2.2. Fieldwork

Field works were conducted for fifteen days and involved different activities. The first two days of the field work involved road geology by which the overall geology of the area was outlined. The major activities conducted during the fieldwork were a description of lithostratigraphy in relation to accurate measurement, observation and recording of all the

lithological variation in color, texture, mineral composition, kind and degree of weathering, the color of fresh surface. Moreover, tracing of structural continuity, measuring and recording of geological structures, taking of representative and fresh rock samples for further laboratory analysis (petrographic and geochemical analysis). Furthermore, lithological variations, lithological contacts, and the geological structures are transferred to a geological map of scale 1: 25,000.

#### 1.5.2.3. Petrographic analysis

Based on the variety of the lithologies fifteen (15) fresh and representative samples are selected for thin section preparation. The thin sections have been prepared at the laboratory of Geological Survey of Ethiopia. Moreover, thin section samples have been examined under Leica petrographic microscope to determine the modal proportion of minerals and rock fabrics (texture). The petrographic analysis is carried out at Addis Ababa University, School of Earth Science mineralogy laboratory. The main output of the thin section analysis is modal proportion of minerals, largest grain size diameter along their longest dimension of each mineral, the average grain shape of those existed minerals and grain to grain relationship of the phenocrysts. This information will help lastly in the rock classification and understand the magmatic evolution.

#### 1.5.2.4.Geochemical analysis

Fresh samples of basalt and rhyolite were collected from Debre Sahil area, and totally twelve (12) samples were selected for geochemical analysis. Sample preparation for geochemical analysis includes removal of the weathered part; break the sample into desirable sizes, crush the broken sample and the sample have been milled down to micron size particles. The sample preparation is done in Akaki Kaliti, Kebele 10/11 block 03 at ALS milling room Addis Ababa. The samples are submitted to the Australian Laboratory Science (ALS) to determine the concentration of major and trace elements. Major elements (including loss on ignition) were analyzed by Inductively Coupled Plasma Atomic emission spectrometry (ICP-AES). Besides, trace elements were analyzed by Inductively Coupled Plasma Mass Sepectrometry (ICP-MS) and base metal by Multi-Element four acid digestion 81 (ME-4ACD81).

### 1.6. Significance of the Research

The output of this research helps for individual researchers and research organization by providing different data of the local geology. Furthermore, the study may give some understanding of the methodology followed in this research, petrographic and geochemical studies that will be used as a reference framework for the students and other researchers. In this

study, the petrographic and geochemical details of the flood basalt with their field observations will have a paramount importance to determine Petrogenesis of the rocks in southeastern Ethiopian plateau that will again useful as a reference for the scientific community.

### 1.7. Review of previous works

Previous works in the study area have been carried out at regional scale such as geologic and structural mapping (EIGS, 1978). Some notable works in the surrounding area include those of Nelson (2009) suggested that the Ethiopian plateau basalt evolved through mantle plume contribution beneath Ethiopian lithosphere. Corti (2009) described the Ethiopian plateau volcanism and evolution of the flood basalt volcanic province as well as rifting. The chemical composition of the flood basalt both in the north and southern sector of the Somalian and Ethiopian plateau have been discussed by (Mohr, 1983; Giday WoldeGabriel et al., 1990); and Kieffer et al. (2004), among others. Some detailed geological description of the Southeastern Ethiopian Plateau, including some stratigraphy, geochemistry and geochronology, as well as the structural context, has been given by Seife Michael Berhe et al. (1987) and Workineh Haro et al. (2014).

The work by (Eberz et al.,1988) shows that the uplifting of the Ethiopian and Arabian platform happened during Cretaceous followed by down warping of Afar and Ethiopian proto rift in mid-Tertiary. This led to the outpouring of voluminous flood basalt volcanism with transitional to tholeiitic composition in the northern sector of the plateau and mildly alkaline in the southern sector (Mohr, 1983; Giday WoldeGabriel et al., 1990). Following the trap series, the early Miocene, a resurgence of volcanism occurred throughout the region with increased basaltic activity in Turkana and shield volcanism and fissural basalts on the Ethiopian plateau (Rooney, 2017). In addition, following the resurgence phase welded and non-welded tuffs of Pliocene volcanism were formed unconformably overlaying the basalts (Mohr, 1968) and locally interbedded with lacustrine sediments (Eberz et al., 1988). Major uplift of the rift margins did not begin before late Pliocene suggesting that the silicic volcanic rocks were not formed before the major episode of Ethiopian rifting stage (Mohr, 1968; Meyer et al., 1975). Besides the work by Rooney et al. (2011) shows that Subsequent magmatism largely localized to the developing MER and took the form of large silicic centers and smaller basaltic eruptions.

### 1.8. Thesis Overview

The thesis is organized in six chapters. Chapter one gives general information about the area of study, the purpose and methods followed in the research. The second chapter provide a regional scale overview. Chapter three deals with a detailed description of the lithology and petrographic of the study area. Chapter four provide the geochemical results with their interpretations. In chapter five the discussion and petrogenetic evolution of Debre Sahil bimodal volcanic rocks are presented. Eventually, in chapter six, conclusion and recommendations for further study are presented.

# CHAPTER TWO

# 2. REGIONAL GEOLOGY

## 2.1. Magmatism on the Ethiopian Plateau

Cenozoic magmatic activity in Ethiopian and East African plateaus started some 45 Ma before the formation of the EARS (Davidson and Rex ,1980; Ebinger et al., 1993; George et al., 1998). However, the most flood basalt successions in the Ethiopian plateaus (northwest and southeast) formed during the period of 31–28 Ma (Hofmann et al. 1997; Dereje Ayalew et al., 2002; Ukstin et al., 2002). This Large-scale flood basalts were emplaced as a result of the impingement of the Afar plume (Baker et al., 1996; Hofmann et al., 1997; Pik et al., 1999; Dereje Ayalew et al., 2002; Kieffer et al., 2004) and related to uplift and extension (Marty et al. 1996; Dereje Ayalew et al., 2002). This plume related uplift caused deep-seated faults within the lithosphere, leading to the initiation of the Afar Depression (Alebachew Beyene and Mohammed Abdelsalam, 2005), the rifting of MER, and sporadic formation of shield-volcanoes around 26 to 22 Ma (Kieffer et al., 2004). The activity of shield volcanoes migrated southeastward at 15–13 Ma in central Ethiopia (Zanettin et al., 1978).

Moreover, the Ethiopian volcanic event is classified into three main stages (Mohr and Zanettin, 1988; Peccerillo et al., 2003; 2007). The large-scale flood basalts were erupted during first stage where voluminous eruption had taken place during a short 1–2 Ma period, forming a vast volcanic plateau (Baker et al. 1996 and Hofmann et al. 1997). Latest phases of this stage were characterized by alternating basalt and ignimbritic eruption, forming the so-called Alaji Rhyolitic Formation (e.g., Merla et al., 1979). A second stage of activity is Miocene in age and is characterized by the construction of huge basaltic shield volcanoes (Termaber Basalt Formation) (e.g., Piccirillo et al., 1979; Peccerillo et al., 2003; 2007; Kieffer et al. 2004). This province covers an area of 600,000 km2 and has an estimated volume of volcanic rocks greater than 350,000 km3 (Mohr 1983). Compositionally the Trap series are mostly tholeiitic flood basalts and alkaline shield volcanoes (Pik et al., 1998; Kieffer et al., 2004).

In addition, on base of geochemistry, the Trap series basalts divided into Low-Ti tholeiitic and High-Ti alkali basalts (Pik et al., 1998). The Low-Ti tholeiitic flood basalts have relatively low concentrations of highly-incompatible trace elements, variable depletions at Rb, Th, U, Nb and Ta, exhibit the lowest rare earth element (REE) contents and nearly flat patterns whereas the High-Ti flood basalts are enriched in strongly-incompatible trace elements and have depletions at Rb, K and Sr (Pik et al.,1999). High Titanium basalts are found in the south and eastern part whereas Low Ti basalts are found in the northern part of plateau (Pik et al., 1998).

Based on K-Ar dating Seife Michael Berhe et al. (1987) recognized that Ethiopian flood basalts were formed during three stages: at>40Ma, 40-30Ma and 30-21Ma, though they are not the same in the northwest and southwest Ethiopian plateaus. This is also supported by Peccerillo et al. (2003; 2007). Seife Michael Berhe et al. (1987) suggests that stage one and stage three did not develop in the northwest, while Tertiary volcanism develops during stage three in southeast Ethiopia. The geology and geochronology of rocks in the southeast plateau suggests the existence of flood basalt volcanism since the earliest eruption at 30- 22 Ma (Seife Michael Berhe et al., 1987). Accordingly, four units are recognized in the Bale area: 30-22Ma lower stratoid basalts; Riera basalts (15-5Ma); Dodola basalts (undetermined age) and 6-2Ma Arorso trachyte (Merla et al., 1979) and 2.1 Ma Sante Basalts and Batu trachyte on the top. The lower stratoid basalts are overlain by 10-15m thick Damole ignimbrite in the east and by Riera basalts further to the west in the direction of the rift (Seife Michael Berhe et al., 1987). Riera basalts, pyroxene and plagioclase phyric basalt, form 600m thick succession of different units separated by scoriceous basaltic horizons and paleo soils. This unit is overlain by Dodola ignimbrite and Trachyte consisting of rhyolite ignimbrite, trachyte and ash flow tuff. The existence of intercalated volcano-sedimentary rocks is also recognized by Seife Michael Berheet al. (1987) and all together is considered as the 6-2 Ma old Ghinir unit (Merla et al., 1979). Shield volcanoes of 2.1Ma age form the Sante and Batu trachytes forming large volcanic edifies. In addition, Workineh Haro et al. (2014) recognize various units in the Bale - Asela area: lower lava flows, middle lava flows, plateau basalts and upper pyroclastics to plateau basalts and Quaternary basalts, trachyte and scoria cones on the top. Workineh Haro et al. (2014) recognized fine to medium plagioclase phyric basalts, medium to course plagioclase phyric basalts, scoriceous basalts, as well as olivine-plagioclase phyric basalts, olivine-pyroxene-plagioclase phyric basalts and pyroxene-olivine-plagioclase basalts in the area.

In summary, the work by Rooney (2017) confirms that magmatism on the Southeastern Ethiopian plateaus has some distinctions to that on the northwest Ethiopian Plateau in that Oligocene flood basalts do not constitute the most significant volume of the Somali Plateau. The earliest phase of volcanism in this region appears to be dominantly Early Miocene in age with the exception of some late Oligocene HT1 flows at Asebe Teferi, near the Afar margin (Nelson, 2009), and there is a lack of widespread silicic activity following the termination of the flood basalts. However, the ca. 25–26Ma resurgence in basaltic volcanism appears to be a common feature of both plateaus, potentially earlier on the Somali Plateau (Rooney, 2017).

Generally, the Ethiopian flood basalts are derived from one or more mantle sources with geographically varying mineralogy and depth of melting (Furman et al., 2016). These flood basalts could be generated by melting a different portion of the mantle with increasing depth, temperature and degree of metasomatism from the outer margin of the province (the LT basalts) to the center, where HT2 basalts and picrites sample ‘‘the core of the plume head” Beccaluva et al. (2009).

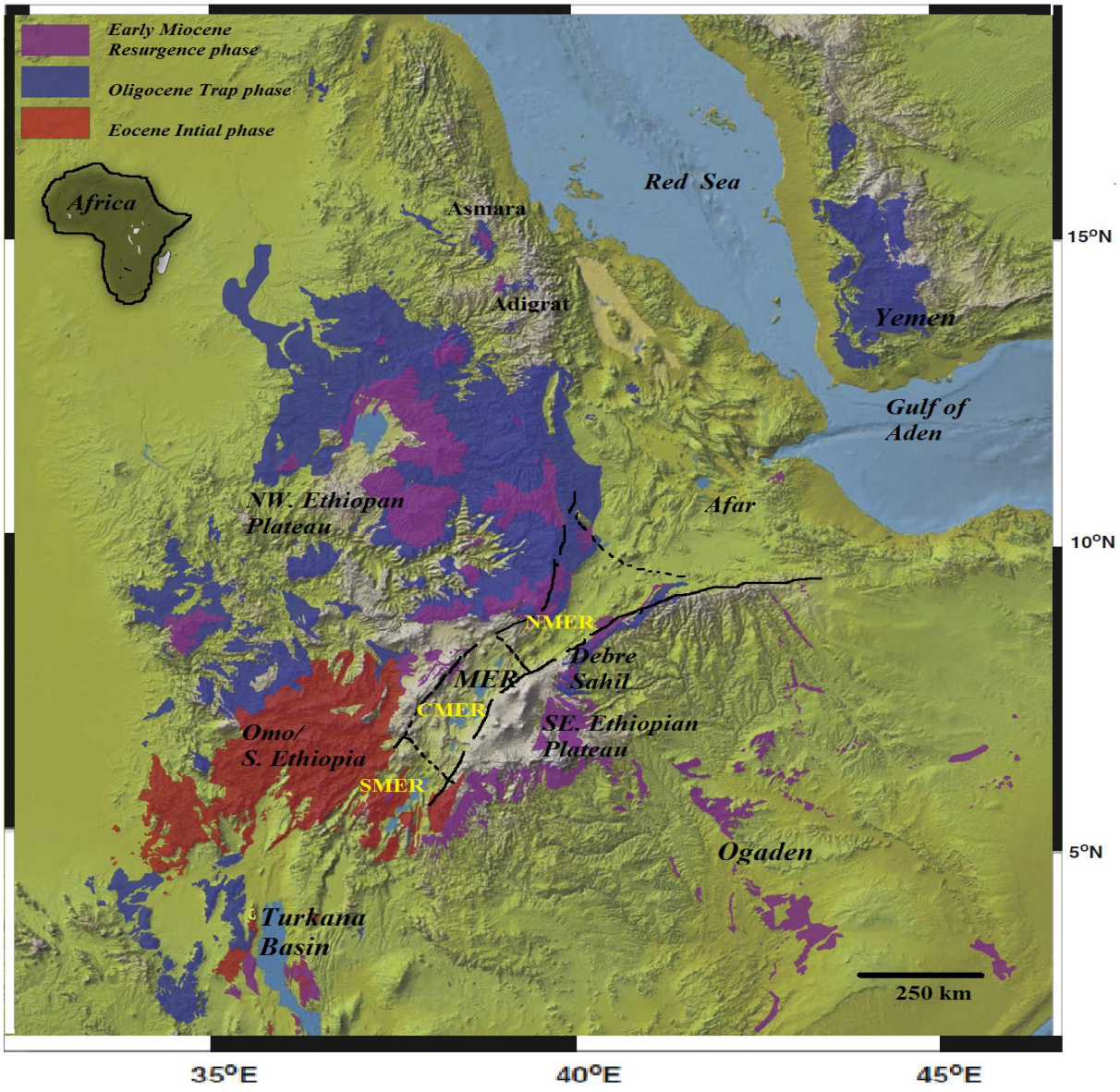


**Fig. 2.1**. Magmatic activity in Africa and parts of the Arabian Peninsula from 45 to 22 Ma and divided into three broad periods of magmatic activity: (A) Eocene Initial Phase (45–34 Ma), (B) Oligocene Traps phase (~33.9–27 Ma), (C) Early Miocene resurgence phase (26.9 Ma to 22 Ma). (*modified after Rooney, 2017)*.

## 2.2. Main Ethiopian rift volcanism

The main Ethiopian rift (MER) represents the northernmost volcanically active portion of the EARS (Bekele Abebe et al., 2007) which is bounded by the Afar depression to the North, the Gregory Rift (Kenya rift) to the South, and the Somali Plateau to the East and the Ethiopian Plateau to the West (Boccalleti et al., 1999; Ronga et al., 2010). It is a main sector of the EARS that records the history of episodic magmatic events throughout the rift (Giday WoldeGabriel et al., 1990). The northern most part is mainly characterized by widespread basaltic lava flows, associated with shield volcanoes or erupted fissures (Hayward and Ebinger, 1996) these basalts constitute most of the floor of the northern MER (e.g. Tadiwos Chernet et al., 1998). Conversely, felsic central volcanoes, usually characterized by calderas, are responsible for the formation of rhyolite ignimbrites and predominate in the central and southern part of the rift (Gidey WoldeGabriel et al., 1990; Tadiwos Chernet et al., 1998; Ebinger and Casey, 2001; Acocella et al., 2003). These deposits are usually intercalated with sedimentary syn-rift deposits (Le Turdu et al., 1999). Moreover, Peccerillo et al. (2003; 2007) ascribed the occurrence of the majority of silicic products and subordinate basalts in MER during Pliocene to present times to the final stage of volcanic activity.

Basically, the development of the MER was accompanied by extensive bimodal volcanic activity that occurred both inside the rift and along its shoulders (e.g., Gasparon et al., 1993; Natali et al., 2011). Basalts and silicic products are characteristics of the rift floor whereas trachyte magmas evolved along the rift shoulder, for instance the Ziquala and Yerer volcanic centers (Gasparon et al., 1993; Peccerillo et al., 2007). Subsequent volcanic activity started at ~ 14 Ma and was linked with the initial development of the MER and Afar (Mengesha Tefera et al., 1996). This activity is roughly coincident with the onset of rifting, voluminous felsic volcanism, and the establishment of a bimodal volcanic system in the transition of the northern MER and the southern Afar region (Natali et al., 2011). These the Rift stage is characterized by emplacement of fissural basalts belonging to the Anchar Formation (~12– 10 Ma, Gidey Woldegabriel et al., 1990; Tadiwos Chernet et al., 1998), followed by the voluminous fissural volcanism of the Nazret Group (~9.5–5.8 Ma Gidey Woldegabriel et al. 1990; Tadiwos Chernet et al. 1998). After the emplacement of the Nazret Group, mainly cropping out along the rift flanks, and including abundant evolved rocks and minor basic products, fissural volcanism became gradually confined to the present rift floor, with the emplacement of basalts of the Bofa Formation ~3.5–1.5 Ma (eg. Gidey Woldegabriel et al. 1990; Tadiwos Chernet et al.1998).

Moreover, the MER volcanic activities yielding 10-5Ma transitional and Na- alkaline basalts with minor trachyte shield volcanoes are considered as secondary phases (Peccerillo et al., 2003). In addition, Wolfenden et al. (2004) have found 10.5Ma trachyte flows from the base of Megezez volcano. Further to the NMER, Kurkura Kabeto et al. (2009) dated 9-7Ma transitional–alkaline Addis Ababa basalts, suggesting the presence of volcanic gap between the two pre-rift volcanic activities (Tadiwos Chernet et al., 1998; Kurkura Kabeto et al., 2009). This shows southward migration and younging of volcanism following the rift shoulder (Dereje Ayalew et al., 2006). Bimodal volcanism in Southern Afar Rift floor close to SA-NMERTZ has taken place during the period 7Ma- recent, with the chemical composition ranging from tholeiitic – alkaline basalts and basanites to trachyte and rhyolite (Tadiwos Chernet et al., 1998). The youngest rock of the Nazreth group in the NMER, for example is dated to 5.8Ma (Tadiwos Chernet et al., 1998). Even though volcanic gap is reported between 6.6 and 3.5Ma by Wolfenden et al. (2004) in the Adama basin, 7-5 Ma silicic rift margin transition zone magmas overlain by 5.6-4.5 Ma Afar Stratoid Series are recognized by Tadiwos Chernet et al. (1998). Using chrono-stratigraphic evidence it is followed by 4.5-3 Ma volcanic rocks of the Addis Ababa rift embayment (Tadiwos Chernet et al., 1998). Lastly young age rift floor basalts and Quaternary bimodal volcanic rocks (*ca*. 2Ma) have formed (Tadiwos Chernet et al., 1998; Kurkura Kabeto et al., 2009).

After these episodes of pre-rift activity widespread late Miocene-Pliocene rhyolitic ignimbrites (_7–3 Ma) with intercalated mafic lavas also occur in the Northern and Central MER [e.g., Gidey WoldeGabriel et al., 1990; Tadiwos Chernet et al., 1998]. The upper Pliocene basalts of the rift are variously named as the Wolenchiti basalts, Bishoftu basalts and Rhyolite, and Bofa basalts (Tadiwos Chernet and Hart, 1999). The NMER Bofa basalts and Melkasa units are considered as rift center basic volcanic centers, while the felsic rocks of Nazareth, Keleta, Boku –Tede and Dera – Sodere units are termed as Nazreth Group (Kurkura Kabeto et al., 2009). The Bofa basalts largely cover the northern and central sector of MER forming the barrier between ignimbrites of the Nazareth and Wonji group (Tadiwos Chernet et al., 1998; Tadiwos Chernet and Hart, 1999). The Nazreth Group volcanics consist of welded ignimbrite, pumice, ash; rhyolite flows and domes with minor intercalated basalts where the lower series are associated with earliest stage of rifting (Tadiwos Chernet and Hart, 1999). The ignimbrite of the Nazreth Group is formed from volcanic eruptions of the marginal centers (Peccerillo et al., 2003) covering large portions of rift margin and escarpments whereas basaltic magmas of this group are exposed along the fault scarps (Tadiwos Chernet et al., 1998). However, the

formation of ignimbrite is not restricted to swelling fractures of the marginal centers, but could also be formed from central volcanoes, e.g., Fantale (Peccerillo et al., 2003).

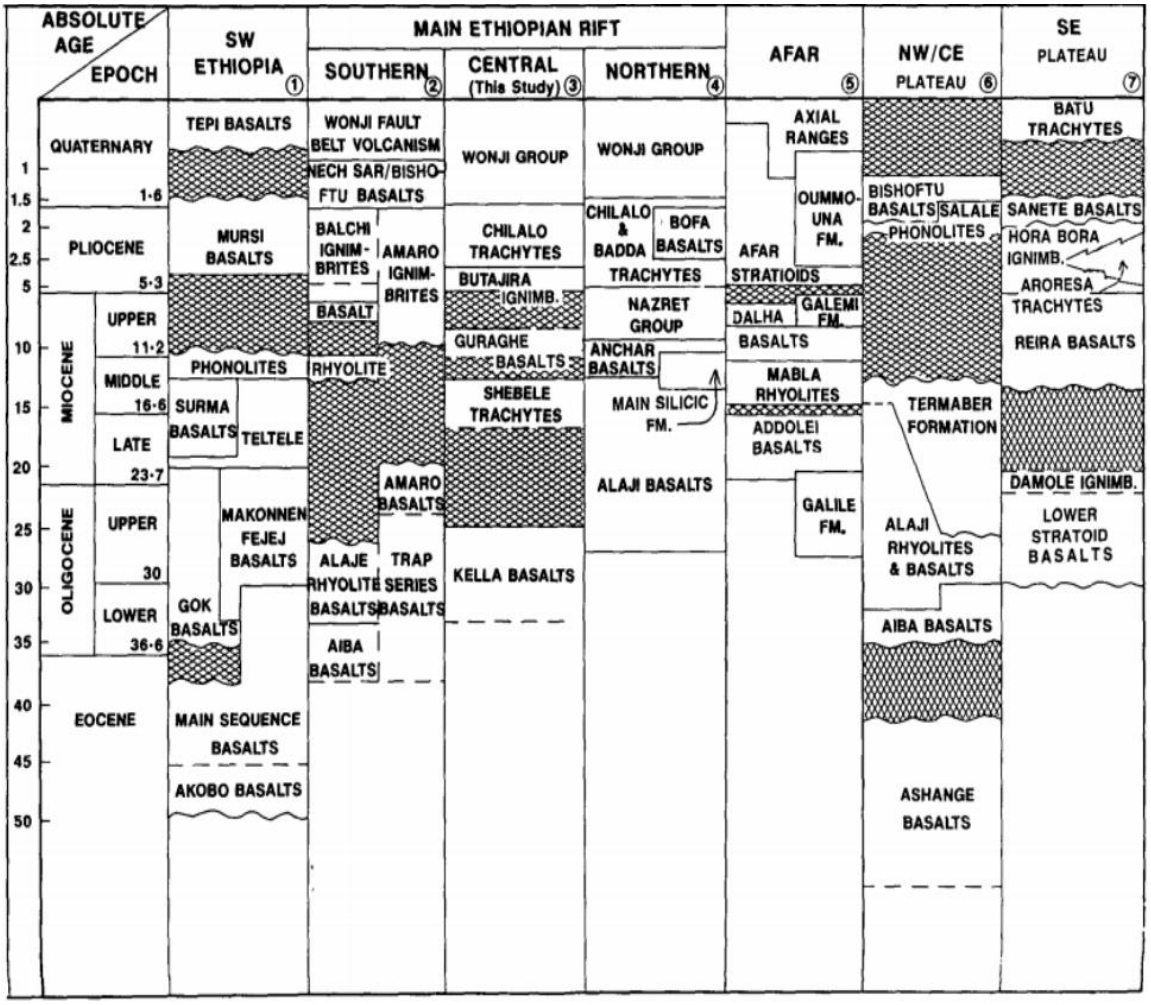


**Fig. 2.2.** Correlation chart of Cenozoic volcanic rocks in Ethiopia (from Giday WoldeGabriel et al., 1990).

The Quaternary volcanic activity < 2.6 Ma (Rooney, 2017) was associated with the Wonji Fault belt (WFB) affecting the rift floor [e.g. Gidey WoldeGabriel et al., 1990; Tadiwos Chernet et al., 1998] and characterized by both silicic rocks (Bora-Bericham Rhyolites and basalts (Wonji Basalts of Tsegaye Abebe et al., 2005). The silicic rocks compositions ranges from trachyte to peralkaline rhyolites (Tsegaye Abebe et al., 2005). In the SMER, volcanic activity was resumed in the Pliocene-early Pleistocene with bimodal character with eruption of ignimbrites (1.6-0.5 Ma), (Zanettin et al., 1978) followed by the Nechsar olivine basalt (1.34-0.77Ma) [Ebinger et al., 1993]. Quaternary basalts in the MER were predominantly formed by melts derived from the 'tail' of the Afar plume (Furman et al., 2006; Dereje Ayalew & Gibson, 2009).

A numerous petrological and geochemical studies in the region suggested that silicic volcanic rocks from the rift margin as well as the rift centers and adjacent plateaus are generated from fractional crystallization of basaltic magmas and variable degrees of crustal contaminations (e.g. Gasparon et al., 1993; Tadiwos Chernet and Hart 1999; Peccerillo et al., 2003; 2007; Dereje Ayalew et al., 2006; Kurkura Kabeto et al., 2009; Rooney et al., 2012; Giordano et al., 2014). In contrast, Trua et al. (1999) and Deniel, 2000) stated that the Asela–Ziway-pantellerite ignimbrite is formed from small degree partial melting of lower crust basaltic magmas (10%) followed by low pressure fractionation (40%) of mostly Na- plagioclase.

### 2.3. Tectonic Setting of the Region

The northwest and southeast uplifted Ethiopian volcanic province are separated by a roughly NNE–SSW trending MER (e.g. Gidey WoldeGabriel et al., 1990; Boccalleti et al., 1999; Wolfenden et al., 2004; Ukstins et al., 2002; Feyissa et al., 2017) and forming large escarpments extends from the Afar in northern Ethiopia to and the Kenya Rift to the South (Boccalleti et al., 1999; Agostini et al., 2011). It is a section of rifting that accommodates the active extension between the Nubia and Somalia Plates (e.g. Corti, 2009; Ebinger, 2005). This rift system shows different stages of development from initiation through break up to oceanic spreading in the north (Hayward and Ebinger et al., 1996). Bonini et al. (2005) suggested a heterogeneous time–space evolution, with initial extension in the Southern MER at 20–21 Ma, followed by extension in the Northern MER at 11 Ma and finally formation of the Central MER at about 5–6 Ma. Irregular rift propagation due to the presence of preexisting structures has also been proposed by Keranen and Klemperer (2008). This is also supported by work of Wolfenden et al. (2004).

The MER is divided into three main sections (NMER; CMER and SMER) differing in terms of trend, fault patterns and lithospheric characteristics [e.g., Mohr, 1983; Gidey WoldeGabriel et al., 1990; Hayward and Ebinger, 1996; Bonini et al., 2005]. The work by Hayward and Ebinger (1996) show that the variations of the thickness of the lithosphere in these different segments, were interpreted as reflecting a variation in rift evolution from mature rifting in the NMER to early continental rifting in the Southern MER. The crustal thickness measured along the rift axis varies from ~32 km in the central part of the northern MER to ~24 km south of Afar (Abera Tessema and Antoine, 2004). Moving off the rift axis, crustal thickness increases up to ~36–40 km below the rift shoulders and below the plateau (Abera Tessema and Antoine, 2004).

The SMER extends south from Lake Awasa into the largely rifted part of southern Ethiopia (Ebinger et al., 2000) with faults trending N-S to N20°E. Faulting in the SMER was well-established by ~18 Ma (Ebinger et al., 1993; Gidey WoldeGabriel et al., 1990). In the SMER the boundary faults are oriented N0°E to N20°E due to rotation of the rift valley from N20°-35° to N 5°-20° (Corti, 2009). It is characterized by the Chencha major fault in the west, which is curvilinear in shape-oriented N–S and N40°E and the Agereselam linear shaped NNE–SSW trend boundary fault in the east (Corti, 2009). According to Gidey WoldeGabriel et al. (1990) the Agereselam boundary fault was formed at 10 Ma whereas south of Lake Abaya extensional deformation initiated at 20-21 Ma ago (Bonini et al., 2005).

The CMER is bounded by the Boru-Toru Structural High (BTSH) and the Goba-Bonga structural lineament (Bonini et al., 2005). The main border fault in this area of the CMER, known as the Asela-Sire border fault. These trend at approximately N30°E-N40°E in this area and define the rift, separating the CMER from the Somali plateau to the east (Gidey Woldegabriel et al., 1990; Boccaletti et al., 1998; Tsegaye Abebe et al., 2010), and are mid-Miocene (Ebinger and Casey, 2001), no older than ~8 Ma (Gidey Woldegabriel et al., 1990; Bonini et al., 2005; Tsegaye Abebe et al., 2010). Based on gravity and seismic data, crustal thickness of the CMER increases rapidly from the boundary with the NMER (33–35 km) to the middle of the CMER (38–40 km) (e.g. Keranen and Klemper, 2008).

The Northern MER is characterized by two well developed fault systems: (1) a set of roughly NE–SW-trending boundary faults and (2) a set of roughly NNE–SSW-trending faults affecting the rift floor, usually referred to as (WFB) (Boccaletti et al., 1998; Acocella et al., 2003; Corti, 2009). This sector is the merger of the southern Afar marginal faults and the MER border faults, which have formed since 10–11 Ma (Wolfenden et al., 2004). Furthermore, the NMER is bounded by the Arboye and Sire boundary faults in the southeastern and by the Ankobor and Boru-Tura structural high in the Northwest side and whose trend is N40°E (Wolfenden et al., 2004). The boundary faults are generally long, widely spaced and characterized by large vertical offset and are interpreted to have accommodated the tectonic deformation during the initial stages of rifting (Hayward and Ebinger, 1996; Boccaletti et al., 1998). On the basis of seismicity (Keir et al., 2006) and local geological data (Wolfenden et al., 2004) the boundary fault set is thought to have been deactivated and mostly eroded in the northern MER. The WFB is a tectono-volcanic system characterized by short, closely spaced, active faults that exhibit minor vertical throw, which developed essentially in the last 2 my [e.g., Boccaletti et al., 1999; Ebinger and Casey, 2001]. The WFB structures form clearly defined right-stepping en echelon segments obliquely cutting the rift floor (Boccaletti et al., 1999. The work by (Keranen and

Klemper, 2008) show that the NMER has the lowest elevation and consequently thin crust compared to the CMER. The crust progressively thins towards the southern Afar from 33–35 km adjacent to the CMER to ~26 km near the AAZ (Keranen and Klemper, 2008). Apparent and abrupt change in physiography and crustal properties is observed at the junction between the central and northern rift segments.

The rift floor of the MER is affected by widespread deformation related to faulting along the WFB formed at 2 Ma (Bonini et al., 2005; Kurz et al., 2007). It is oblique to the direction of main rift margins forming 'S' shaped curvature resulting in sigmoidal geometry (Corti, 2009). N-S trending Kenyan rift gives rise to the development of SMER at about 20-21 Ma and lasted up to 11 Ma in which the northward spread of the Kenyan rift is hindered by Goba Bonga transverse lineament (Wolfenden et al., 2004; Bonini et al., 2005). Accordingly, this propagation is due to the combined effect of mantle plume movement and the existence of pre-existing structures (Bonini et al., 2005). In addition, southward migration of deformation from Afar (Bonini et al., 2005) is evident from the existence and re-activation of pre-existing tectono-magmatic structures in southern Afar at around 10-11Ma (Wolfenden et al., 2004).

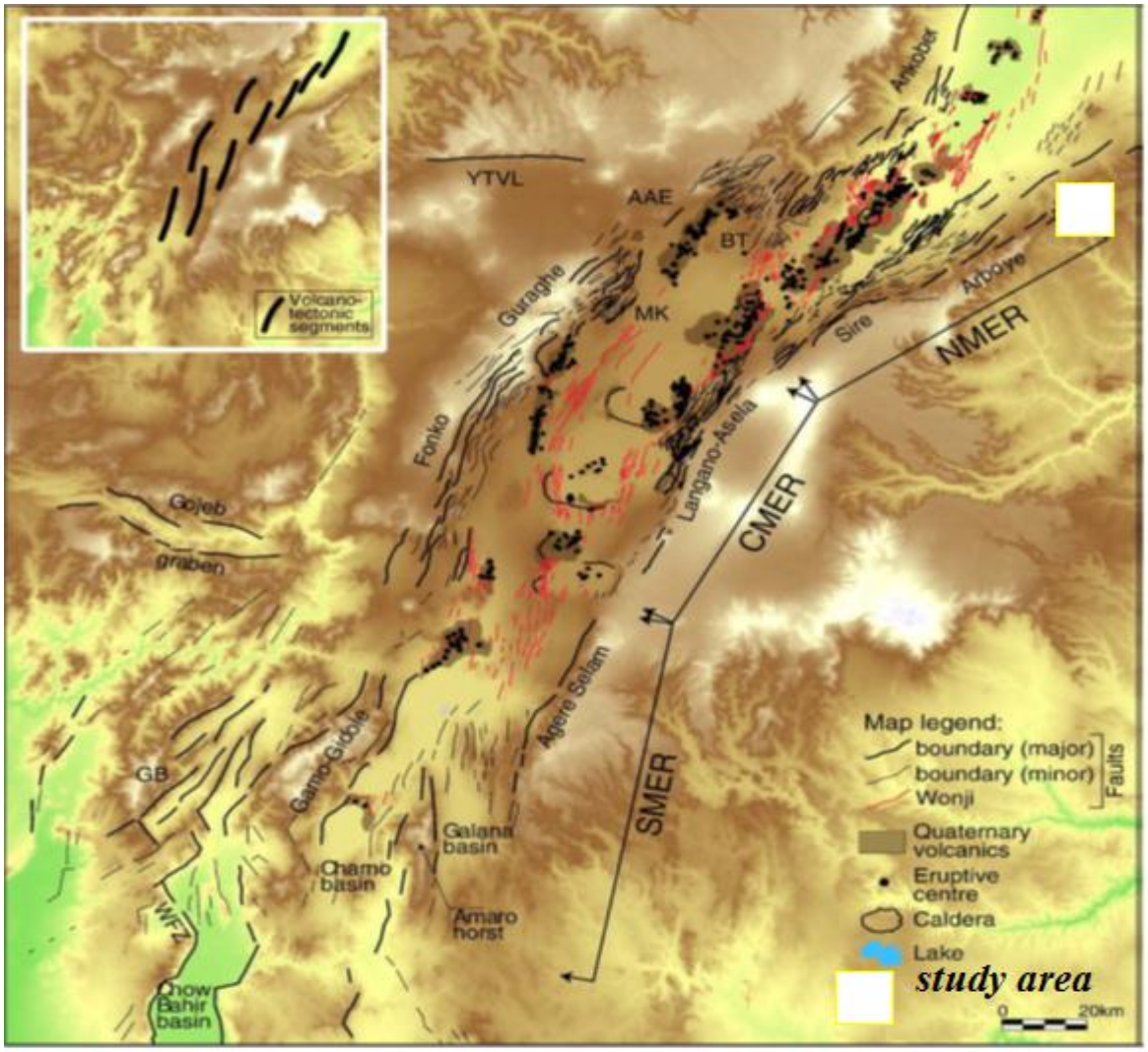


**Fig. 2.3**:Tectonic sketch map of the Main Ethiopian rift (from Corti, 2009). Inset shows the en-echelon, right-stepping arrangement of the volcano-tectonic segments of the WFB. AAE: Addis Ababa Embayment; BT: Boru Toru structural high; MK: Midre Kebd structural high; WFZ: Woito fault zone; YTVL: Yerer–Tullu Wellel volcano-tectonic lineament. The black lines are major and minor boundary faults whereas the red lines are Wonji faults.

# CHAPTER THREE

# 3. GEOLOGY OF DEBRE SAHIL/ GUNA AREA

## 3.1.Introduction

The Debre Sahil area is a part of the southeastern Ethiopian volcanic province that is dominated by bimodal basalt-rhyolite rock units (Fig.3.1). Basaltic rocks are exposed in the western, northeastern, central and southeastern part of the study area, whereas the felsic rock units are exposed in the northern, southern and southeastern part of the study area. The maximum thickness of these units is exposed by NE -SW tending major fault and river cut exposure. The orientation of this fault is N032$^{o}$E and dipping towards NW direction. The study area has different types of rock units which are differentiated by their lithological and textural description, and degree of weathering. Based on the stratigraphy succession the major rock units recognized from the youngest to the oldest are: upper basalt, lower basalt, rhyolitic ignimbrite, white rhyolite and glassy rhyolite. Moreover, based on their textures, color, hardness at outcrop scale, the silicic rock unit in the study area are classified into three groups. These are glassy rhyolite, white rhyolite and highly welded rhyolitic ignimbrite. However, on the geological map, they are mapped together as rhyolite rock units (Fig. 3.1) this is due to their similarity in petrographic analysis and geochemistry. But on the litho-stratigraphic section they are described separately (Fig.3.3).

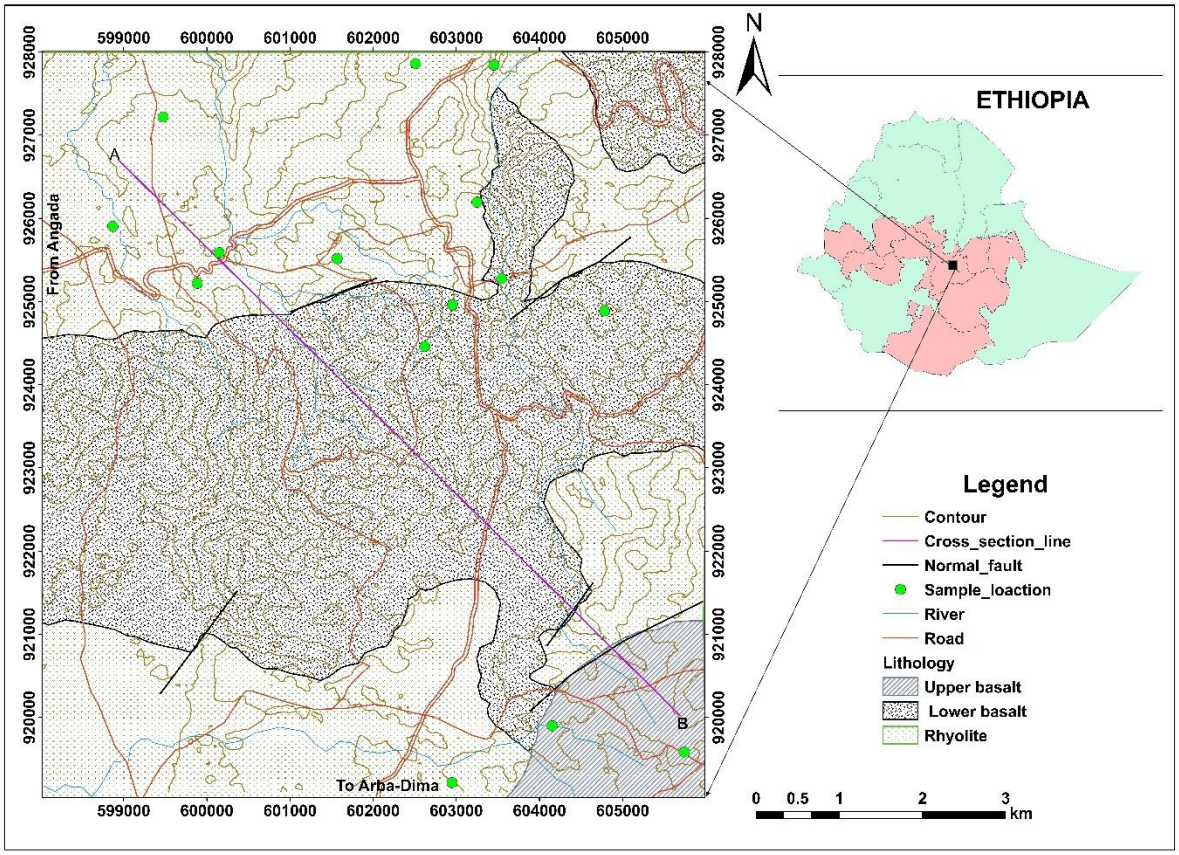


**Fig. 3.1 A.** Geological map of the study area with representative samples location

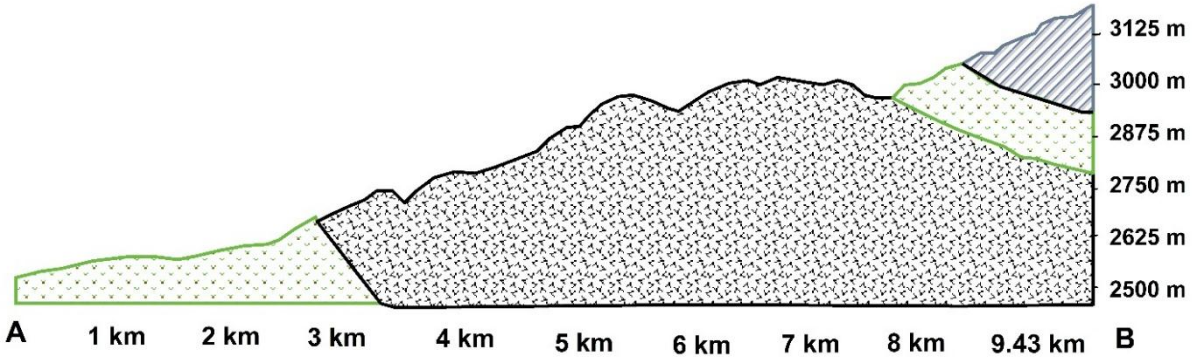


**Fig. 3.1 B.** Geological cross-section of the study area

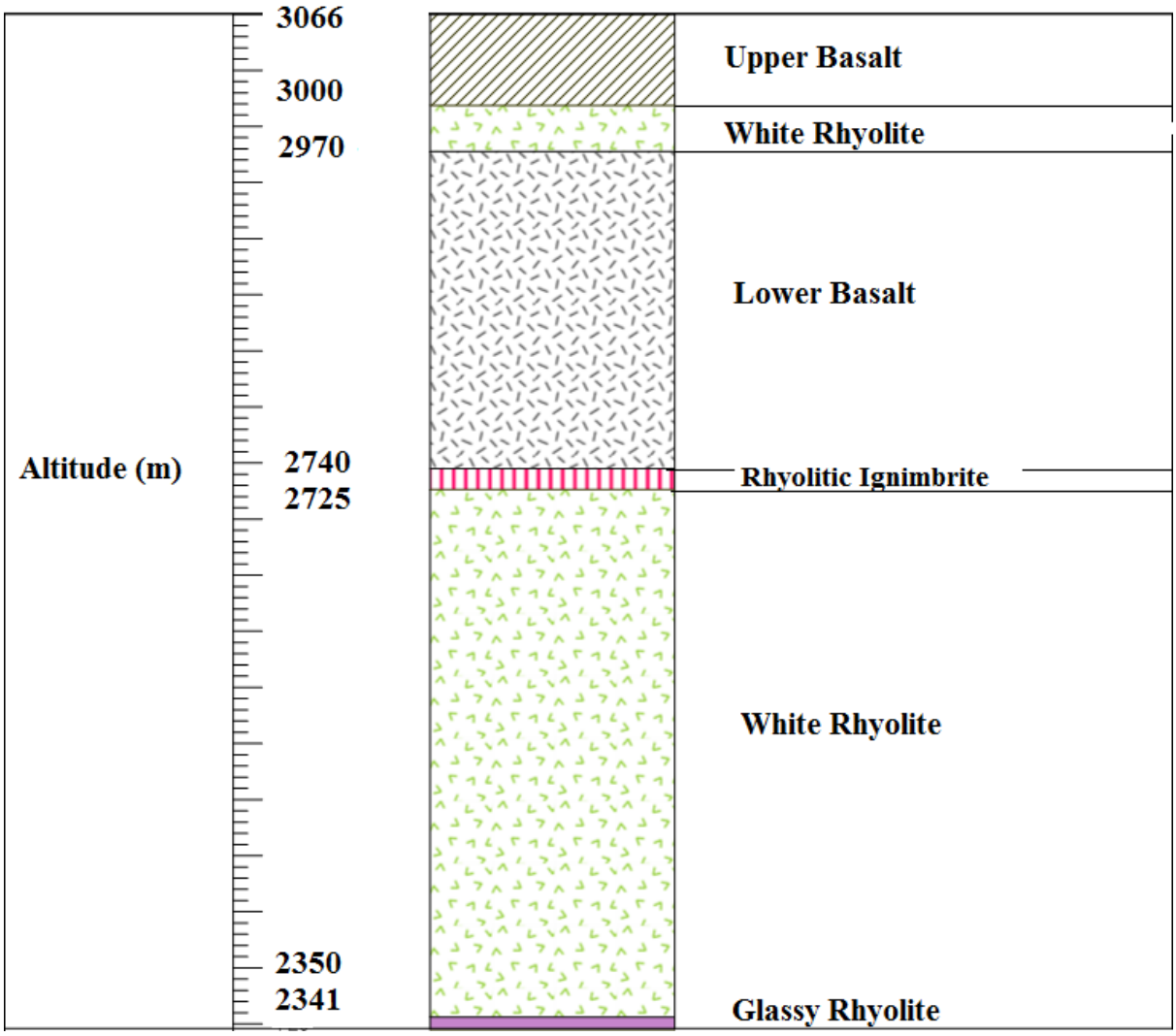


**Fig. 3.2**. Lithostratigraphic section of the study area

## 3.2. Lithology and petrography of the study area

### 3.2.1. Glassy Rhyolite

Glassy rhyolite unit is one of the lithological units found in the study area which is not mappable; that means the rock unit area coverage is below the scale of the geological map (1:25,000). Stratigraphically, it is overlain by white rhyolite rock unit. The glassy rhyolite is exposed on the northern part of the study area at location *(0602509E: 0927861N)* and elevation 2340 m above sea level. It is characterized by big phenocrysts of plagioclase feldspar and alkali feldspar within a glassy matrix. Minor quartz and rock fragments are visible both in hand specimen as well as in thin section. One thin section is prepared from this unit and the petrographic analysis show that porphyritic texture with phenocrysts range of <1mm to 8mm big, euhedral to subhedral, preferred and elongated orientation of plagioclase and rock fragments. The modal composition of the glassy rhyolite contains 35-40 % of phenocrysts. These phenocrysts are (15-20) % plagioclase, (8-10) % alkali feldspar, 5 % rock fragments, 3 % quartz and 2%) of opaque. However, plagioclase and alkali feldspar with a characteristic of flat to elongated crystal shape are the dominant phenocrysts. The other 60-65 % modal proportion is covered by glassy groundmass. In addition, the optically uniform plagioclase-feldspar phenocrysts themselves contain crystals of quartz, and minor accessory minerals forming poikilitic texture. Furthermore, the presence of inclusions in the phenocrysts with different characteristics suggest that they are older and included at depth prior to the crystallization of plagioclase during the way of the magma to the surface.

**Fig. 3.3**. Photograph of glassy rhyolite outcrop taken from the field at location (0602509 E:0927861N.

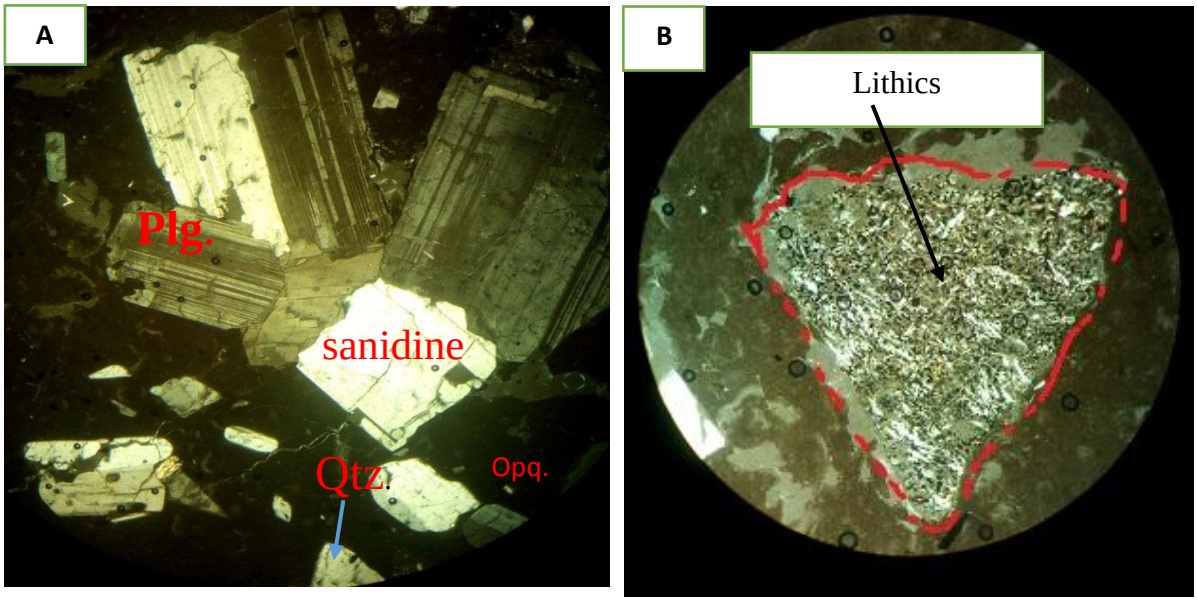


**Fig. 3.4.** Microphoto-picture of glassy rhyolite sample # T6S1, location (0602509 E:0927861N) under optical microscope in XPL view. The labels stand for; Plg- plagioclase, Qtz-Quartz and Opq-Fe-Ti oxides. The photo is taken at 10X magnification.

### 3.2.2. White Rhyolite

From the major lithological units, white rhyolite is the main unit with a maximum thickness relative to the other rock succession in the study area. The maximum thickness of this unit reaches 376 m along Sorbayi river cut exposure in northern part of the study area. This units are mostly exposed on the northern, southern and northeastern part of the study area which is characterized by white color, fine to medium grained texture and the weathered part has brownish color. In addition to these, columnar structures are also observed on the upper part of rhyolite. Mostly, the columnar joint structures show vertical fractures in multi-direction. The strike of fractures ranges between $N50^0$-$60^0$ E. This unit covers approximately around (40-45%) total study area.

From different location five samples (T1S2, T1S3, T1S4, T3S3 and T6S2) were collected and prepared for thin section study. The petrographic analysis of this rock unit shows a porphyritic texture with volumetric proportion 40 % of phenocrysts (Fig.3.7). The phenocrysts are 10-15% sanidine, 5-10% plagioclase, 5-8% quartz, 5% rock fragments and 3 % Fe-Ti oxides. The maximum grain lengths of each phenocryst are 0.3 mm Fe-Ti oxides, 4 mm sanidine, 6 mm plagioclase feldspar, 0.64 mm quartz and 0.8 mm rock fragments. The grain shape of each phenocryst shows anhedral (quartz, Fe-Ti oxides and rock fragments) and subhedral to euhedral (sanidine and plagioclase). The groundmass takes the maximum modal proportion of (65%), which is composed of microcrystalline quartz, alkali feldspar, lithic fragments and reddish stains (that might be clay minerals from hydrothermal alteration). The plagioclase shows polysynthetic twinning. On sample code T1S4, the rock shows radiate texture (Fig.3.7b). This radiate texture is formed by the overgrowth of alkali feldspar on existing phenocrysts. The phenocrysts in the radiate microstructure is dominantly alkali feldspars and quartz. Although Sample T3S3 shows sieve texture.

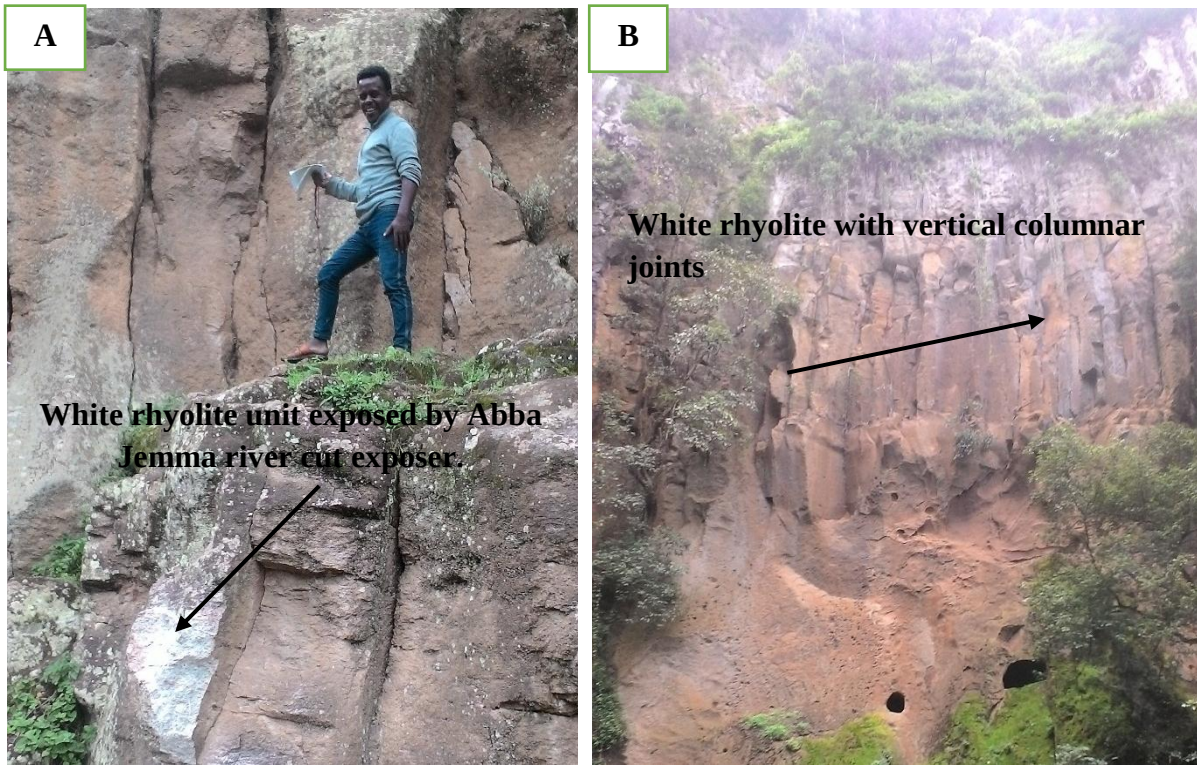


**Fig.3.5.** Photograph of representative white rhyolitic out crop taken from the field, (**A**) at (0600328 E & 0925905 N) and **(B**) This unit is exposed by Sorbayi river cut exposure and characterized by relatively having the maximum thickness among the lithologies found in the study area. In addition, it shows vertical columnar joints (0603451E:0927843N).

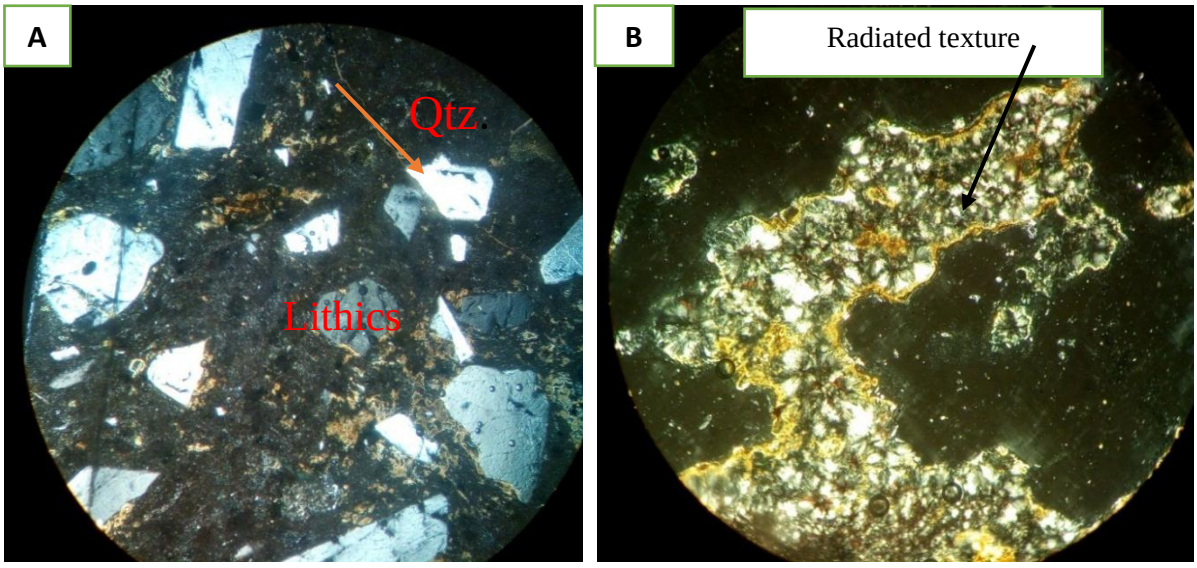

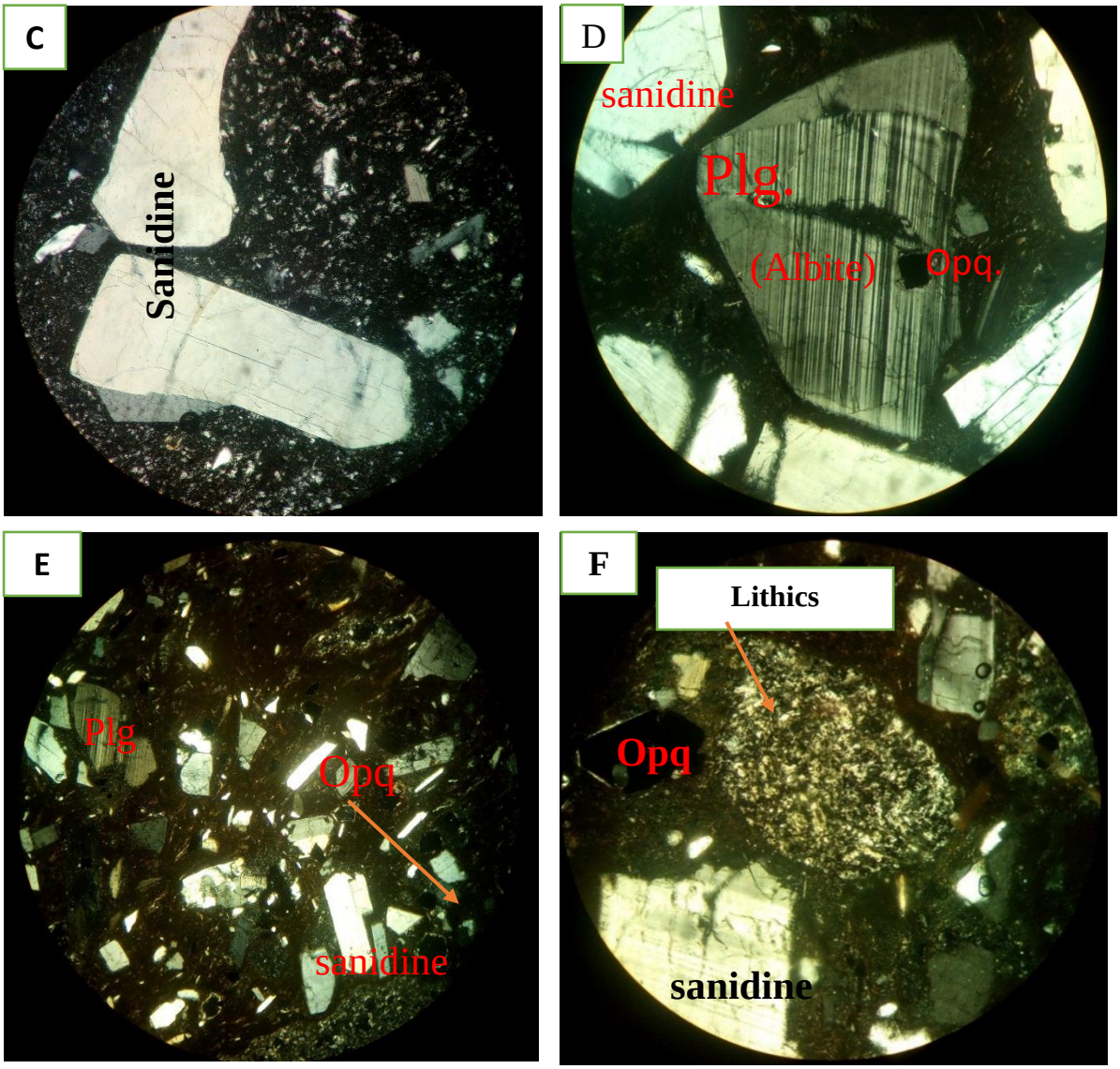


**Fig. 3.6**. Microscopic photo- picture of rhyolite lava samples; T1S4 (**A**), T1S3 (B), T1S2 (C), T3S3 (**D & E**) and T6S2 (F) under optical microscope in cross polarized light (XPL) view. (**A**&**C**) The labels stand for; Qtz-Quartz, Plg- Plagioclase feldspar and Opq-Fe-Ti oxides. All photos are taken at 10x magnification except photo (C), which is taken at 4x magnification.

Sample # T3S3 in XPL (**D & E**), in 10x and 4x magnification respectively, location (0602946 E, 0919214 N). This rock unit exhibit porphyritic texture i.e. relatively larger grains of sanidine and plagioclase are set in a cryptocrystalline groundmass. The plagioclase shows polysynthetic twining.

### 3.2.3. Rhyolitic Ignimbrite

This rock unit is exposed in the northwestern and western part of the study area. The rhyolitic ignimbrite unit is characterized by gray color, medium to coarse grained, massive & dense rock. The maximum thickness of this unit is around 15 meter which is exposed by Abajema river cut exposure. The quartz phenocrysts are shown at hand specimen level on this unit. Stratigraphically it is underlain by white rhyolite and overlain by lower basalt (olivine-pyroxene phyric basalt). This rock unit is mapped together with rhyolite because of the petrographic and geochemical data analysis indicate that they are similar in chemical composition and mineralogical composition with rhyolite, only differing in color, hardness and texture from rhyolite. Three samples (T4S1, T4S3 and T5S1) are collected from different location and prepared for petrographic examination. The petrographic study of this unit shows porphyritic texture in which sanidine and quartz phenocrysts are set in glassy groundmass. Although, sample # T4S3 shows radiated texture. In addition, the phenocrysts are smaller in size than those in the glassy ignimbrite. Some minor reddish minerals in one sample indicate slight alteration due to weathering.


**Fig. 3.7.** Photograph of representative outcrop of rhyolitic ignimbrite. **(A)** rhyolitic- ignimbrite with some geological structure (joints) (0601566 E :0925515 N) and elevation 2726 m a.s.l. (**B**) massive, fresh highly welded rhyolitic- ignimbrite rock unit exposed by Abajema river cut (0600643 E :0924997 N) and elevation 2735 m above sea level (a.s.l).

The modal composition of the welded rhyolitic- ignimbrite is 10-15% sanidine, 5-10% quartz, 5% opaque + rock fragments, and 70% is covered by glassy matrix groundmass. The grain shape of each phenocrysts exhibits anhedral to subhedral (sanidine) and anhedral (quartz and opaque (Fe-Ti oxide)). The size of the grains ranges from < 1mm to 3mm.

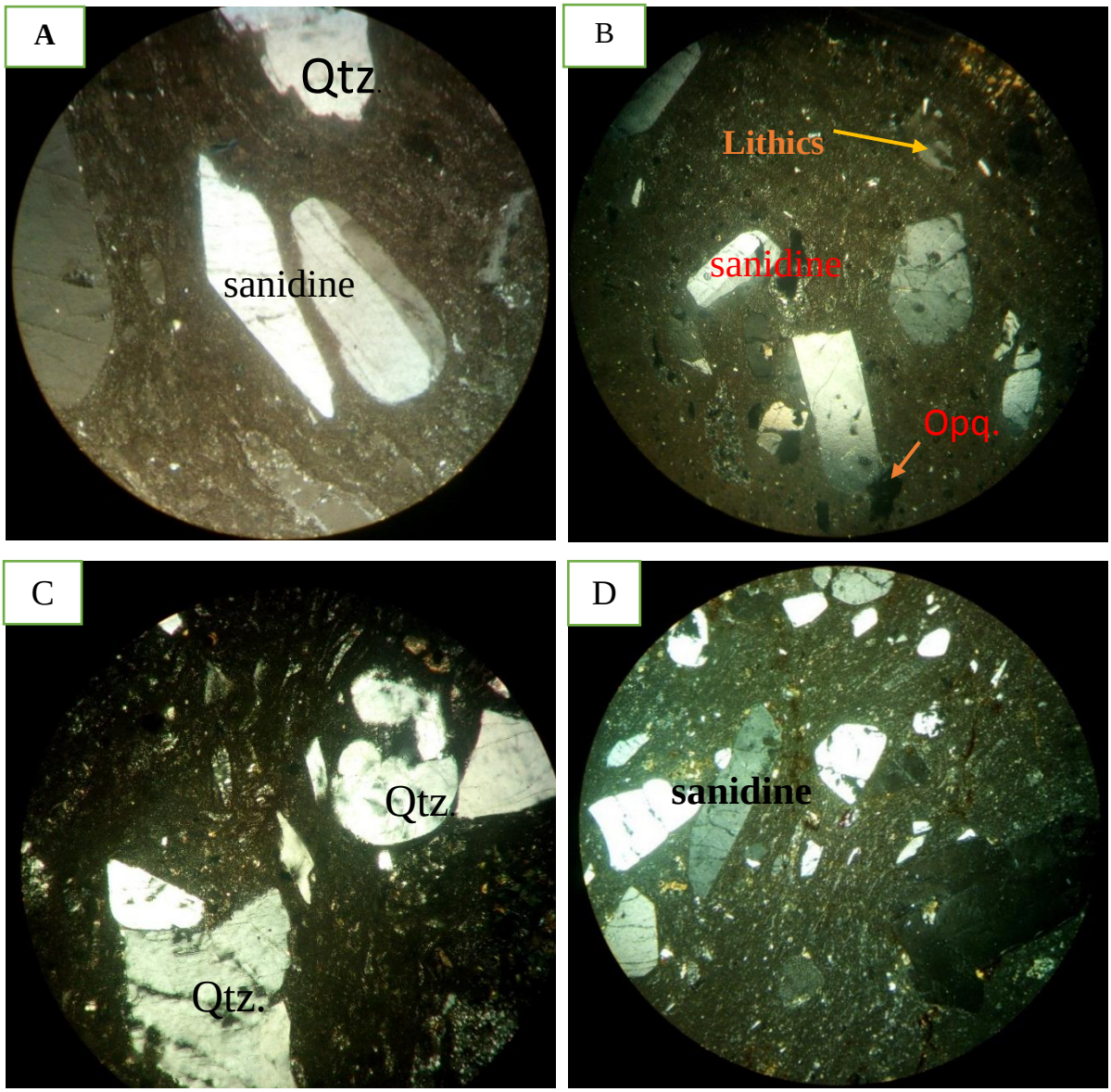


**Fig. 3.8.** Microphoto picture of welded rhyolitic ignimbrite sample, T4S1 (**A**), T4S3 (**B & D)** and T5S1 (**C**) in 10X magnification under XPL view. The labeles are phenocrysts of (Qtz-Quartz, Opq-Fe-Ti oxides), Lithics–Lithic fragment.

### 3.2.4. Lower Basalt

This rock unit is exposed on the western, central and eastern part of the study area. Stratigraphically the lower basalt is found above the rhyolitic ignimbrite. Most of these basalts are fine to medium grained, dark grey, massive and fresh basalts. It contains various phenocrysts of olivine and other crystal both at hand specimen scale and under thin section. In addition to these it is characterized by forming a gentle slope and steep topography along fault and river cut exposure. This unit has a maximum of around 230 meters estimated thickness. Some 45% of the total study area is covered by lower basalt (olivine- pyroxene phyric basalt) rock unit.


**Fig. 3.9.** Photograph of lower basalt out crop taken from the field at (0602625 E: 0924469 N).

From different localities four samples (T5S2, T5S3, T5S4 and T5S6) were collected and prepared for petrographic analysis. The Petrographic analysis of the representative samples indicates that these rocks are mainly composed of olivine, clinopyroxene and plagioclase minerals. The groundmass is dominated by microcrystalline plagioclase, clinopyroxene, olivine, and Fe-Ti oxides. The samples show a porphyritic texture (Fig.3.11) which is the grain size has a large variation. The modal composition of the lower basalt is 70% microcrystalline ground mass and 30 % phenocrysts. These phenocrysts are (10-12) % olivine, (8-10) % clinopyroxene, 5% opaque, <3% orthopyroxene together with minor elongated shape plagioclase crystals. The groundmass is composed microcrystalline of mainly plagioclase, olivine and Fe-Ti oxides.

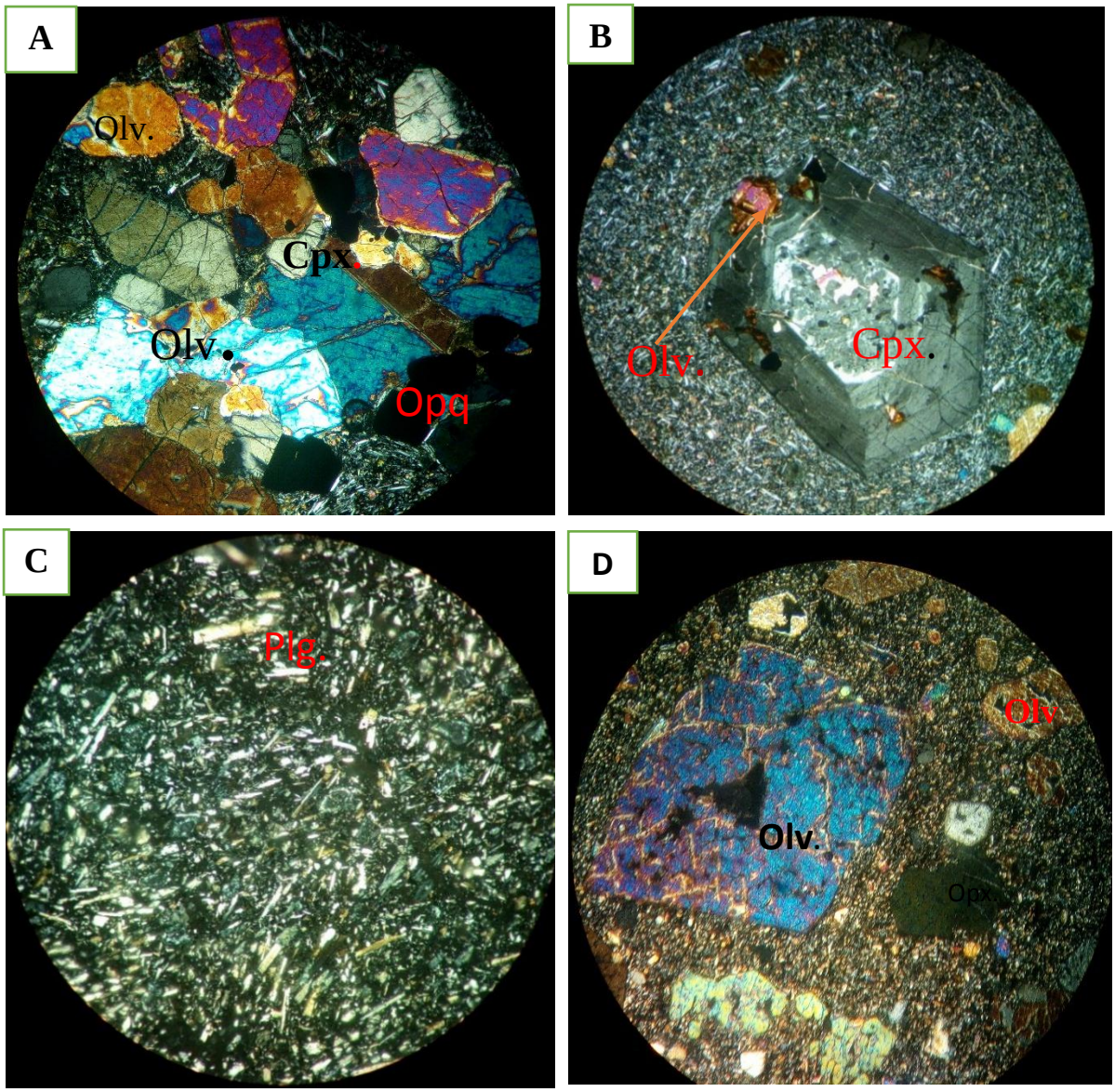


**Fig. 3.10**. Microphoto of lower basalt samples, T5S3 **(A),** T5S2 **(B),** T5S4 **(C)** and T5S6 **(D**) in XPL view at 10x magnification. The labels stand for (Olv- olivine, cpx-clinopyroxene, plg- plagioclase, opq- opaque or Ti-Fe oxide).

**(B)** Sample number T5S2 in XPL, 10 X magnifications, location (0602620 E: 0924461N). This rock unit exhibit porphyritic texture i.e. relatively well-developed shape of larger crystal of clinopyroxene are set in a fine-grained matrix of olivine, clinopyroxene and plagioclase. The clinopyroxene crystal shows zoning which indicates the fractional crystallization of early mineral phases from the magma. In addition, it shows poikilitic texture.

(**C**) Sample number T5S4 in XPL, 10x magnifications, location (0603543 E: 0925274 N). This rock unit show crystal phases dominated by plagioclase and opaque (Fe-Ti oxide) and micro porphyritic texture. In addition, it also shows plagioclase grains which are highly fractured and show skeletal structure; the crystal occupying the bulk has a complex interior form and alteration. The rock unit is composed of 35 % plagioclase and (5- 10) % opaque or Ti-Fe oxide.

The maximum dimension of each largest visible mineral grains is measured and the result shows; 1 mm Fe-Ti oxides, 8 mm clinopyroxene, 0.8 mm plagioclase feldspar and 3 mm olivine. The average grain shape is euhedral to subhedral (clinopyroxene & olivine) and elongated plagioclase feldspar and anhedral (Fe-Ti oxides).

### 3.2.5. Upper Basalt

This rock unit is exposed in southeastern part of the study area. The upper basalt (pyroxene-Olivine phyric basalts) are course grained and dark grey in color. It is mainly massive and hard rock. The pyroxene and olivine phenocrysts area visible at hand specimen scale. Moreover, different geological structures are observed on this unit. The orientation of the joints varies from $N25^0$-$35^0E$ and its dip from $50^0$-$60^0$ NW. The maximum thickness of this rock unit reaches 60m near to the Welargi Mountains southeastern part of the study area.

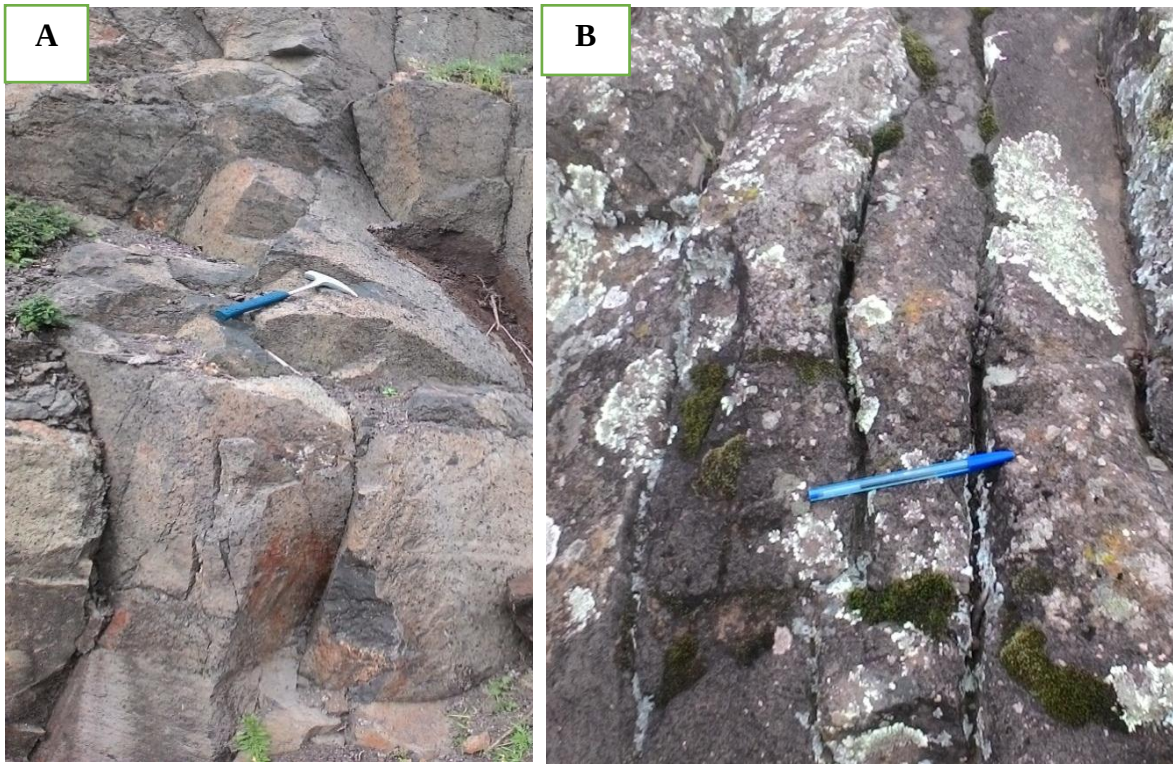


**Fig. 3.11**. Photograph of representative upper basalt (pyroxene-olivine phyric basalt) sample taken from the field at (0603431 E and 0922801 N). (**A**) and (**B**) show Parallel joints.

Two samples collected from lower basalt are prepared for petrographic analysis by considering their variation in mineralogy. The sample codes are T3S1 and T3S2. The analysis shows a seriate texture (Fig.3.13). This type of texture is a porphyritic texture in which the phenocrysts show a wide range of grain size. The Petrographic examination of T3S1 indicates that the phenocrysts is dominantly clinopyroxene with modal proportion of 30-35%, 9% olivine and 1% orthopyroxene (only observed on T3S1) and another sample T3S2 shows 30% clinopyroxene, 10% olivine and 10% Fe-Ti oxides. The maximum grain size along the longest

length of the phenocrysts is 5 mm clinopyroxene, 2 mm olivine, 0.1 mm Fe-Ti oxides and 0.14 mm orthopyroxene. Grain shape of the phenocrysts show euhedral to subhedral (olivine, clinopyroxene) and anhedral (orthopyroxene and Fe-Ti oxides).

In addition, the olivine phenocrysts exhibit alteration along fracture and the groundmass is dominated with microlites (the crystals are more visible but still extremely small) refers to the extent to which a magma has crystallized.

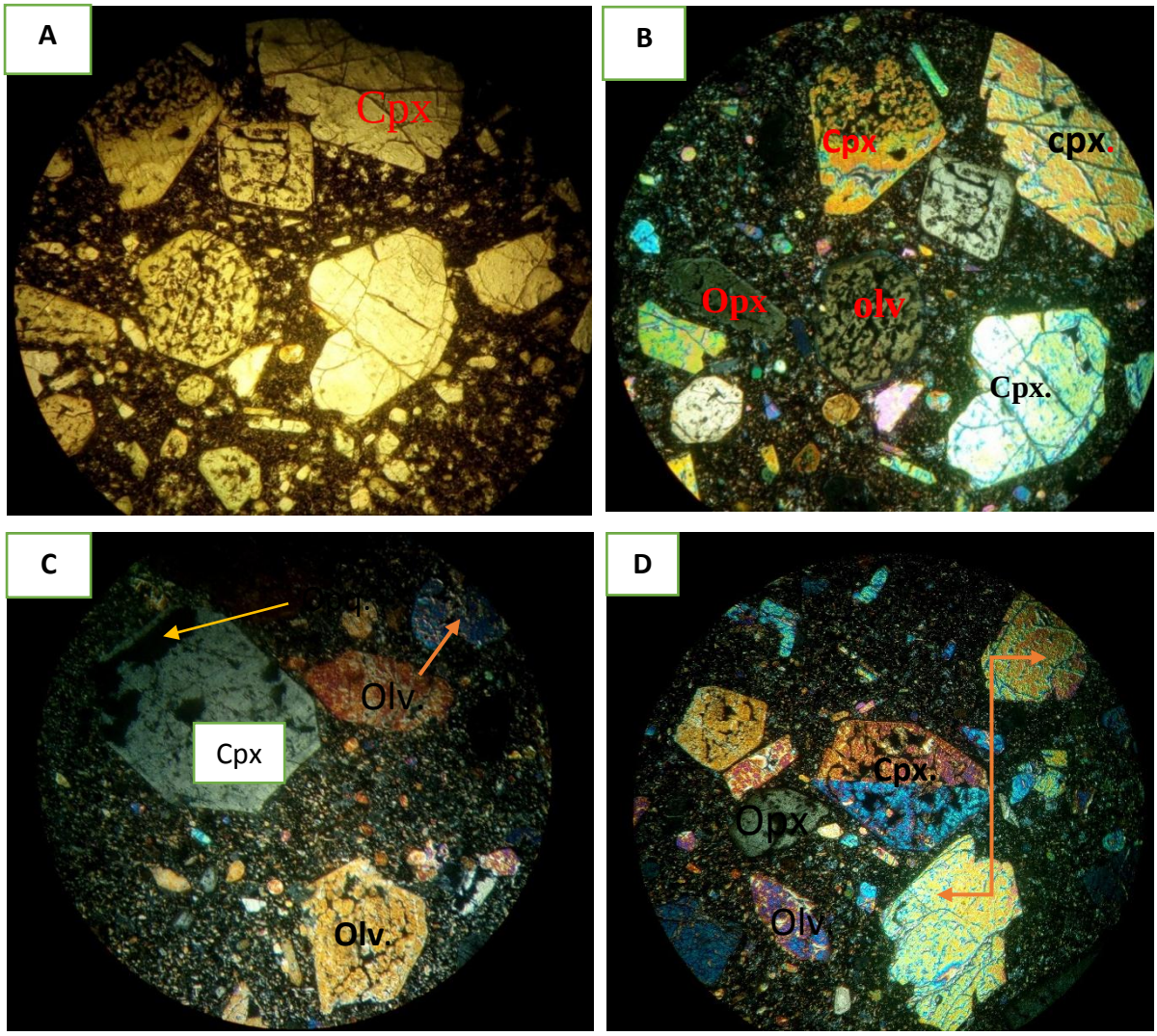


**Fig. 3.12**. Micro photo of pyroxene-olivine phyric basalt samples, T3S1 (A & B) in XPL and PPL view. T3S2 (C & D) in XPL view. The photos are taken at 4x magnification while they are porphyritic. The labels are phenocrysts of (Olv-olivine, opx- orthopyroxene, cpx- clinopyroxene, Opq- opaque or Ti-Fe oxide).

### 3.3.Summary of Petrographic description of the study area

The specimens collected from the Debre Sahil/Guna area can be described as massive, non-vesicular basalts with sparse, 1-3mm scale crystals of olivine and pyroxene and the rhyolite with quartz and some sanidine crystals.

In thin section, the basaltic rock samples collected from the Debre Sahil area exhibit crystal phases dominated by olivine, clinopyroxene, plagioclase and include lesser abundances of orthopyroxene with microcrystalline groundmass (Fig. 3.12 & 3.13). These crystal phases rarely display skeletal textures, and most appear to be in equilibrium with the groundmass (Fig.3.13). Some samples are observed to contain plagioclase laths within an aphanitic groundmass. In addition, some phenocrysts of clinopyroxene and plagioclase display a seriate texture. The clinopyroxene crystal shows zoning and poikilitic texture (Figure 3.11b). The presence of zonation indicates that the crystallization of early mineral phases. Moreover, Olivine and some clinopyroxene display alteration along rims and through fractures.

The overall petrographic analysis of the rhyolitic rock units displays crystal phases dominated by alkali feldspar (sanidine), plagioclase, quartz and lithic fragments with a cryptocrystalline groundmass. The plagioclase phenocrysts show multiple twinning and the crystal size ranges from<1 mm to 8 mm. Most of the sample shows porphyritic texture. In addition, some of the sanidine phenocrysts exhibits radiated texture and sieve texture.

**Table 3.1:** The description of minerals found in thin-sections.

| **Phenocrysts** | **Petrographic Descriptions** |
|---|---|
| Olivine | Euhedral to subhedral in shape and the size ranges from <1 mm to 3 mm along the maximum length and <1mm to 3 mm width. The groundmass shows micro porphyritic texture. The olivine phenocryst shows lesser alteration along fracture. In addition, it shows intergrowth texture with clinopyroxene. |
| Clinopyroxene | This mineral assemblage characterized by well-developed euhedral to subhedral hexagonal crystal shape and shows simple twinning. The size of the phenocrysts ranges from 1mm to 7mm. In addition, it shows zoning. |
| Orthopyroxene | Pale colored in thin section with subtle pinkish to greenish pleochroism. It has subhedral to anhedral shape. The size of the grains ranges from <1mm to 1.5mm. |
| Alkali feldspar (sanidine) | Light color, euhedarl to subhedral in shape, elongated and rectangular shaped crystals are also observed. Size ranges from<1mm to 8 mm along the maximum length and <1mm to 2mm width. Generally, the samples show minor sign of alteration along the margins and sparsely within the phenocrysts itself. In some cases, the cleavage direction is not clearly visible due to the composite effect of included lithic fragment and alteration effect. |
| Plagioclase | Light in color, shows multiple twinning, perfect cleavage, subhedral in shape, 5mm along the longest dimension and 2mm width, no fracture and shows oscillatory zoning. |
| Quartz | It is generally fine grained in size, unhedral in shape, showing light color and randomly oriented, served as pokioclast within the lithic fragments. |
| Rock fragments /Lithic fragments | These vary in shape and size with numerous included crystals of feldspar, quartz, minor sanidine and opaque. Theses crystals serve as pokiolites. It shows irregular to sub-rounded and occasionally elongated shape; no deformed lithics. It ranges from <1mm to 4 mm in size; with sign of alteration along the boundaries. |
| Volcanic glass | Volcanic glass is the matrix in which the large alkali feldspar grains, quartz, opaque minerals as well as minor constituents and lithic fragments are set. It shows flow banding structures elongated along one direction. It is devoid of pokioclasts. It is light color in PPL and dark under XPL. In addition, the directional arrangement of fiammes indicates post-eruptive welding effect during pyroclastic flow. |
| Opaque (Ti-Fe oxide) | Are minor constituent in the samples, <1mm to 1mm in length, some of them are anhedral in shape, and dark in both XPL and PPL. |

# CHAPTER FOUR

# 4. GEOCHEMISTRY

## 4.1. Introduction

Twelve (12) representative samples (7-rhyolite and 5- basalt rock) were selected for whole-rock geo-chemical analyses from Debre Sahil area. The analyzed samples are fresh and show no evidence of alteration. The sample preparation was taken place in Akaki Kaliti Kebele 10/11 block 03 milling room. Then, the samples were crushed to 70% less than 2mm, riffled to split off 1kg and the splits were pulverized to 75 microns. The pulverized samples were sent to the Australian Laboratory Science (ALS) to determine the concentration of major and trace elements.

Major element oxide abundances and loss on ignition (LOI) values were determined via Inductively Coupled Plasma Atomic emission spectrometry (ICP-AES) analysis in Ireland by Australian Laboratory Science. Trace elements were analyzed by Inductively Coupled Plasma Mass spectrometry 81 (ICP-MS) using lithium borate fusion, whereas base metals (Ag, Co, Cu, Ni, Pb, Sc and Zn) were determined by multi element four acid digestion 81 (ME-4ACD81). Further information on the procedure, precision, accuracy, and detection limits of ALS of ME-ICP06 and ME-MS81 analyses could be found at www.alsglobal.com. The sample locations are illustrated in Fig.3.1 and their assigned sample names and corresponding major element (wt %) and trace elements (ppm) values are listed in Table 4.1 and 4.2 respectively. In addition, the analyzed geochemical data have been integrated through different software packages such as Microsoft excel 2016 (xls) sample worksheet, Petrograph version 2beta and GCDKit 3.00 version. Petrograph version 2beta and GCDKit 3.00 version software packages are used to produce different geochemical variation diagram that help to understand mainly the magmatic evolution of the rock of area by depending on those representative geochemical samples.

## 4.2. Whole- Rock Geochemical Results

Whole-rock chemical analyses for the Debre Sahil volcanic rocks are presented in Table 4.1 and 4.2. The analyzed basalt and rhyolitic samples have< 4.2% lose on ignition (LOI). The LOI enrichment is usually occurred by post deposition alteration process (Peccerillo et al., 2003). The effect of the volatile enrichment is checked by comparing selected mobile and immobile elements trend by plotting them with LOI in binary diagram. The trend of mobile major element for example Na2O against LOI has negative correlation (Fig.4.2b). In contrast to this the immobile elements, for example Al2O3, plot with LOI show no variation in the samples (Fig.4.1a). Following these results, the data is recalculated, structured and presented on

volatile-free base. All diagrams, descriptions and interpretation are according to the recalculated volatile-free base results.

**Table 4.1:** Major element Geochemical analysis result and the CIPW norm of Debre Sahil bimodal basalt -rhyolite samples.

| | **Basalt** | | | | | **Rhyolite** | | | | | | |
|---|---|---|---|---|---|---|---|---|---|---|---|---|
| **Sample** | **T5S4** | **T3S2** | **T3S1** | **T5S2** | **T5S3** | **T6S2** | **T1S3** | **T1S2** | **T5S1** | **T4S1** | **T4S3** | **T1S4** |
| SiO2 | 41.2 | 43.7 | 43.9 | 46.4 | 46.4 | 72.7 | 73 | 73.5 | 73.7 | 74.4 | 74.7 | 74.7 |
| TiO2 | 2.77 | 1.76 | 1.77 | 1.73 | 1.75 | 0.65 | 0.4 | 0.65 | 0.41 | 0.35 | 0.35 | 0.35 |
| Al2O3 | 11.7 | 9.37 | 9.56 | 13.85 | 14.05 | 12.55 | 11.05 | 12.75 | 10.65 | 10.5 | 10.6 | 10.45 |
| FeOt | 13.81 | 10.89 | 10.98 | 12.33 | 12.46 | 3.34 | 4.75 | 3.29 | 5.07 | 4.40 | 4.30 | 4.5 |
| MnO | 0.22 | 0.17 | 0.18 | 0.2 | 0.21 | 0.19 | 0.1 | 0.14 | 0.15 | 0.09 | 0.06 | 0.13 |
| MgO | 7.39 | 14.15 | 14.2 | 6.27 | 6.25 | 0.38 | 0.22 | 0.12 | 0.2 | 0.15 | 0.16 | 0.14 |
| CaO | 13.2 | 12.7 | 12.75 | 9.89 | 10.25 | 0.28 | 0.31 | 0.14 | 0.32 | 0.28 | 0.29 | 0.29 |
| Na2O | 2.71 | 2.64 | 2.74 | 3.37 | 3.14 | 5.13 | 4.06 | 4.14 | 4.52 | 3.81 | 3.85 | 3.83 |
| K2O | 0.54 | 1.06 | 1.12 | 1.46 | 1.48 | 4.49 | 4.42 | 4.36 | 4.5 | 4.46 | 4.49 | 4.49 |
| P2O5 | 0.59 | 0.26 | 0.25 | 0.52 | 0.54 | 0.01 | 0.02 | 0.02 | 0.01 | 0.01 | 0.01 | 0.01 |
| LOI | 4.16 | 0.88 | 0.79 | 2.62 | 2.38 | 0.92 | 2.18 | 2.07 | 1.05 | 2.31 | 2.29 | 2.06 |
| **Total** | 99.83 | 98.79 | 99.46 | 100.01 | 100.3 | 101.01 | 101.04 | 101.55 | 101.14 | 101.25 | 101.58 | 101.45 |
| Mg# | 48.82 | 69.85 | 69.75 | 47.55 | 47.2 | 16.87 | 7.63 | 6.1 | 6.57 | 5.73 | 6.22 | 5.26 |
| CIPW norm | | | | | | | | | | | | |
| Q | 0 | 0 | 0 | 0 | 0 | 25.71 | 32.32 | 32.31 | 31.51 | 35.36 | 35.29 | 35.57 |
| Or | 3.19 | 6.26 | 6.62 | 8.63 | 8.75 | 26.54 | 26.12 | 25.77 | 26.59 | 26.36 | 26.54 | 26.54 |
| Ab | 20.27 | 10.35 | 9.58 | 28.53 | 26.57 | 39.55 | 32.23 | 35.03 | 29.73 | 29.18 | 29.52 | 28.75 |
| An | 18.17 | 10.59 | 10.48 | 18.35 | 19.87 | 0 | 0 | 0.564 | 0 | 0 | 0 | 0 |
| Ne | 1.44 | 6.49 | 7.37 | 0 | 0 | 0 | 0 | 0 | 0 | 0 | 0 | 0 |
| Ac | 0 | 0 | 0 | 0 | 0 | 3.40 | 1.87 | 0 | 7.51 | 2.70 | 2.69 | 3.22 |
| Di | 26.99 | 35.23 | 35.56 | 17.18 | 17.27 | 0 | 0.32 | 0 | 0.53 | 0.36 | 0.303 | 0.517 |
| Hy | 0 | 0 | 0 | 1.09 | 3.03 | 0.95 | 0.40 | 0.3 | 0.25 | 0.21 | 0.26 | 0.109 |
| Ol | 4.129 | 13.25 | 13.24 | 4.60 | 3.18 | 0 | 0 | 0 | 0 | 0 | 0 | 0 |
| Il | 0.471 | 0.36 | 0.39 | 0.43 | 0.449 | 0.41 | 0.21 | 0.29 | 0.32 | 0.19 | 0.128 | 0.278 |
| Hm | 13.81 | 10.89 | 10.98 | 12.33 | 12.46 | 2.164 | 4.103 | 3.293 | 2.471 | 3.467 | 3.37 | 3.39 |
| Tn | 0 | 0 | 0 | 3.69 | 3.72 | 0.933 | 0.706 | 0 | 0.592 | 0.61 | 0.69 | 0.5 |
| Pf | 4.29 | 2.67 | 2.67 | 0 | 0 | 0 | 0 | 0 | 0 | 0 | 0 | 0 |
| Ru | 0 | 0 | 0 | 0 | 0 | 0.056 | 0 | 0.493 | 0 | 0 | 0 | 0 |
| Ap | 1.41 | 0.616 | 0.59 | 1.23 | 1.28 | 0.024 | 0.047 | 0.047 | 0.024 | 0.024 | 0.024 | 0.024 |
| Total | 94.17 | 96.71 | 97.46 | 96.05 | 96.56 | 99.721 | 98.33 | 99.12 | 99.53 | 98.45 | 98.81 | 98.89 |

Normative minerals: Ab = albite; Ac = acmite; An = anorthite; Ap = apatite Di = diopside; Hy = hypersthene; Ol = olivine; Or = orthoclase Q = quartz; Ne = nepheline; Il = ilmenite; Hm = hematite; Pf = perovskite; Ru = rutile; Tn = titanite

**Table 4.2:** Whole rock trace element geochemical data for Debre Sahil volcanic rocks.

| | **Basalt** | | | | | **Rhyolite** | | | | | | |
|---|---|---|---|---|---|---|---|---|---|---|---|---|
| **Sample** | **T5S4** | **T3S2** | **T3S1** | **T5S2** | **T5S3** | **T6S2** | **T1S3** | **T1S2** | **T5S1** | **T4S1** | **T4S3** | **T1S4** |
| Ppm | | | | | | | | | | | | |
| Sc | 33 | 35 | 36 | 25 | 24 | 6 | 3 | 6 | 3 | 2 | 2 | 2 |
| V | 420 | 277 | 264 | 298 | 317 | 22 | 11 | 14 | 14 | 6 | 6 | 9 |
| Cr | 50 | 1260 | 1220 | 70 | 70 | <10 | <10 | <10 | <10 | <10 | <10 | 10 |
| Co | 55 | 63 | 64 | 51 | 51 | <1 | <1 | <1 | <1 | <1 | <1 | <1 |
| Ni | 62 | 293 | 290 | 51 | 50 | 1 | 9 | <1 | 3 | 16 | 11 | 12 |
| Cu | 357 | 153 | 152 | 180 | 180 | 2 | 1 | <1 | 2 | 1 | 1 | <1 |
| Zn | 111 | 86 | 82 | 117 | 116 | 214 | 160 | 168 | 200 | 211 | 208 | 219 |
| Ga | 18.8 | 12.4 | 13 | 20 | 20.5 | 30.8 | 32.8 | 31.5 | 33.1 | 34.2 | 32.4 | 34.5 |
| Rb | 40.2 | 21.1 | 23.9 | 30.8 | 28.3 | 128 | 112.5 | 121 | 121 | 113 | 111 | 121.5 |
| Sr | 416 | 367 | 379 | 695 | 757 | 24.1 | 14.9 | 12 | 12.5 | 12.7 | 13.4 | 13.2 |
| Y | 23.6 | 15.5 | 16.2 | 24.4 | 24.5 | 86 | 54.8 | 147.5 | 101 | 26.7 | 24.3 | 34.8 |
| Zr | 174 | 104 | 112 | 167 | 170 | 1270 | 791 | 1360 | 989 | 927 | 887 | 965 |
| Nb | 38.3 | 27.6 | 29.7 | 25.7 | 26.4 | 143 | 87 | 153.5 | 98.4 | 95.5 | 93.1 | 98.5 |
| Cs | 0.86 | 0.16 | 0.19 | 0.27 | 0.24 | 0.62 | 0.7 | 0.51 | 0.5 | 0.34 | 0.3 | 0.48 |
| Ba | 476 | 298 | 305 | 559 | 572 | 346 | 115.5 | 254 | 95.4 | 77.9 | 52.5 | 90.3 |
| La | 31.9 | 22.5 | 23 | 24.8 | 25.3 | 103.5 | 76.1 | 96.6 | 83.2 | 62 | 53.8 | 55 |
| Ce | 63 | 43.3 | 44.4 | 49.4 | 50.4 | 248 | 113.5 | 110.5 | 76.7 | 117.5 | 60.9 | 193 |
| Pr | 7.57 | 4.91 | 5.38 | 5.98 | 5.94 | 25.4 | 19.25 | 28.2 | 22.3 | 16.65 | 14.3 | 16.1 |
| Nd | 31.9 | 20 | 21.4 | 24.4 | 25.2 | 95.9 | 70.5 | 108.5 | 87.1 | 60.4 | 52.7 | 59.8 |
| Sm | 6.28 | 4.11 | 4.12 | 4.89 | 5.31 | 18.65 | 14.25 | 23.1 | 17.85 | 11.9 | 10.1 | 13.05 |
| Eu | 2.15 | 1.41 | 1.31 | 1.75 | 1.69 | 4.28 | 1.41 | 6.03 | 1.57 | 0.98 | 0.89 | 1.03 |
| Gd | 6.11 | 3.98 | 4.01 | 5.1 | 5.02 | 16 | 12.1 | 22.9 | 17.7 | 9.27 | 7.68 | 9.87 |
| Tb | 0.85 | 0.57 | 0.6 | 0.72 | 0.77 | 2.6 | 2.06 | 3.97 | 3.03 | 1.43 | 1.16 | 1.58 |
| Dy | 4.8 | 3.51 | 3.53 | 4.7 | 4.98 | 16.55 | 12.45 | 28.2 | 19.1 | 7.74 | 7.08 | 10 |
| Ho | 0.94 | 0.62 | 0.59 | 0.92 | 0.9 | 3.2 | 2.43 | 5.37 | 3.96 | 1.38 | 1.18 | 1.75 |
| Er | 2.17 | 1.53 | 1.53 | 2.38 | 2.28 | 9.36 | 7.18 | 15.75 | 11.65 | 4 | 3.41 | 5.08 |
| Tm | 0.28 | 0.19 | 0.24 | 0.31 | 0.35 | 1.42 | 1.09 | 2.14 | 1.84 | 0.64 | 0.6 | 0.79 |
| Yb | 0.28 | 1.25 | 1.3 | 2.06 | 2.17 | 9.69 | 8.02 | 13.35 | 12.35 | 4.82 | 4.12 | 5.99 |
| Lu | 0.26 | 0.17 | 0.17 | 0.29 | 0.32 | 1.51 | 1.2 | 2.12 | 1.9 | 0.66 | 0.58 | 0.86 |
| Hf | 5.1 | 2.6 | 2.9 | 4.1 | 4.2 | 29 | 20.4 | 30.7 | 24.5 | 23.3 | 21.5 | 22.8 |
| Ta | 2.4 | 1.3 | 1.5 | 1.3 | 1.4 | 9 | 5.3 | 9.9 | 6.2 | 6 | 5.5 | 5.9 |
| Pb | 13 | 5 | 10 | 8 | 11 | 25 | 22 | 25 | 15 | 22 | 17 | 22 |
| Th | 2.81 | 2.37 | 2.39 | 1.92 | 1.9 | 17.35 | 11.8 | 19.15 | 13.35 | 13.25 | 12.45 | 13.1 |
| U | 0.41 | 0.42 | 0.47 | 0.37 | 0.41 | 2.97 | 0.64 | 4.11 | 1.81 | 0.84 | 0.89 | 0.78 |

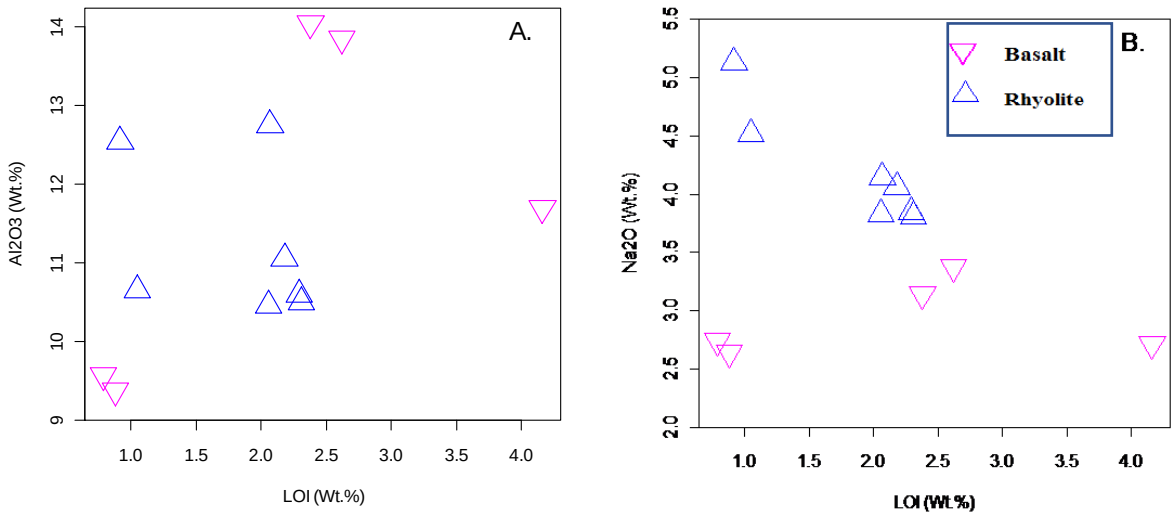


**Fig. 4.1.** Graphs of Al2O3 and Na2O with LOI that show the variation of mobile and immobile major element.

There is a negative correlation between Na2O and LOI for silicic rocks, which suggests that the loss of sodium was accompanied by an increase in volatiles, mostly water.

### 4.2.1. Geochemical classification

On the basis of the Total Alkali Silica (TAS) classification diagram (Le Bas et al., 1986), the samples from the Debre Sahil area plot in the field of tephrite basanite, basalt and rhyolite (Fig.4.2). The distribution of the samples is mainly fall on felsic boundary with silica (SiO2) above 72 wt. % and mafic with silica range of 45 to 50 wt. %. All felsic samples are rhyolitic in composition. From the mafic samples only one sample fall on tephrite basanite range and another two samples straddle on the boundary line between tephrite basanite and basalt, while the other are basaltic in composition. It is observed that the volcanic products define bimodal basalt-rhyolite distribution with a distinct lack of intermediate compositions. There is a noticeable lack of samples with $SiO_2$ content between 47 wt. % to 72 wt. % (Table 4. 1) (Fig. 4.2). This lack of samples is described in many locations in the EARS and is known in the literature as the Daly Gap (Trua et al., 1999; Peccerillo, 2003; Rooney et al., 2012). This gap has been interpreted as a function of differential tapping of magma chambers at depth (Peccerillo et al., 2007), and more recently as the result of a magma mush where more silicic material has evolved and was removed from a magma chamber after partial crystallization to fractionate at shallower levels (Trua et al., 1999; Rooney et al., 2012).

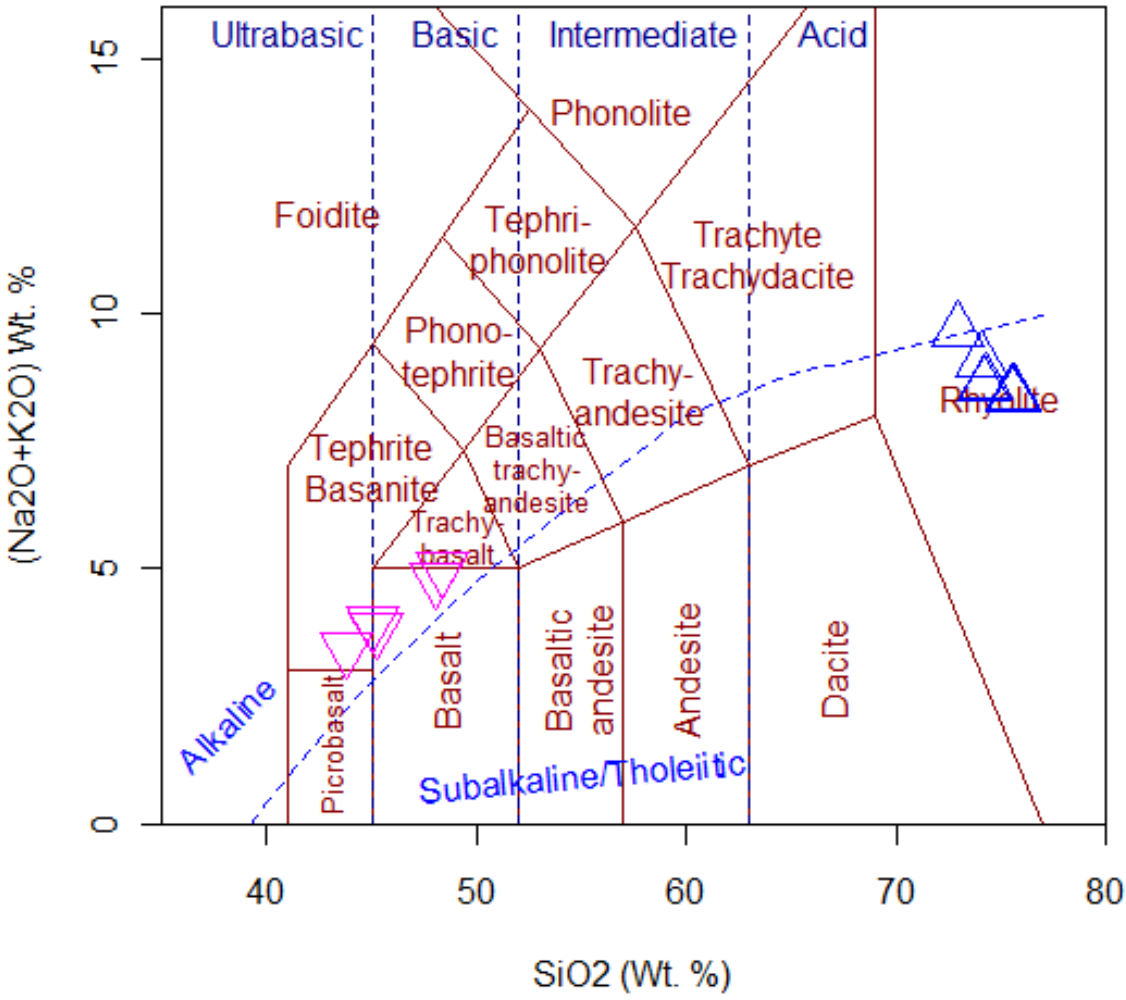


**Fig. 4.2.** Total alkalis vs. silica (TAS, Le Bas et al., 1986) diagram for Debre Sahil lavas showing an alkaline composition for basalt and sub alkaline/ tholeiitic for rhyolite. Alkaline/tholeiitic boundary is after Irvine and Baragar (1971).

### 4.2.2. Major element geochemistry

The major element analytical data of the twelve samples collected from the study area is used in oxide and CIPW norm form. The analyzed data readjusted to volatile free bases to use for the interpretation and to draw the graphs. The volatile free base is calculated by normalizing the major element concentration value to 100% by subtracting the volatile concentration (that is presented as LOI). ICP-AES gives Fe concentration in form of Fe2O3. From the volatile free base FeO is calculated by multiplying Fe2O3 by 0.8998. Then FeOt calculated by the mathematical formula; FeOt=FeO+Fe2O3 (Rollinson, 1993).

The CIPW norm calculation is a method of working out the mineralogy of a rock from a chemical analysis. Because the mineralogy of the norm is entirely dependent on chemistry, a texture, finally it gives a different mineralogical percentage distribution compare to the modal

proportion result from the petrographic analysis. The volatile free base geochemical data and the CIPW norm calculation results are presented in Table 4.1. The CIPW norms of mafic rocks range from nepheline -normative (maximum nepheline = 7.37 wt%) through hy-normative (maximum hypersthene = 3.026 wt%) and no quartz-normative. Based on this the three samples (T5S4, T3S1 & T3S2) are grouped in silica-undersaturated basalt (alkali basalt) which is characterized by the presence of normative olivine and nepheline whereas, the other two samples (T5S2 &T5S3) are silica saturated basalts (olivine tholeiites) which is characterized by normative hypersthene and olivine. The rhyolite rocks are rich in normative quartz (25.707–35.57 Wt.%) and acmite (1.874– 3.396 Wt%) (Table 4.1). The rhyolites show a peralkaline affinity which is reflected by the presence of normative acmite ($NaFe^{+3}Si_2O_6$). However, one sample (T1S2) do not have normative acmite.

The analyzed samples show large variations in $SiO_2$ and MgO, varying from 41.2 to 74.7 wt.% and 0.12 to 14.2 wt.%, respectively. The MgO contents of mafic series ranges from 6.25 to 14.2 wt.%. and Mg# value (Mg# = 100(MgO/40.32)/((MgO/40.32)+(FeO/71.85)) (Wager and Deer, 1939) between 47.2 and 69.85. Two alkali basalts (samples T3S1 and T3S2) have relatively high MgO contents (14.15–14.2 wt.%) and Mg # values (69.75–69.85), and are inferred to have undergone only limited fractionation. Moreover, the other three mafic samples displays concentrations of MgO (6.25-7.39) Wt.% and have Mg# between 47.2 and 48.82, respectively, suggesting a moderate degree of differentiation. Whereas, the seven highly evolved rhyolitc samples have (0.12-0.38) Wt.% MgO contents. In addition, the concentrations of $TiO_2$, ranges from (1.73 -2.77) Wt.% for mafic rock samples whereas between (0.35-0.65) Wt.% for highly evolved felsic rock samples. These indicate that the Debre Sahil/ Guna basalt are Low Titanium (LT) basalt type that is consistent with (Pik et al., 1998) classification.

Selected major element variations diagram against to $SiO_2$ (wt.%) are illustrated in Fig. 4.3. MgO, FeOt, CaO, $TiO_2$, and $P_2O_5$ exhibit almost negative trend with increasing $SiO_2$ concentrations while, $K_2O$ is correlated positively with $SiO_2$ implies that successively enriched in the lavas during the course of differentiation (i.e no fractionation of potassium bearing mineral such as k- feldspar). The $Al_2O_3$ and $Na_2O$ versus $SiO_2$ variaton diagram displays inflected trends. In this case the inflection is generelly taken to indicate either the entry of a new phase during crystal fractionation or loss of phase during partial melting.

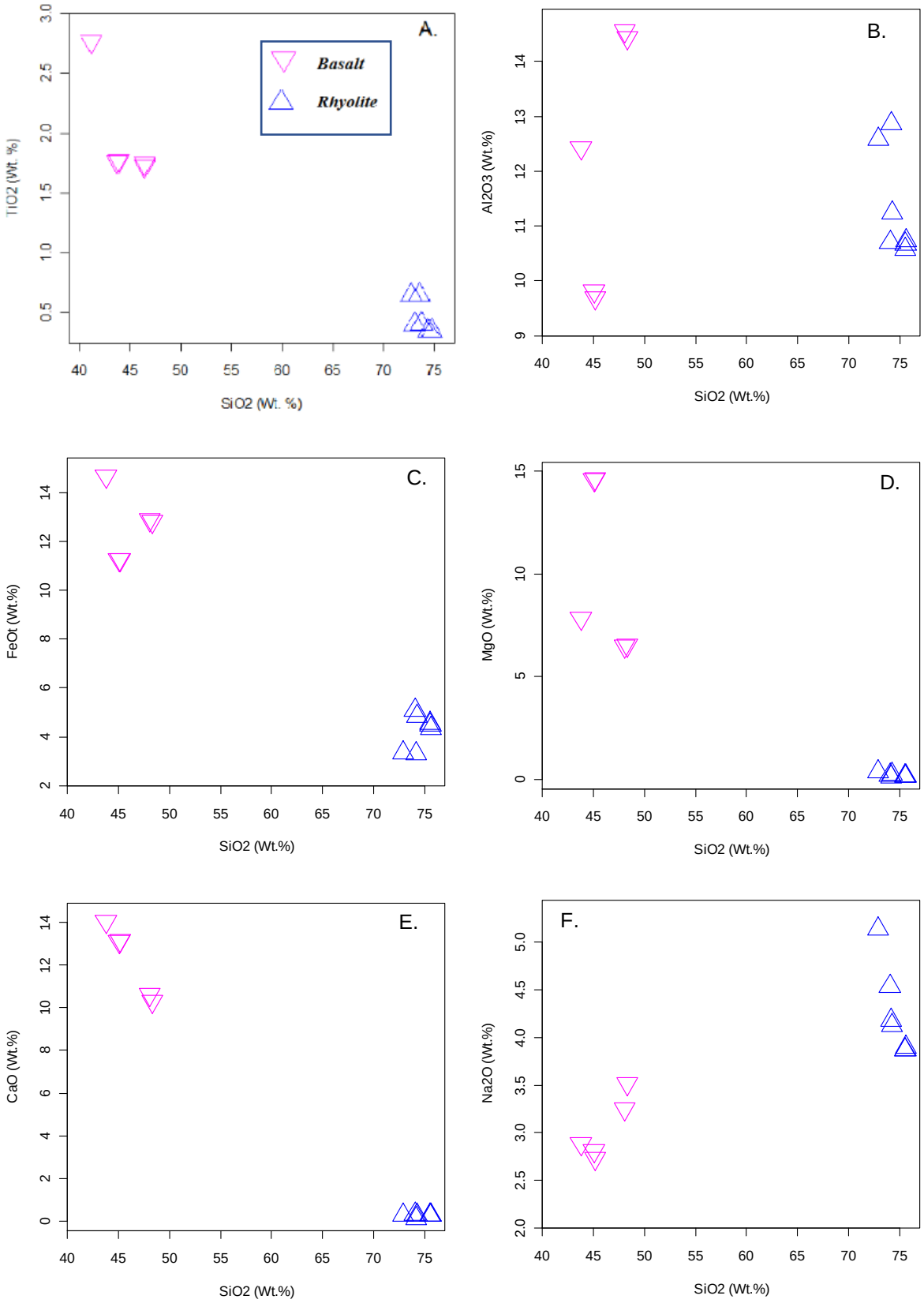
A.
Basalt
Rhyolite
TiO2 (Wt. %)
SiO2 (Wt. %)
B.
Al2O3 (Wt.%)
SiO2 (Wt.%)
C.
FeOt (Wt.%)
SiO2 (Wt.%)
D.
MgO (Wt.%)
SiO2 (Wt.%)
E.
CaO (Wt.%)
SiO2 (Wt.%)
F.
Na2O (Wt.%)
SiO2 (Wt.%)

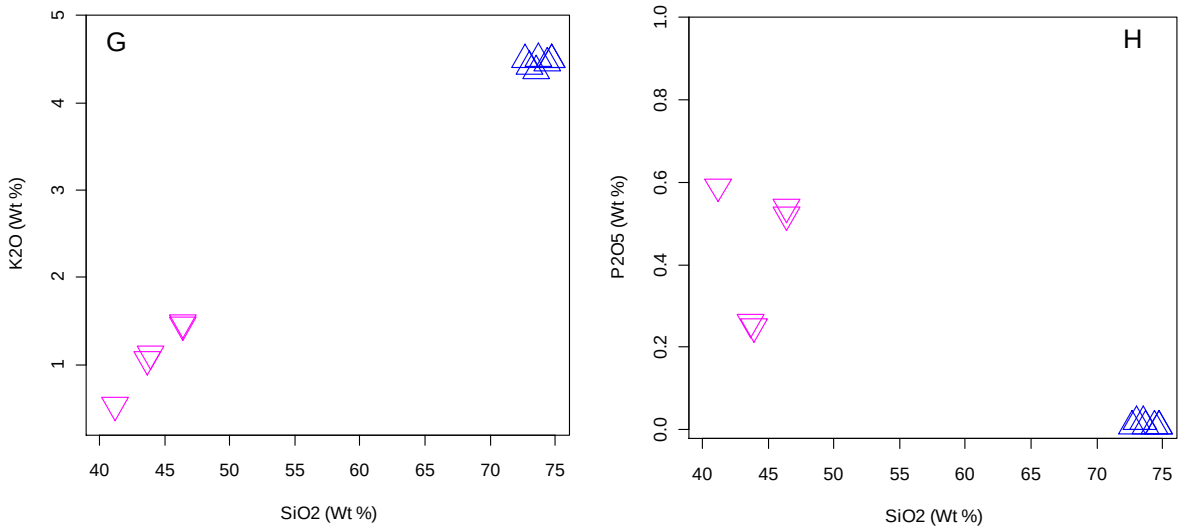


**Fig. 4.3**. Harker variation diagram of whole rock composition for all representative rock samples collected from Debre Sahil area. Major elements are plotted against SiO2 and their concentration is volatile free base and expressed by wt. %.

### 4.2.3. Trace Elements Geochemistry

#### 4.2.3.1. Compatible Trace Elements

The whole rock samples trace element concentrations are presented in table 4.2. According to Ronald et al. (2014) a compatible element is one that is preferentially fractionated from a melt into the crystallizing phases. In other words, the element is compatible with the crystallizing minerals. Because these elements are preferentially extracted during crystallization, the abundances of compatible elements in the melt should decrease with increasing fractionation.

The Debre Sahil volcanic rock exhibits a wide range of compatible trace element concentrations. The two high-MgO lavas samples (T3S1 & T3S2) have relatively higher Ni (290–293 ppm) and Cr (1220-1260 ppm) contents which indicates limited olivine and relatively high pyroxene accumulation, and the other mafic samples have low contents of Ni of 50–62 ppm and Cr of 50–70 ppm, suggesting that these rocks do not represent primary magmas rather underwent olivine and clinopyroxene fractionation. Moreover, highly fractionated silica rich lavas have ( Ni ≤16 ppm, Cr ≤16 ppm and V (6-22 ppm) contents.

The concentration of Compatible trace elements such as Ni, Cr, Sc, V and Sr decrease from mafic to felsic rocks ( table 4.2). The variation diagram of compatible elements Ni, Cr, V, Sc and Sr against SiO2 shows negative trend (Fig. 4.4). The scandium concentrations are slightly higher (24-36 ppm) for mafic samples than felsic suites (2-6 ppm) with comparable wt % SiO2, indicating a later onset of clinopyroxene fractionation in this suite. Scandium concentrations

do not indicate clinopyroxene accumulation but the negative Sc-SiO2 correlation indicates clinopyroxene fractionation was important in Debre Sahil suites.

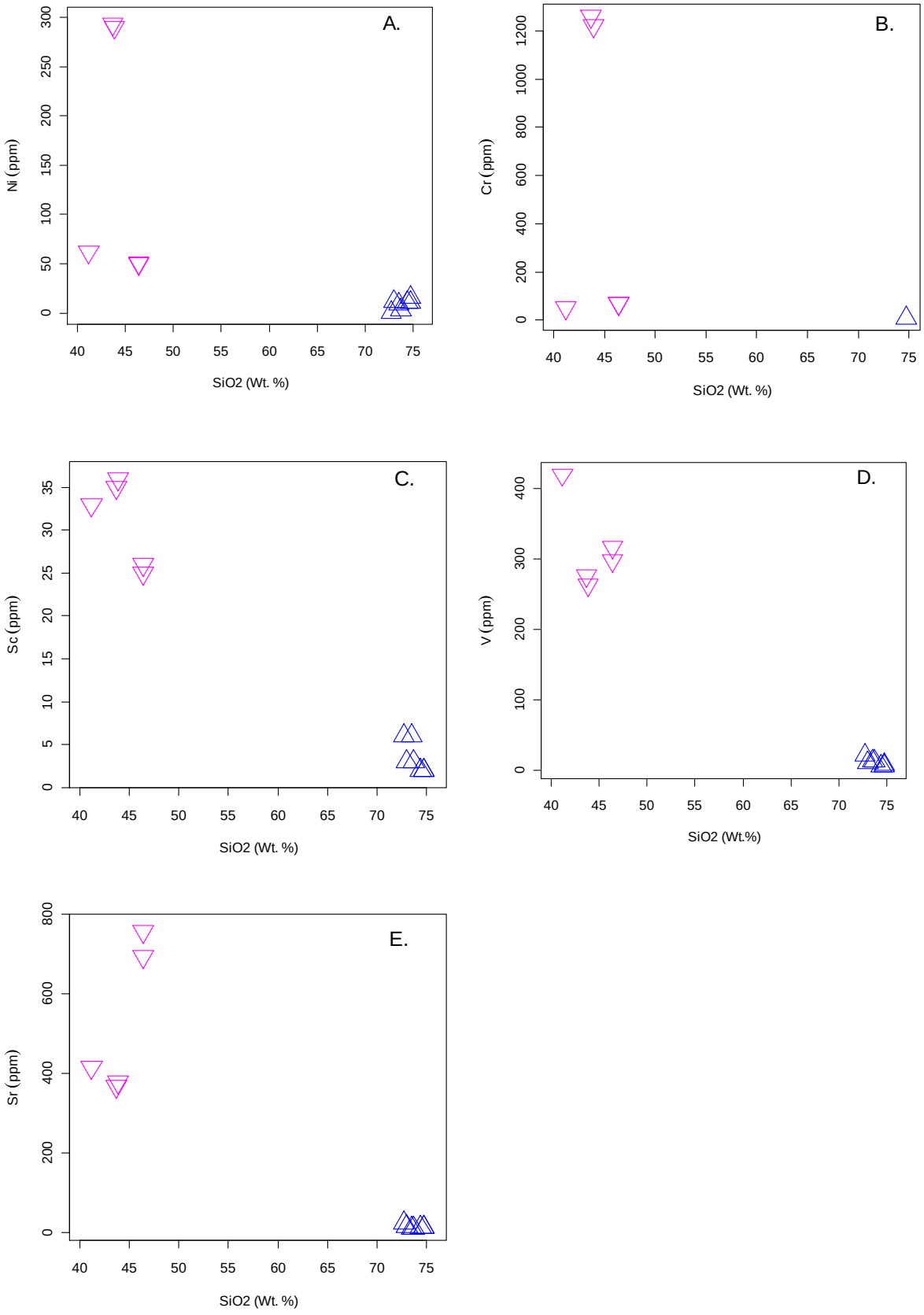


**Fig. 4.4.** Variation diagram of compatible element against SiO2 for Debre Sahil bimodal lava suite.

The trace elements are in ppm whereas the major elements are expresed in Wt. %.

### 4.2.3.2. In compatible elements

Incompatible elements are defined as those elements that partition readily into a melt phase when the mantle undergoes melting (White, 2005). The incompatible trace element concentrations of the Debre Sahil bimodal volcanic rock area are plotted against SiO2 (Fig. 4.5). Rb, Th, Nb, Hf and Y demonstrate a negative correlation with SiO2 for all mafic samples and positive and some vertical trends in rhyolitic sample suites. Moreover, Ba show inflected trend with increasing SiO2. Except Ba and Y, all the other incompatible element shows curvilinear almost positive trends between the mafic and rhyolitic samples.

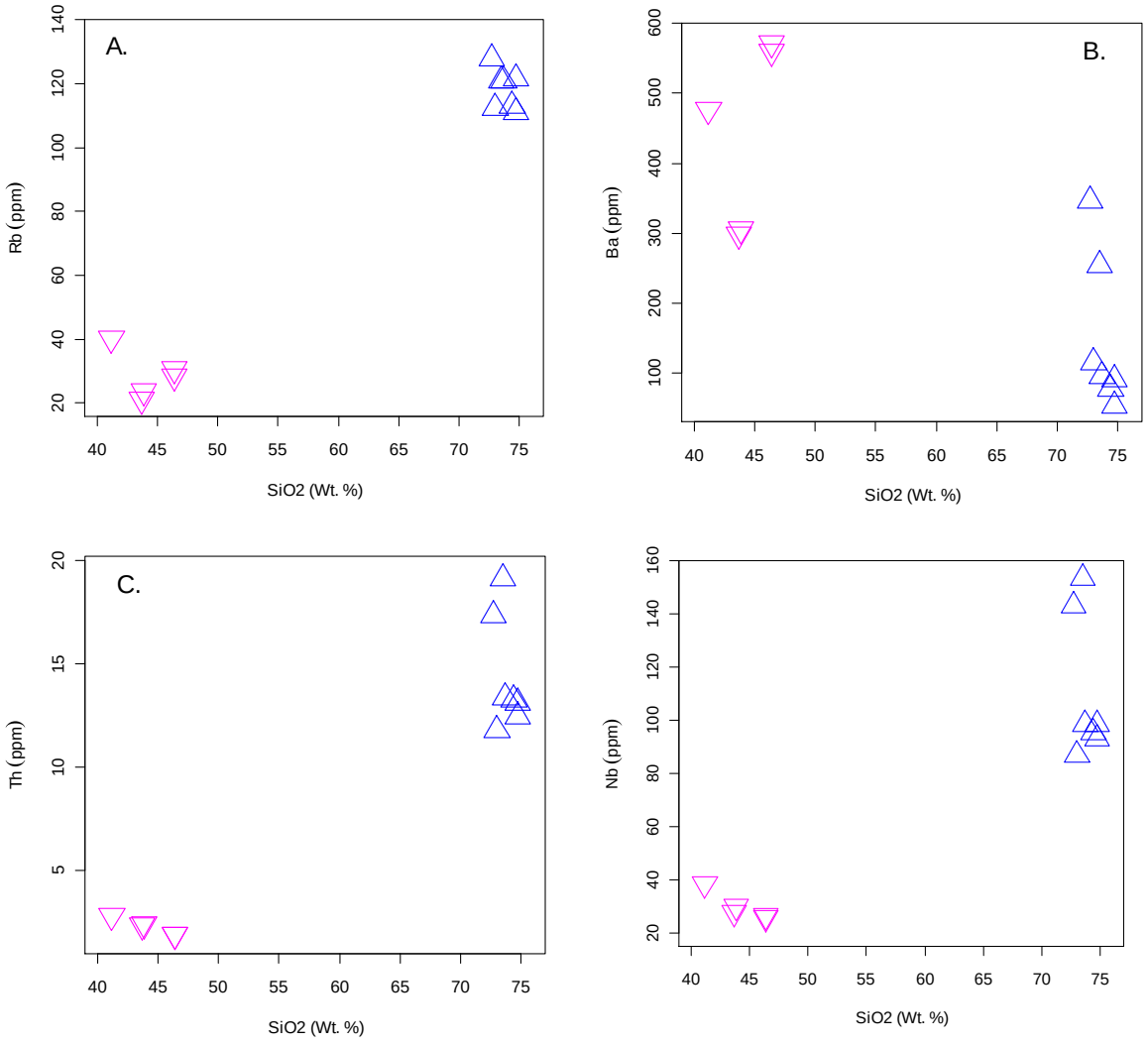

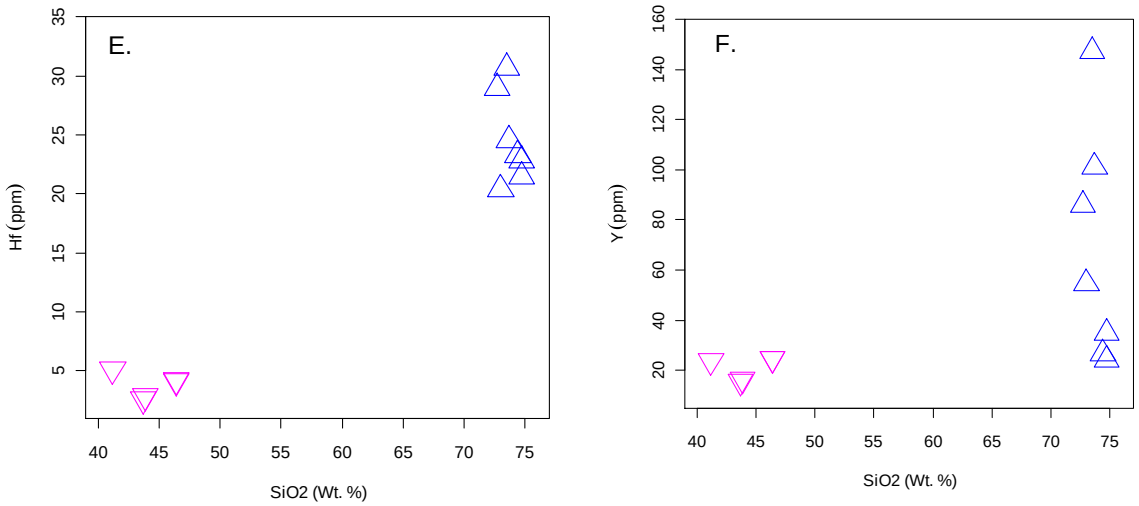


**Fig. 4.5**.Variation diagram of selected incompatible trace elements against SiO2 for Debre Sahil bimodal lava suites.

In addition, incompatible against incompatible elements are plotted to check whether the basaltic and rhyolitic rocks are genetically related or not (Fig. 4.6). (Nb, Ta, Rb and Th) against Zr show a well-defined positive trend generally passing through the origin. This show that the basalt and rhyolite rocks have a similar source (co-genetic). In addition, the Nb, Ta and Th vs Zr plot shows that spatially related basalts and rhyolites define single trends (Fig. 4.6 a, b & d), supporting the view that the rhyolites may be genetically related to the associated basalts either by fractional crystallization (FC) or partial melting (PM).

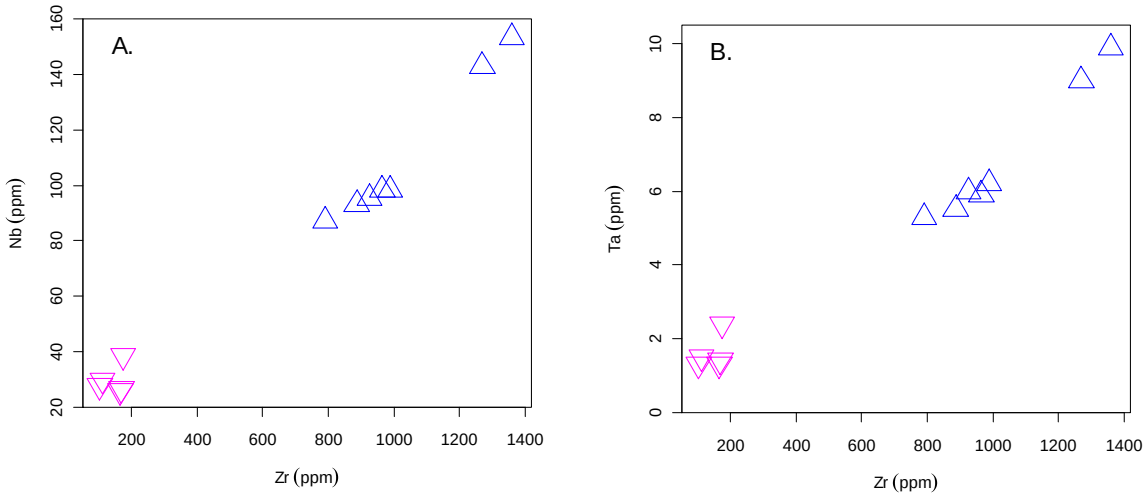

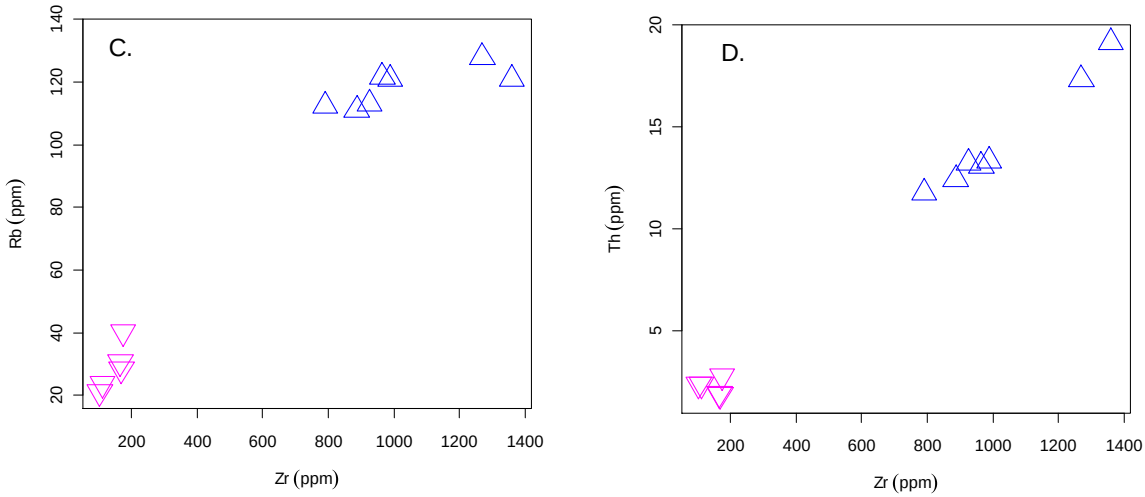


**Fig. 4.6.** Highly incompatible against incompatible trace elements bi-variant plot in which Zr is used as index of differentiation in the horizontal axis and Nb, Ta, Rb and Th vary positively with Zr during magmatic differentiation.

Plots for selected trace element against trace element ratio (Fig.4.7) give information about the evolution of the mafic and silicic magma that is discussed and elaborated further on section 4.6. For samples of silicic volcanic product; Rb/Sr against SiO2 is plotted and show a positive trend. This indicates the fractionation of plagioclase is high relative to alkali feldspar. The sharp drop in Ti/Zr in the less differentiated lava indicates significant removal of Fe-Ti oxides and/or pyroxenes in the initial stage of differentiation of silicic lava.

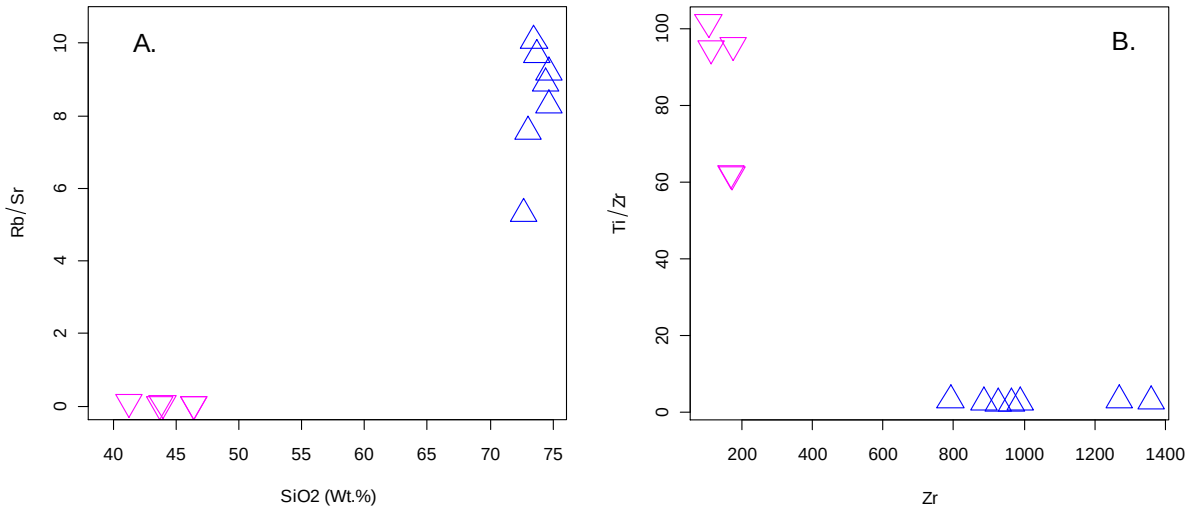

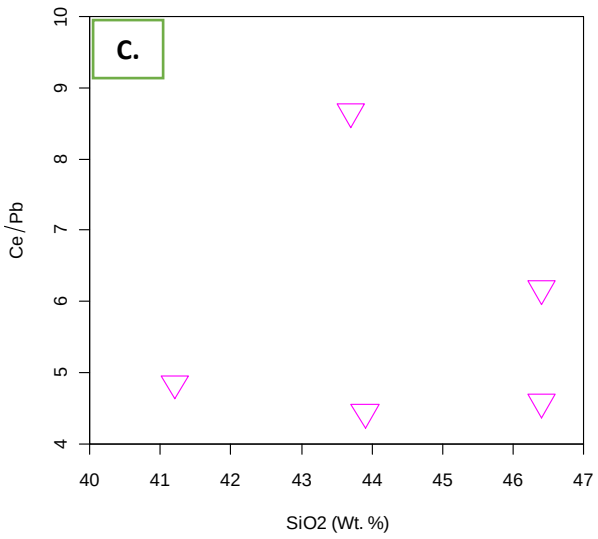


**Fig. 4.7. (**a) Trace element ratio against SiO2 and Ti/Zr- Zr. The unit for the concentration is in ppm (for trace element) and wt. % for major element.

#### 4.2.3.3. Rare Earth element (REE)

The REE concentrations are normalized to chondrite according to the values of Boynton (1984). Chondrite-normalized rare earth element (REE) patterns are shown in (Fig. 4.9). The REE analysis is made separately for mafic and silicic rocks. The analyzed mafic and rhyolitic rock shows enrichment of light rare earth element relative to heavy rare earth elements. All of the mafic lavas are enriched in light-REE to varying degrees. The enrichment of the LREE in mafic rock range, in terms of $(La/Yb)_N$, between (7.86-12.14), while the heavy REE are moderately fractionated with almost flat pattern [$(Gd/Yb)_N$ 1.87- 2.77]. The pattern of the REE diagram show nearly parallel for all of the samples. This indicates almost their derivation from similar source. The Eu concentration of mafic lavas shows a slight positive anomaly (Eu/Eu*~0.99-1.07)) that likely comes from accumulation of plagioclase feldspar (Wilson, 1989; Rollinson, 1993). The REE diagram pattern of the rhyolite rock shows enrichment in the light rare earth element (LREE) and gentle heavy rare earth element (HREE). The enrichment of LREE range between, in terms of $(La/Yb)_N$, 4.54-8.8). Similar to mafic samples, the silicic samples show parallel pattern in the HREE. In addition, all samples show a negative Eu anomaly (Eu/Eu* 0.27- 0.8). This is a typical indication for the fractionation of plagioclase feldspar (Wilson, 1989; Rollinson, 1993). The strong negative anomaly of Eu is observed in rhyolite samples (Eu/Eu*=0.27). On rhyolite samples we can observe three ways of trend (negative, positive and flat) on the Ce concentration due to alteration.

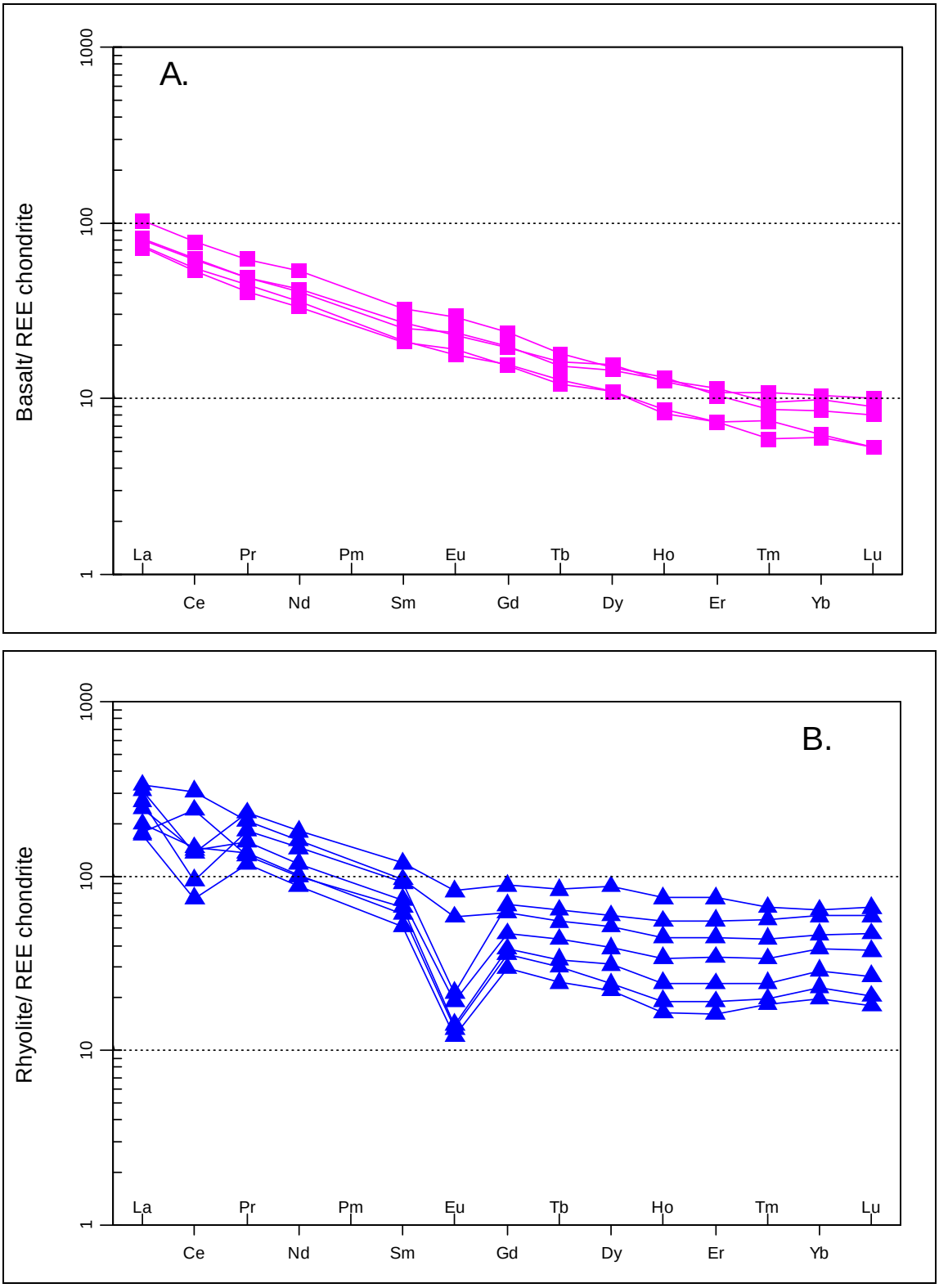


**Fig. 4.8.** REE chondrite normalized variation diagram of representative samples for basaltic (A) and rhyolitic (B) rocks. The concentration value of the rock sample is normalized to chondrite value determined by Boynton (1984).

Primitive mantle-normalised multi-element variation diagrams (Fig.410a & b) for bimodal basalt-rhyolite suite are plotted to further understand the evolution of the rocks from Debre Sahil area. The Primitive mantle-normalised multi-element variation diagram for mafic rock shows a positive anomaly at Ba, Nb, Pb, and negative anomaly at U. The combination of minor enrichment in Ba and the absence of troughs at Nb indicates no significant crustal contamination of the mafic lava during the fractionation process. Over all enrichment in the incompatible elements show fractionation of phases specially plagioclase feldspar. The spider diagram for the rhyolite rock display marked troughs at Ba, U, Ce, Sr, P, Ti and positive anomaly at Rb, Th, Nb, Nd, Pb, Zr and Dy. The negative anomaly at Ba, Sr, P and Ti, are show the fractionation or removal of alkali feldspar, plagioclase feldspar, apatite and Fe–Ti oxide (accessory ilmenite) respectively from the magma. More over some elements show slight enrichment as well as depletion on the spider diagram which indicate that the involvement and removal of some minerals during the evolution of magma.

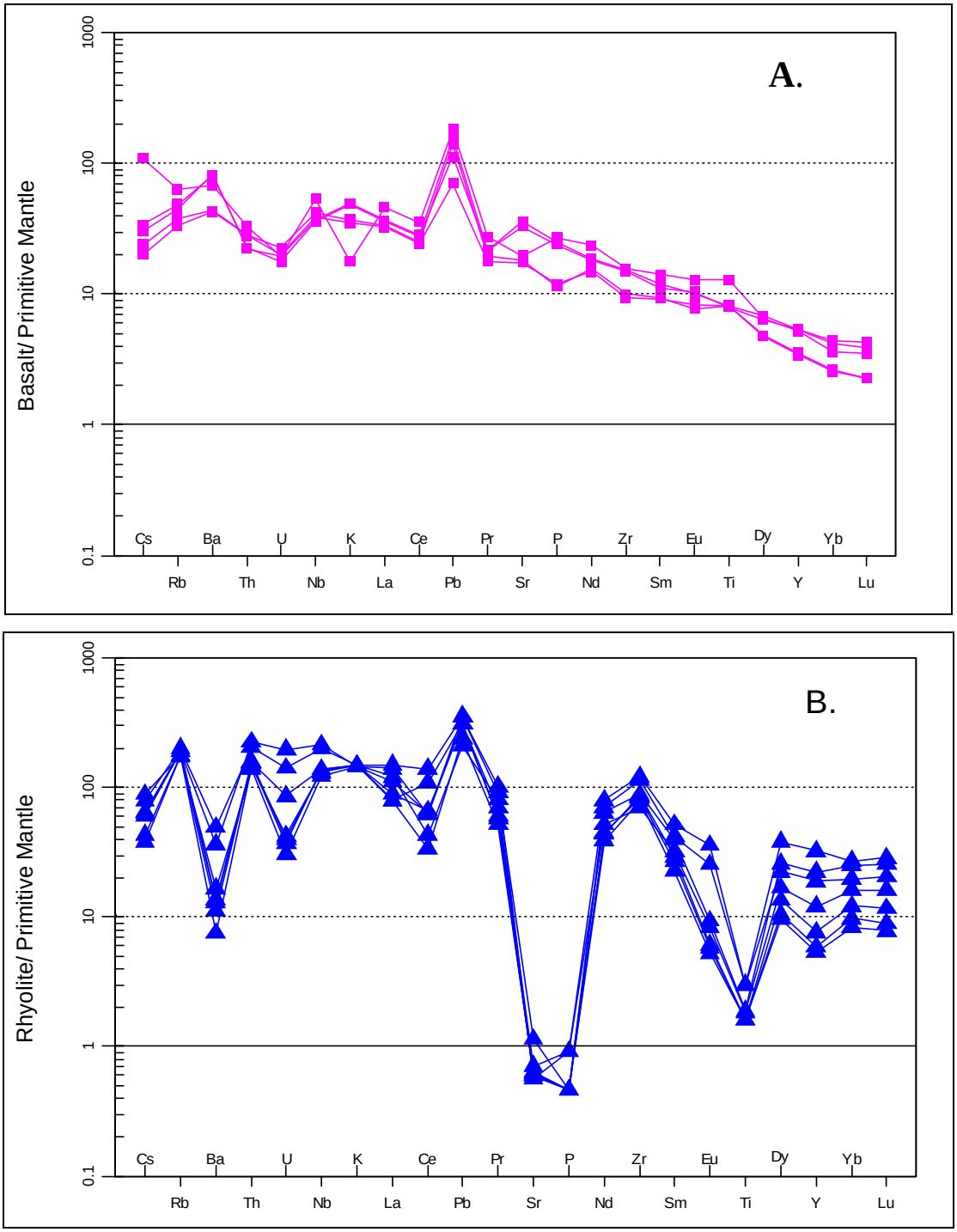


**Fig. 4.9**. Primitive-mantle-normalized multi-element variation diagram of representative basaltic (**A**) and rhyolitic (**B**) rocks from Debre Sahil area. The samples are normalized to primitive mantle of value determined by Sun and McDonough (1989).

# CHAPTER FIVE

# 5. DISCUSION

## 5.1. Fractional Crystallization

The Debre Sahil bimodal volcanic products strictly show a major and trace element variation that mainly affected by fractionation of mineral phases. The overall distribution of the samples and the slopes of the trend in the major element variation diagrams (Fig. 4.3 a, c, d e & h) suggest that early fractional crystallization controlled by olivine followed by clinopyroxene, plagioclase, Fe-Ti oxides and apatite occurring over the course of magmatic evolution. A steep slope break in the variation diagram of MgO against SiO2 indicates the control of olivine fractionation from the system in the initial level and then dominated by clinopyroxene, plagioclase and ilmenite (Fe-Ti oxides) (after 46 to 47 wt. % of SiO2). This were consistent with the phenocrysts identified during petrographic analysis. The variation of the major elements for the silicic analyzed rocks against SiO2; different fractionation histories may be responsible for the trend. The variation of SiO2 (specifically above a value of 72.7 wt. %) against Na2O and Al203 shows a negative trend in rhyolite samples. In this group of rock, it appears to be the major element variation is controlled by the fractionation of alkaline feldspar (sanidine) in the final stage of the magma evolution. Accordingly, the dominancy of alkali feldspar phenocryst in highly evolved rhyolite thin section samples also supports the late fractionation of alkali feldspar. Furthermore, the CaO and MgO against SiO2 clearly show a trend change from steep negative to gentler slope. The trend change is an indication of CaO and MgO bearing mineral removal is less dominant in silicic magma relative to mafic.

In addition, the fractionation process is also shown by the trace element geochemistry with plots of trace element against SiO2 & Zr variation diagrams that discussed in section 4.4,4.5 &4.6. The marked fall in the abundance of compatible trace elements such as Ni (293 to <1) ppm and Cr from (1260 to <10) ppm strongly suggests that fractional crystallization of olivine and clinopyroxene has been important in early evolution of the suite. The plots of the compatible trace element (e.g. Ni, Cr, V, Sc and Sr) against SiO2 show a negative correlating line. The declines in these elements reflect early fractionation of Ni, Cr, Sc,Vand Sr bearing minerals. In addition, incompatible trace element plot with SiO2 and Zr (e.g. Nb, Ta, Rb and Th) show a positive trend lines that confirms that fractionation played a major role in the evolution of the rocks of the area. The rhyolitic chondrite normalized REE diagram show negative Eu anomaly that support the fractionation of plagioclase feldspar. On multi-element variation diagram the trough at Ba, Sr, Ti and P also evidenced the fractionation of mineral

phases specially alkali feldspar, plagioclase feldspar, accessory ilmenite or titanomagnetite and apatite.

In general, the variations in major and trace element concentrations and petrographic observations, indicate that fractionation of olivine, clinopyroxene, plagioclase, alkali feldspar apatite and Fe-Ti oxide) or opaque minerals occurred during the evolution of the Debre Sahil bimodal basalt - rhyolite lava suite. This has been further refined by incompatible trace-element plots (e.g. Zr Vs Th, Nb and Ta) of the Debre Sahil basalts and rhyolites define positive linear trends that pass through the origin show the genetic relationship or co-genetic nature of the basaltic and rhyolitic rocks. This together with their parallel REE patterns suggests that fractional crystallization has been the dominant process in the evolution of the basalt–rhyolite suite of the area.

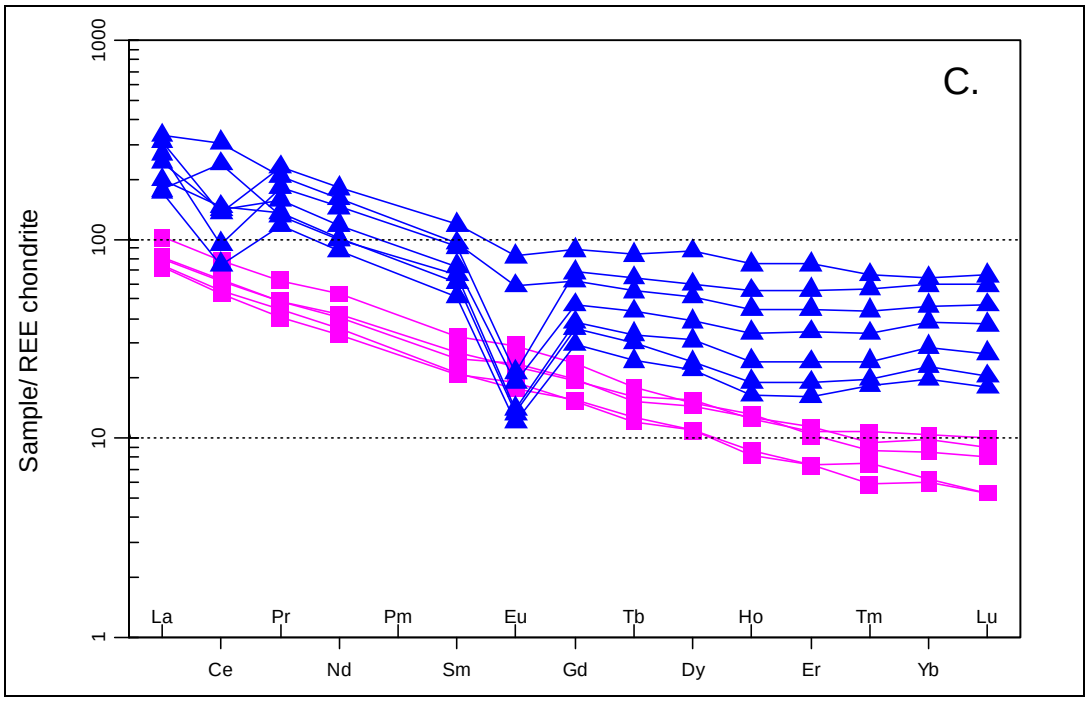

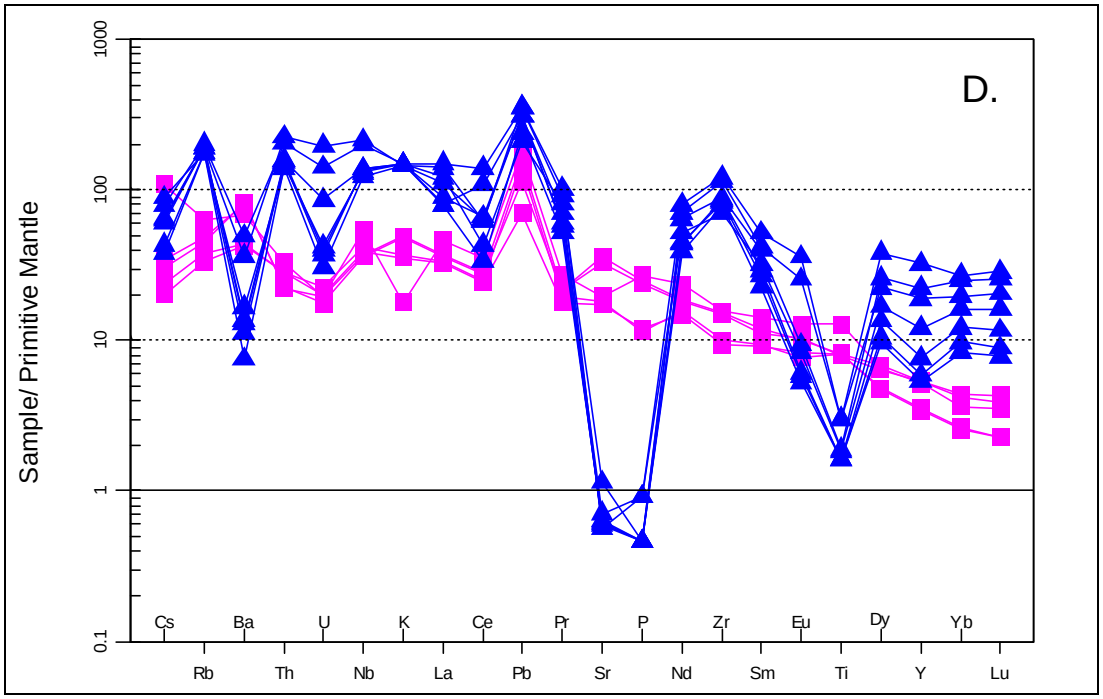


**Fig. 5.1.** Chondrite normalized REE diagram (C) and primitive-mantle normalized diagram (D). Normalization values are from Boynton, 1984 and Sun and McDonough (1989).

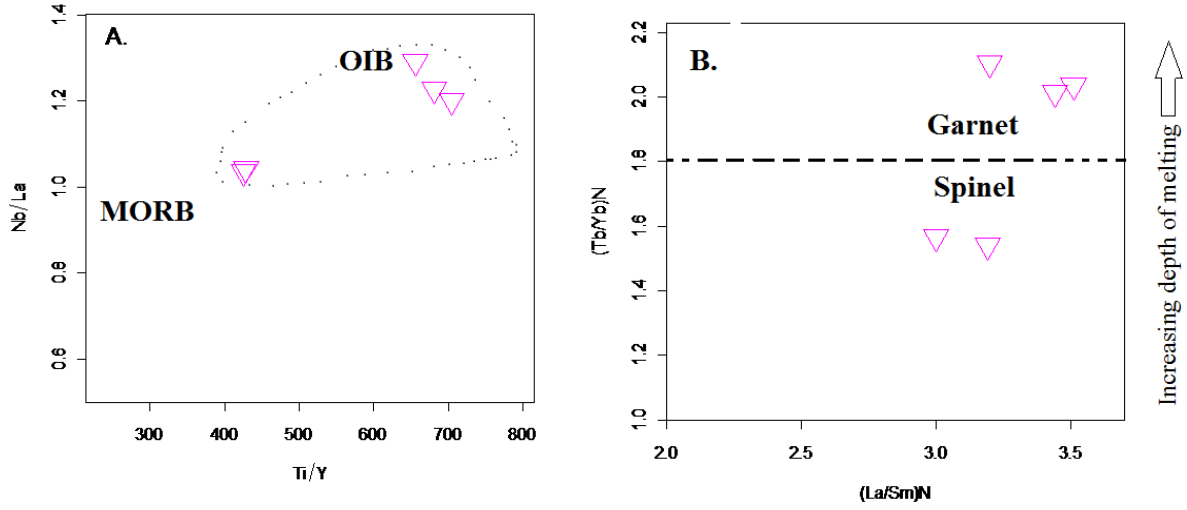


**Fig. 5.2.** Nb/La vs Ti/Y and $(Tb/Yb)_N$ versus $(La/Sm)_N$, ratios for Debre Sahil flood basalts.
**(A).** Nb/La vs. Ti/Y for Debre Sahil flood basalts MORB and OIB compositions are from Sun and McDonough, 1989 And **(B)** $(Tb/Yb)_N$ versus $(La/Sm)_N$, ratios. Chondrite normalization factors from Boynton (1984). Dashed line represents approximate division between melts derived from mantle lithologies dominated by garnet as the aluminous phase versus those dominated by spinel. (after Mulugeta Alene et al., 2017).

### 5.2. Crustal Contamination

The analyzed samples are characterized by strong enrichment in LREE and in highly incompatible trace elements. The enrichment in LREE and in highly incompatible elements may either be a consequence of crustal contamination or derivation from enriched mantle source (e.g. Thompson, 1984; Dereje Ayalew et al., 1999. The crustal contaminating material involvement is mainly verified from the contamination index (La/Nb). The mafic samples from Debre Sahil lavas show La/Nb ratio between (0.77-0.96) that indicate slight contamination by crustal material (Thompson, 1984, Rooney et al.,2007). The diagram Ce/Pb ratio against SiO2 (Fig. 4.7 c) which show scatter plot with a slight sub horizontal trend (Fig.5.1b) suggest a minor contamination. The Debre Sahil lavas, Ce/Pb ratios values range from (4.44-8.66) suggest all sample suites are out of the range of primitive or uncontaminated melts (Ce/Pb = 20-30; and crustally contaminated melts (Ce/Pb <20); Hoffman et al. (1986). Moreover, the Nb/Th ratio of primitive mantle is ≥8, whereas in continental crust it is around 1.1 (Taylor and McLennan, 1985; Sun and McDonough, 1989; Rollinson, 1993). The analyzed Debre Sahil basaltic rock samples display Nb/Th ratio (11.65 to 13.89) ranges which is consistent with that of primitive mantle values thereby reflecting insignificant crustal contamination during magma ascent. The trace element ratio values are fully presented in appendix II. In addition, the presence of high positive Pb anomalies in primitive mantle normalized trace element diagrams also indicative of crustal input in all lavas.

Additionally, the absence of negative anomalies at Nb in the primitive mantle-normalized multi-element variation diagrams (Fig.5.2 d) indicate that a significant crustal contribution is absent in the genesis of the Debre Sahil bimodal volcanic rock units investigated here.

### 5.3. Mantle melting conditions (Magma generation)

Rare-earth element (REE) compositions provide important constraints in understanding the mantle melting conditions because their relative abundances in mantle-derived melts are strongly dependent on the degree of partial melting and the nature of aluminous phase (spinel or garnet) in the mantle source (Lassiter et al., 1995). Furthermore, the relative REE abundances are highly dependent upon source lithology and can indicate the presence of spinel versus garnet (Furman et al., 2016). In general, heavy rare Earth element (HREE) especially Yb is compatible in garnet, whereas La (LREE), Sm and Gd (MREE) are incompatible (e.g. Rollinson, 1993). La/Yb and Sm/Yb are strongly fractionated when melting occurs in the garnet stability field, and in contrast to this La/Yb is slightly fractionated and Sm/Yb is nearly unfractionated during melting in the spinel peridotite domain (Yaxley, 2000; Xu et al., 2005; Lai et al., 2012). Gd/Yb and Sm/Yb are distinct indicators of the presence of residual garnet

during partial melting. The REE signatures of Debre Sahil bimodal volcanic products are marked by $(La/Yb)_N$ = 4.54-12.14, $(Sm/Yb)_N$ = 1.55-3.78 and $(Gd/Yb)_N$ = 1.16-2.77) with parallel chondrite-normalized REE patterns (Fig.5.2 c) reflect moderate to high fractionation of HREE and thus suggest that the parental magmas were derived by partial melting of a mantle source at variable depths extending from spinel to garnet stability fields (Safonova et al., 2008; Buslov et al., 2010; Manikyamba et al., 2015)). Similar inferences are derived from a plot of $(La/Sm)_N$ vs. $(Tb/Yb)_N$ ratios (Fig. 5.3 b) (Mulugeta Alene et al., 2017).

In addition, the Debre Sahil basalts rocks are characterized by relatively moderate CaO/Al2O3 ratios (0.714–1.36) and relatively parallel HREE patterns $(Tb/Yb)_N$ = 1.54–2.11)) together with slightly elevated HREE concentrations higher than 10-times chondritic values for two samples and the other three basaltic samples show HREE concentration (< 10- times chondritic values), which most likely suggest a mantle source containing spinel bearing peridotite with residual garnet (Dereje Ayalew et al., 2016; 2018 in press).

The Primitive mantle-normalized multi-element patterns and chondrite normalized REE patterns (Fig. 5c & d) exhibit higher abundances of LILE and LREE of these basalts suggesting that their parent magma had a mantle source which had experienced sufficient enrichment in these elements. The Nb/Ta (15.96-21.23), Zr/Sm (25.3- 34.15) and Zr/Hf (34.12-40.73) ratios against respective primitive mantle values of 17, 25 and 36 indicates that an enriched mantle source for the derivation of parent magma producing Debre Sahil basalts (Sun and McDonough,1989). These basalts have Nb (25.7-38.3 ppm) and Zr (104-174 ppm) contents higher than those of the N-MORB (Nb =2.33 ppm, Zr = 74 ppm) and lower than that of OIB (Nb = 48 ppm, Zr = 280 ppm) implying their generation from an enriched mantle source (Sun and McDonough,1989). Moreover, the studied basalt sample have relatively higher Zr/Nb ratios (3.77-6.5) than those of the OIB (4.2). In addition, the La/Nb (0.77-0.96), Nb/La (1.04-1.29) and Ba/Nb (10.27-21.67) ratios also indicates that the Debre Sahil basalts are derived from OIB type source (Sun and McDonough,1989).

# CHAPTER SIX

# 6. CONCLUSION AND RECOMMENDATION

## 6.1. Conclusion

A combination of, field mapping, petrographic and geochemical analysis provide new insights regarding the Petrogenetic evolution of the Debre Sahil bimodal lava suite. The main results of this study are:

1. The geochemistry tells that the analyzed rocks are bimodal, which lacks intermediate composition. The chemical compositions are mainly basaltic and silicic. The basalts are alkaline whereas the silicic rocks are peralkaline rhyolite.
2. The overall elemental variation in the bimodal basalt-rhyolite suite shows two important fractionation trends. A first one dominated by fractionation of mafic phases (olivine, clinopyroxene, plagioclase feldspar, apatite and Fe-Ti oxides) and a second dominated by a fractionation of alkali feldspar.
3. The new major and trace element data indicate that the Debre Sahil bimodal basalt- rhyolite suite mostly evolved by fractional crystallization process with minor crustal material involvement, and the perfect positive correlation between highly incompatible elements in the Harker diagram is the reflection of co genetic origin of the basalt and rhyolite suites.
4. The trace element data suggests that the Debre Sahil mafic rocks are derived by partial melting of spinel bearing peridotite with some residual garnet mantle source, whereas the rhyolite rocks are derived from mafic rocks by fractional crystallization process.
5. Finally, the analyzed selected trace element ratio such as Zr/Sm (25.3- 34.15), Zr/Hf (34.12-40.73) and Nb/Ta (15.96-21.23) ratios against respective primitive mantle values of 25, 36 and 17 indicates to an enriched mantle source for the derivation of parent magma producing Debre Sahil basalts.

## 6.2. Recommendation

- Isotope geochemistry is a strong tool to understand magma evolution. Hence, more samples for geochemical analysis and isotope geochemistry is suggested for further substantiation of the source and petrogenesis of the bimodal basalt-rhyolite rocks.

# References

Abera Tessema and Antoine, L.A.G. (2004). Processing and interpretation of the gravity field of the East African Rift: implication for crustal extension. *Tectonophysics,* **394:** 87– 110.

Acocella, V.,Tesfaye Korme and Salvini, F. (2003). Formation of normal faults along the axial zone of the Ethiopian Rift. *Journal of Structural Geology*, **25:** 503-513.

Agostini, A., Bonini, M., Corti, G., Sani, F. and Manetti, P. (2011). Distribution of Quaternary deformation in the central Main Ethiopian Rift, East Africa. *Tectonics,* **30**, TC4010.

Alebachew Beyene and Mohamed Abdelsalam, 2005. Tectonics of the Afar Depression: a review and synthesis. *Journal of African Earth Sciences*, **41**: 41–59.

Baker, J., Snee, L. and Menzies, M. (1996). A brief Oligocene period of flood volcanism in Yemen. *Earth and Planetary Science Letters,***138**: 39–55.

Beccaluva, L., Bianchini, G., Natali, C. and Siena, F. (2009). Continental flood basalts and mantle plumes: a case of the Northern Ethiopian Plateau. *Journal of Petrology,* **50**: 1377–1403.

Bekele Abebe, Acocella V., Tesfaye Korme and Dereje Ayalew (2007). Quaternary faulting and volcanism in the Main Ethiopian Rift. *Journal of African Earth Sciences,* **48**: 115–124.

Boccaletti, M., Bonini, M., Mazzuoli, R., Bekele Abebe, Piccardi, L. and Tortorici, L. (1998). Quaternary oblique extensional tectonics in the Ethiopian Rift (Horn of Africa). *Tectonophysics,* **287**: 97-116.

Boccaletti, M., Mazzuoli, M., Bonini, R., Trua, T. and Bekele Abebe (1999). Plio- Quaternary volcano tectonic activity in northern sector of the Main Ethiopian Rift: Relationship with oblique rifting. *Journals of earth sciences*, **29**(4):679-698.

Bonini, M., Corti, G., Innocenti, F., Manetti, P., Mazzarini, F., Tsegaye Abebe and Pecskay, Z. (2005). Evolution of the Main Ethiopian Rift in the frame of Afar and Kenya rifts propagation. *Tectonics* **24**: TC1007. doi:10.1029/2004TC001680.

Boynton, W.V. (1984). Geochemistry of Rare Earth Elements: Meteoritic Studies, *Elsevier, Amsterdam*, 63-114pp.

Buslov, M.M., Safonova, I.Yu, Fedoseev, G.S., Reichow, M., Davies, C., Babin, G.A. (2010). Permo-Triassic plume magmatism of the Kuznetsk Basin, Central Asia: geology, geochronology and geochemistry. *Russian Geology and Geophysics,* **51:** 901-916.

Corti, G. (2009). Continental rift evolution: From rift initiation to incipient break-up in the Main Ethiopian Rift. East Africa. *Earth-Science Reviews*, **96**: 1–53.

Davidson, A. and Rex, D.C. (1980). Age of volcanism and rifting in south-western Ethiopia. *Nature* **283**: 654–658.

Deniel C., Trua T. and Mazzuoli, R. (2000) Crustal control in the genesis of Plio-Quaternary bimodal magmatism of the Main Ethiopian Rift (MER): geochemical and isotopic (Sr, Nd, Pb) evidence—reply. *Chemical Geology*, **168**:5–7.

Dereje Ayalew, Gezahegn Yirgu and Raphael Pik (1999). Geochemical and isotopic (Sr, Nd and Pb) characteristics of volcanic rocks from southwestern Ethiopia. *Journal of African Earth Sciences*,**29**: 381-391.

Dereje Ayalew (2000). Origin by fractional crystallization of transitional basalt for the Asela-Ziway pantellerites. Crustal control in the genesis of Plio-Quaternary bimodal magmatism of the Main Ethiopian Rift MER: geochemical and isotopic Sr, Nd, Pb evidence by Trua et al. 1999.*Chemical Geology*, **168**: 2000 1–3.

Dereje Ayalew, Pierre Barbey, Bernard Marty, Laurie Reisberg, Gezahegn Yirgu, and Raphael Pik (2002). Source, genesis, and timing of giant ignimbrite deposits associated with Ethiopian continental flood basalts. *Geochimica et Cosmochimica Acta*,**66**(8): 1429–1448.

Dereje Ayalew and Gezahegn Yirgu (2003). Crustal contribution to the genesis of Ethiopian plateau rhyolitic ignimbrites: Basalt and rhyolite geochemical provinciality. *Journal of the Geological Society*, **160**: 47-56. Doi: 10.1144/0016-764901-169.

Dereje Ayalew, Ebinger, C., Bourdon, E., Wolfenden, E., Gezaheng Yirgu and Grassineau, N. (2006). Temporal compositional variation of syn-rift rhyolites along the western margin of the southern Red Sea and northern Main Ethiopian Rift. In: Gezaheng Yirgu, Ebinger, C.J., Maguire, P.K.H. (Eds.), the Afar Volcanic Province within the East African Rift System: *Geological Society Special Publication, **259***: 121–130.

Dereje Ayalew; Gibson, S.A. (2009). Head-to-tail transition of the Afarmantle plume: geochemical evidence from a Miocene bimodal basalt-rhyolite succession in the Ethiopian Large Igneous Province. *Lithos*, **112**: 461–476.

Dereje Ayalew, Jung, S., Romer, R.L., Kersten, F., Pfander, J.A. and Garbe-Schonberg, D. (2016). Petrogenesis and origin of modern Ethiopian rift basalts: constraints from isotope and trace element geochemistry. *Lithos*, **258-259**: 1–14.

Dereje Ayalew, Jung, S., Romer, L. and Garbe-Schonberg, D. (2018). Trace element systematics and Nd, Sr, and Pb isotopes of Pliocene flood basalt magmas (Ethiopian rift): A case for Afar plume-lithosphere interaction. *Chemical Geology*, in press.

Eberz, G.W., Williams, F.M., Williams. M.A.J. and Clayton (1988). Plio-Pleistocene volcanism and sedimentary facies changes at Gadeb pre-historic site, Ethiopia. *Geologische Rundschu*, 513-527.

Ebinger, C.J., Tilahun Yemane, Gidey WoldeGabriel, Aronson, J.L. and Walter, R.C. (1993). Late Eocene Recent volcanism and faulting in the southern main Ethiopian rift. *Journal of the Geological Society of London*, **150**: 99–108.

Ebinger, C. and Casey, M. (2001). Continental breakup in magmatic provinces: An Ethiopian example. *Geology*, **29**:527-530.

Ebinger, C. (2005), Continental break-up: The East African perspective, *Astron. Geophys*., **46**: 2.16–2.21.

EIGS _Ethiopian Institute of Geological Surveys, Ministry of Mines and Energy., 1978. Geological Map of the Nazret Sheet_NC37-15., scale 1: 250,000.

Feyissa, D.H., Shinjo, R. Kitagawa, H., Daniel Meshesha, and Nakamura, E. (2017). Petrologic and geochemical characterization of rift-related magmatism at the northernmost Main Ethiopian Rift: Implications for plume-lithosphere interaction and the evolution of rift mantle sources. *Lithos*, **282–283**: 240–261.

Furman, T., Bryce, J., Rooney, T., Hanan, B., Gezahegn Yirgu and Dereje Ayalew (2006). Heads and tails: 30 million years of the Afar plume. *Geol. Soc. London Spec. Publ*. **259**: 97–121.

Furman, T. (2007). Geochemistry of East African Rift basalts: An overview. *Journal of African Earth Sciences*, **48**: 147–160.

Furman, T., Nelson W.R., Elkins-Tanton, L.T. (2016). Evolution of the East African rift: Drip magmatism, lithospheric thinning and mafic volcanism. *Geochimica et Cosmochimica Acta*, **185**: 418–434.

Gasparon, M., Innocenti, F., Manetti, P., Peccerillo, A. and Tsegaye Abebe (1993). Genesis of the Pliocene to Recent bimodal mafic–felsic volcanism in the Debre–Zeyt area, central Ethiopia: volcanological and geochemical constraints. *Journal of African Earth Sciences*, **17**: 145–165.

George, R., Rogers, N. and Kelly, S. (1998). Earliest magmatism in Ethiopia: evidence for two mantle plumes in one flood basalt province. *Geology*, **26**: 923-926.

Gidey WoldeGabriel, G., Aronson, J.L. and Walter, R.C. (1990). Geology, geochronology, and rift basin development in the central sector of the Main Ethiopia Rift. *Geological Society of America Bulletin,***102**: 439–458.

Giordano F., D'Antonio M., Civetta L., Tonarini S., Orsi G., Dereje Ayalew, Gezahegn Yirgu, Dell'Erba F., Di Vito M.A. and Isaia R. (2014). Genesis and evolution of mafic and felsic magmas at Quaternary volcanoes within the Main Ethiopian Rift: Insights from Gedemsa and Fanta 'Ale complexes. *Lithos,***188**: 130–144.

Hayward, N.J. and Ebinger, C.J. (1996). Variations in the along-axis segmentation of the Afar Rift system. *Tectonics*, **15**: 244–257.

http://en.climate-data.org/location/2108/ accessed on 04,25,2018.

Hofmann, C., Courtillot, V., Féraud, G., Rochette, P., Gezahegn Yirgu, Ketefo, E., and Pik, R. (1997). Timing of the Ethiopian flood basalt event and implications for plume birth and global change: *Nature*, **389**: 838–841.

Hofmann, A.W., Jochum,K.P., Seufert,M. and White,W.M. (1986). Nb and Pb in oceanic basalts: new constraints on mantle evolution. *Earth Planet. Sci. Lett*., **79**: 33-45.

Irvine, T.N. and Baragar, W.R.A., 1971. A guide to chemical classification of common volcanic rocks. *Canadian Journal of Earth Science*, **8:** 523–548.

Keranen K. and Klemperer S.L. (2008). Discontinuous and diachronous evolution of the Main Ethiopian Rift: Implications for development of continental rifts. *Earth and Planetary Science Letters,***265**: 96–111.

Keir, D., Ebinger, C.J., Stuart, G.W., Daly, E. and Atalay Ayele (2006). Strain accommodation by magmatism and faulting as rifting proceeds to break-up: seismicity of the northern Ethiopian rift. *J. Geophys. Res*, **111**, B05314. doi:10.1029/2005JB 003748.

Kieffer, B., Arndt, N., LaPierre, H., Bastien, F., Bosch, D., Pecher, A., Gezahegn Yirgu, Dereje Ayalew, Weis, D., Jerram, D., Keller and F., Meugniot, C. (2004). Flood and shield basalts from Ethiopia: magmas from the African Super swell. *Journal of Petrology*, **45**: 793–834.

Kurkura Kabeto, Sawnda, Y.and Roser B. (2009). Compositional differences between felsic volcanic rocks from the margin and center of the northern Main Ethiopian Rift. *MEJS*, **1**(1): 4-35.

Kurz, T., Gloaguen, R., Ebinger, C., Casey, M. and Bekele Abebe (2007). Deformation distribution and type in the Main Ethiopian Rift (MER): a remote sensing study. *Journal of African Earth Sciences*, **48**: 100–114.

Lai, S., Qin, J., Li, Y., Li, S. and Santosh, M. (2012). Permian high Ti/Y basalts from the eastern part of the Emeishan Large Igneous Province, southwestern China: petrogenesis and tectonic implications. *Journal of Asian Earth Sciences*, **47**: 216-230

Lassiter, J.C., DePaolo, D.J. and Mahoney, J.J. (1995). Geochemistry of the Wrangellia Flood Basalt Province: implications for the role of continental and oceanic lithosphere in Flood Basalt Genesis. *Journal of Petrology*, **36**: 983-1009.

Le Bas, M. J., Le Maitre, R. W., Streckeisen, A. and Zanettin, B. (1986). A chemical classification of volcanic rocks based on the total alkali–silica diagram. *Journal of Petrology*, **27**: 745–750.

Le Turdu, C., Tiercelin, J.J., Gibert, E., Travi, Y., Lezzar, K.E., Richert, J.P., Massault, M., Gasse, F., Bonnefille, R., Decobert, M., Gensous, B., Jeudy, V., Tamrat, E., Mohammed, M.U., Martens, K., Balemwal Atnafu, Tesfaye Chernet, Williamson, D. and Taieb, M. (1999). The Ziway–Shala lake basin system, Main Ethiopian Rift: influence of volcanism, tectonics and climatic forcing on basin formation and sedimentation. *Palaeogeography, Palaeoclimatology and Palaeoecology*, **150**: 135–177.

Manikyamba, C. Sohini Ganguly, M. Santosh, Abhishek Saha, G. and Lakshminarayana, (2015). Geochemistry and petrogenesis of Rajahmundry trap basalts of Krishna-Godavari Basin, India. *Geoscience Frontiers*, **6**: 437-451.

Marty, B., Pik, R. and Gezahegn Yirgu (1996). Helium isotopic variations in Ethiopian plume lavas: nature of magmatic sources and limit on lower mantle contribution. *Earth Planetary Science Letters*, **144**: 223–237.

Mengesha Tefera, Tadiwos Chernet and Workineh Haro (1996). Exploration of the geological map of Ethiopia (1:20,000,000). Ethiopian institutes of geological surveys Addis Ababa, Ethiopia, 83pp.

Merla, G., Abbate, E., Azzaroli, A., Bruni, P., Canuti, P., Fazzuoli, M., Sagri, M. and Tacconi, P. (1979). A geological map of Ethiopia and Somalia (1973) and comment with a map of major landforms. C.N.R., Firenze, Italy.

Meyer, W., Pilger, A., Rosler, A. and Stets, J. (1975). Tectonic evolution of the northern part of the Main Ethiopian Rift in Southern Ethiopia. **In**: Pilger, A., Rosler, A. _Eds.., Afar Depression of Ethiopia. *Schweizerbart, Stuttgart*. 352–362.

Mohr, P. A. (1968): The Cenozoic volcanic succession in Ethiopia. - Bull. *Volcanol*. **32**: 5-14. (1983): Ethiopian flood basalt province. – *Nature,* **303**:577-584.

Mohr, P.A. (1983). Ethiopian Flood basalt provinces. *Nature*, **303**: 577-583.

Mohr, P. and Zanettin, B. (1988). The Ethiopian food basalt province. In: Macdougall, J.D. (Ed.), Continental flood basalts. *Kluwer Academic Publishers*, 63–110.

Mulugeta Alene, William, K. Hart, Beverly, Z. Saylor, Alan Deino, Stanley Mertzman, Yohannes Haile-Selassie and Luis B. Gibert (2017). Geochemistry of Woranso–Mille Pliocene basalts from west-central Afar, Ethiopia: Implications for mantle source characteristics and rift evolution. Lithos, **282–283**: 187–200.

Natali, C., Beccaluva, L., Bianchini, G. and Siena, F. (2011). Rhyolites associated to Ethiopian CFB: clues for initial rifting at the Afar plume axis. *Earth and Planetary Science Letters*, **312 (1):** 59–68.

Nelson, W.R. (2009). Two-Plume Dynamics beneath the East African Rift System: A Geochemical Perspective. The Pennsylvania State University, 231 pp.

Peccerillo, A., Barberio, M.R., Gezahegn Yirgu, Dereje Ayalew, Barberi, M. and Wu, T.W. (2003). Relationships between mafic and acid peralkaline magmatism in continental rift settings: a petrological, geochemical and isotopic study of the Gedemsa volcano, central Ethiopian Rift. *Journal of Petrology*, **44**(11): 2003-2032. doi: 10.1093/petrology/egg068.

Peccerillo, A., Donati, C., Santo, A.P., Orlando, A., Gezahegn Yirgu and Dereje Ayalew (2007). Petrogenesis of silicic peralkaline rocks in the Ethiopian rift: geochemical evidence and volcanological implications. *Journal of African Earth Sciences*, **48**: 161–173.

Piccirillo, E. M., Justin-Visentin, E., Zanettin, B., Joron, J. K. and Treuil, M. (1979). Geodynamic evolution from plateau to rift: major and trace element geochemistry of the central eastern Ethiopian plateau volcanics. *Neues Jahrbuch fur Geologie and Palaontologie*, **258:** 139-179.

Pik, R., Deniel, C., Coulon, C., Gezahegn Yirgu, Hofmann, C. and Dereje Ayalew (1998). The Northwest Ethiopian plateau flood basalts: classification and spatial distribution of magma types. *Journal of Volcanology and Geothermal Research*, **81**: 91–111.

Pik, R., Deniel, C., Coulon, C., Gezahegn Yirgu and Marty B. (1999). Isotopic and trace element signatures of Ethiopian flood basalts: Evidence for plume–lithosphere interactions. *Geochimica et Cosmochimica Acta*, **63**(15): 2263–2279.

Rollinson H. (1993). Using geochemical data: evaluation, presentation, interpretation. *Pearson, prentice hall*, 380pp.

Ronald B. F. and Carol D. F. (2014). Essentials of Igneous and Metamorphic Petrology. *New York*, 331p.

Ronga, F., Lustrino, M., Marzoli A. and Melluso L. (2010). Petrogenesis of a basalt-comendite-pantellerite rock suite: the Boseti Volcanic Complex (Main Ethiopian Rift). *Miner Petrol*, **98**: 227–243. doi 10.1007/s00710-009-0064-3.

Rooney, T., Furman, T., Bastow, I., Dereje Ayalew and Gezahegn Yirgu (2007). Lithospheric modification during crustal extension in the Main Ethiopian Rift. *Journal of Geophysical Research,***112:** B10201. doi:10.1029/2006JB004916.

Rooney, T.O., Bastow, I.D. and Keir, D. (2011) Insights into extensional processes during magma assisted rifting: Evidence from aligned scoria cones. *Journal of Volcanology and Geothermal Research **201:** 83-96.*

Rooney, T.O., Hart, W.K., Hall, C.M.,Dereje Ayalew, Ghiorso, M.S., Hidalgo, P. and Gezahegn Yirgu (2012). Peralkaline magma evolution and the tephra record in the Ethiopian Rift. *Contributions to Mineralogy and Petrology*, **164**: 407-426.

Rooney, T.O. (2017) The Cenozoic magmatism of East-Africa: Part I–Flood basalts and pulsed magmatism. *Lithos*, **286–287**: 264–301.

Safonova, I.Yu, Simonov, V.A., Buslov, M.M., Ota, T. and Maruyama, Sh, (2008). Neoproterozoic basalts of the Paleo-Asian Ocean (Kurai accretion zone, Gorny Altai, Russia): geochemistry, petrogenesis, geodynamics. *Russian Geology and Geophysics*, **49**: 254-271.

Siefemichael Berhe, Berhe Desta, Nicoletti, M. and Mengesha Tefera a (1987). Geology, geochronology and geodynamic implications of the Cenozoic magmatic province in W and SE Ethiopia. *Journal of the Geological Society, London.* **144**: 213- 226.

Sun, S.S. and McDonough, W.F. (1989). Chemical and isotopic systematics of oceanic basalts: implications for mantle composition and processes. In: Saunders, A.D., Norry, M.J. (Eds.), Magmatism in Ocean Basins. *Geological Society of London Special Publication*, 42, pp. 313-345.

Tadiwos Chernet, Hart, W.K., Aronson, J.L. and Walter, R.C. (1998). New age constraints on the timing of volcanism and tectonism in the northern Main Ethiopian Rift-southern Afar transition zone (Ethiopia). *Journal of Volcanology and Geothermal Research*, **80**: 267–280.

Tadiwos Chernet and Hart W.K. (1999). Petrology and Geochemistry of volcanism in the northern main Ethiopian rift- southern Afar transition region. *Actavolcanologica,***11**(1): 21-41.

Taylor, S.R. and McLennan, S.M. (1985). The Continental Crust: Its Composition and Evolution. Oxford. *Blackwell Scientific publications, London*, 312 p.

Thompson, R.N., Morrison, M.A., Hendry, G.L. and Parry, S.J. (1984). An assessment of the relative roles of crust and mantle in magma genesis: an elemental approach. *Philosophical Transactions of the Royal Society of London,* A**310**: 549-590.

Trua, T., Deniel, C. and Mazzuoli, R. (1999). Crustal control in the genesis of Plio-Quaternary bimodal magmatism of the Main Ethiopian Rift (MER): Geochemical and isotopic (Sr, Nd and Pb) evidence. *Chemical Geology*, **155**: 201–231.

Tsegaye Abebe, Manetti, P., Bonini, M., Corti, G., Innocenti, F., Mazzarini, F. and Pecskay, Z. (2005). Geological map (scale 1:200000) of the northern Main Ethiopian Rift and its implication for the volcano-tectonic evolution of the rift. *Geological Society of America*, Boulder Colorado, USA, Maps and Charts series, MCH094.

Tsegaye Abebe, Balestrieri, M. and Bigazzi, G. (2010). The Central Main Ethiopian Rift is younger than 8 Ma: confirmation through apatite fission-track thermochronology. *Terra Nova,**22:*** 470–476. doi: 10.1111/j.1365-3121.2010.00968. x.

Ukstins I. A., Renne P. R., Wolfenden E., Baker J., Dereje Ayalew and Menzies M. (2002). Matching conjugate rifted margins: 40Ar/39Ar chrono-stratigraphy of pre- and syn-rift bimodal flood volcanism in Ethiopia and Yemen. *Earth and Planetary Science Letters*, **198:** 289–306.

Wager, L., R., and Deer, W.A., 1939. Geological investigations in East Greenland, part III. The petrology of the Skaergaard intrusions. Kangerdlugessuaq, East Greenland, Medd.om Gronland, **105**, no. 1-352.

Wilson, M., (1989). Igneous petrogenesis: a global tectonic approach. *Harper Collins Academic, London*, 466p.

White, W. M. (2005). Geochemistry. *John Wiley & Sons*, 413p.

Wolfenden, E., Ebinger, C., Gezahegn Yirgu, Deino, A. and Dereje Ayalew (2004). Evolution of the northern Main Ethiopian rift: birth of a triple junction. *Earth and Planetary Science Letters*, **224**: 213–228.

Workineh Haro, Daba Bulto Mekonen Bekele, Desalegn Debelo, Muluken Kebede and Mohamed Edris (2014). Geology, geochemistry, and gravity survey of Asela area.Geological survey of Ethiopia, basic geo science mapping directorate. Un published technical report, Memoir **38**: 87pp.

Xu, Y.-G., Ma, J.-L., Frey, F.A., Feigenson, M.D., and Liu, J.-F. (2005). Role of lithosphere asthenosphere interaction in the genesis of Quaternary alkali and tholeiitic basalts from Datong, western North China Craton. *Chemical Geology*, **224** (4), 247-271.

Yaxley, G.M. (2000). Experimental study of the phase and melting relations of homogeneous basalt + peridotite mixtures and implications for the petrogenesis of flood basalts. *Contributions to Mineralogy and Petrology*, **139**: 326-338.

Zanettin, B., Justin-Visentin, E., Nicoletti, M. and Petrucciani, C. (1978). Evolution of the Chencha escarpment and the Ganjiuli graben (Lake Abaya) in the southern Ethiopian rift. *NeuesJahrbuch fur Geologie und Palaontologie. Monatshefte,***8:** 473–490.

## Appendix I

Sample location

| Sample code | Northing | Easting | Elevation (m) |
|---|---|---|---|
| T5S4 | 0603543 | 0925274 | 2745 |
| T3S1 | 0604153 | 0919897 | 3020 |
| T3S2 | 0605742 | 0919583 | 3015 |
| T5S2 | 0602620 | 0924461 | 2870 |
| T5S3 | 0602952 | 0924960 | 2920 |
| T5S1 | 0604209 | 0922872 | 2685 |
| T1S2 | 0598869 | 0925903 | 2562 |
| T1S3 | 0599475 | 0927219 | 2575 |
| T1S4 | 0599885 | 0925219 | 2490 |
| T4S1 | 0600643 | 0924997 | 2735 |
| T4S3 | 0601566 | 0925515 | 2720 |
| T3S3 | 0602946 | 0919214 | 2995 |
| T651 | 0602509 | 0927861 | 2348 |
| T6S2 | 0603451 | 0927843 | 2354 |
| T5S6 | 0604782 | 0924886 | 2922 |

## Appendix II

Selected normalized and trace element ratio values.

Normalized by chondritic value of Boynton, 1984.

| | **Basalt** | | | | | **Rhyolite** | | | | | | |
|---|---|---|---|---|---|---|---|---|---|---|---|---|
| **Sample** | **T5S4** | **T3S2** | **T3S1** | **T5S2** | **T5S3** | **T6S2** | **T1S3** | **T1S2** | **T5S1** | **T4S1** | **T4S3** | **T1S4** |
| Ba/Y | 20.17 | 19.23 | 18.83 | 22.91 | 23.35 | 4.023 | 2.108 | 1.722 | 0.945 | 2.918 | 2.161 | 2.595 |
| Ce/Pb | 4.85 | 8.66 | 4.44 | 6.175 | 4.582 | 9.92 | 5.16 | 4.42 | 5.11 | 5.34 | 3.53 | 8.77 |
| Rb/Sr | 0.096 | 0.057 | 0.063 | 0.044 | 0.037 | 5.311 | 7.550 | 10.08 | 9.68 | 8.898 | 8.284 | 9.205 |
| Nb/Th | 13.63 | 11.65 | 12.43 | 13.38 | 13.89 | 8.24 | 7.37 | 8.02 | 7.37 | 7.21 | 7.48 | 7.52 |
| La/Nb | 0.833 | 0.815 | 0.774 | 0.965 | 0.958 | 0.724 | 0.875 | 0.629 | 0.846 | 0.649 | 0.578 | 0.558 |
| $(Gd/Yb)_N$ | 2.77 | 2.57 | 2.489 | 1.99 | 1.87 | 1.33 | 1.22 | 1.38 | 1.16 | 1.55 | 1.50 | 1.33 |
| $(La/Yb)_N$ | 12.08 | 12.14 | 11.93 | 8.12 | 7.86 | 7.2 | 6.4 | 4.88 | 4.54 | 8.67 | 8.8 | 6.19 |
| $(La/Sm)_N$ | 3.20 | 3.44 | 3.51 | 3.19 | 3.00 | 3.49 | 3.36 | 2.63 | 2.93 | 3.28 | 3.35 | 2.65 |
| Eu/Eu* | 1.06 | 1.07 | 0.99 | 1.07 | 1 | 0.76 | 0.33 | 0.8 | 0.27 | 0.29 | 0.31 | 0.28 |
| $(Tb/Yb)_N$ | 2.11 | 2.01 | 2.04 | 1.54 | 1.56 | 1.18 | 1.13 | 1.31 | 1.08 | 1.31 | 1.24 | 1.163 |
| $(Sm/Yb)_N$ | 3.78 | 3.53 | 3.40 | 2.54 | 2.62 | 2.06 | 1.91 | 1.85 | 1.55 | 2.65 | 2.63 | 2.34 |
| Nb/La | 1.2 | 1.23 | 1.29 | 1.04 | 1.044 | 1.382 | 1.143 | 1.589 | 1.183 | 1.540 | 1.73 | 1.79 |
| Nb/Ta | 15.96 | 21.23 | 19.8 | 19.77 | 18.86 | 15.89 | 16.42 | 15.51 | 15.87 | 15.92 | 16.93 | 16.69 |
| Zr/Hf | 34.12 | 40 | 38.62 | 40.73 | 40.48 | 43.79 | 38.77 | 44.30 | 40.37 | 39.78 | 41.26 | 42.33 |
| Zr/Sm | 27.71 | 25.30 | 27.18 | 34.15 | 32.06 | 68.09 | 55.51 | 58.87 | 55.41 | 77.9 | 87.82 | 73.95 |
| Zr/Nb | 4.543 | 3.768 | 3.771 | 6.498 | 6.439 | 8.881 | 9.092 | 8.86 | 10.05 | 9.71 | 9.527 | 9.8 |
| Ti/Y | 704.2 | 681.3 | 655.6 | 425.4 | 428.6 | 45.35 | 43.79 | 26.44 | 24.36 | 78.65 | 86.42 | 60.35 |
| Ti/Zr | 95.52 | 101.5 | 94.82 | 62.16 | 61.76 | 3.071 | 3.034 | 2.868 | 2.487 | 2.265 | 2.367 | 2.176 |
| Ba/Nb | 12.43 | 10.8 | 10.27 | 21.75 | 21.67 | 2.42 | 1.33 | 1.65 | 0.97 | 0.82 | 0.56 | 0.92 |